

# Geodätisch-geophysikalische Arbeiten in der Schweiz

(Fortsetzung der Publikationsreihe  
«Astronomisch-geodätische Arbeiten in der Schweiz»)

herausgegeben von der

Schweizerischen Geodätischen Kommission  
(Organ der Schweizerischen Akademie der Naturwissenschaften)

**Achtundfünfzigster Band  
Volume 58**

**Systematic Investigations of Error  
and System-Modelling of Satellite  
Based Flight Approaches and  
Landings in Switzerland**

Maurizio Scaramuzza

1998



# Geodätisch-geophysikalische Arbeiten in der Schweiz

(Fortsetzung der Publikationsreihe  
«Astronomisch-geodätische Arbeiten in der Schweiz»)

herausgegeben von der

Schweizerischen Geodätischen Kommission  
(Organ der Schweizerischen Akademie der Naturwissenschaften)

**Achtundfünfzigster Band**  
**Volume 58**

**Systematic Investigations of Error  
and System-Modelling of Satellite  
Based Flight Approaches and  
Landings in Switzerland**

Maurizio Scaramuzza

1998

**Adresse der Schweizerischen Geodätischen Kommission:**

**Institut für Geodäsie und Photogrammetrie  
Eidg. Technische Hochschule Zürich  
ETH Hönggerberg  
CH-8093 Zürich, Switzerland**

**Redaktion des 58. Bandes:  
Dr. M. Scaramuzza, Dr. B. Bürki**

**Druck: Print-Atelier E. Zingg, Zürich**

## VORWORT

In der Luftfahrtnavigation stellt sich bei Landeanflügen neben der Genauigkeit auch die Frage nach der Zuverlässigkeit, Verfügbarkeit und Kontinuität. Mit entsprechenden Versuchsanordnungen über die Machbarkeit hat Herr Dr. M. Scaramuzza das Potential von GPS-gestützten Landeanflugverfahren und deren Einsatzmöglichkeiten evaluiert, weiterentwickelt und wissenschaftlich untersucht. Das Projekt war in ein Kooperationskonzept von mehreren Partnern eingebettet. Als Koordinationsstelle fungierte das Bundesamt für Zivilluftfahrt (BAZL). Neben dem BAZL und dem Geodäsie und Geodynamik Labor (GGL) der ETH Zürich nahmen SWISSCONTROL, CROSSAIR, Telematica, Linden (D), und das Bundesamt für Landestopographie (L+T) an den Versuchen teil. Allen Institutionen sei für ihre Beiträge herzlich gedankt.

Der vorliegende Band enthält Analysen und Simulationen bezüglich der sogenannten "Required Navigation Performance Parameter", wobei auf die besondere topographische Situation der Schweiz eingegangen wird. Dabei wurden auch kritische Kurvenflüge in niedriger Höhe berücksichtigt und bei realen Flügen getestet. Einen zentralen Mittelpunkt bildete die Frage, wie schnell, gut und zuverlässig Fehler detektiert und entsprechende Warnungen mitgeteilt werden können. Hierzu wurden Algorithmen entwickelt, die für die Anwendungen sehr wertvoll sind. Für die Anflüge wurde eine mittlere horizontale Abweichung vom vorgegebenen Flugweg von 0.7% der erlaubten Abweichung aufgezeigt. Mit Hinzunahme von weiteren Sensoren, wie z.B. Altimetern, dürften Satellitensysteme die Anforderungen künftiger Standards zur Zertifizierung von neuen Anflugsystemen erfüllen.

Herr Scaramuzza hat mit dem vorliegenden Band der Schweizerischen Geodätischen Kommission (SGK) das anspruchsvolle Problem des automatischen Zuverlässigkeits-Monitoring bei GPS-gestützten Landeanflügen erfolgreich bearbeitet. Mit den erzielten Ergebnissen und den potentiellen Anwendungsmöglichkeiten hat er eine wichtige wissenschaftliche Grundlage geschaffen und einen integrierenden Bestandteil in der Konzipierung zukünftiger satellitengestützter Navigationsanwendungen in der Schweiz geliefert.

Die satellitengestützte Navigation eröffnet die Möglichkeit, auch in der Schweiz vorhandene Bedürfnisse für Instrumentenanflugverfahren zu erfüllen, die mit den bisher vorhandenen Mitteln nicht realisierbar waren. Vom GPS-Einsatz im operationellen Flugverkehr erwartet man eine Entlastung der gegenwärtigen Anflugleitstellen sowie vereinfachte und beschleunigte Anflugverfahren. Dies ist in vielen Fällen mit Verkürzungen der Flugwege verbunden und bringt damit wirtschaftliche und ökologische Vorteile.

Die SGK dankt Herrn Scaramuzza für die Arbeiten als wesentlichen neuen Beitrag zur Geodäsie in der Schweiz. Herr Dr. A. Geiger vom GGL hat sowohl in wissenschaftlicher wie auch in organisatorischer Hinsicht sehr zum Gelingen der Untersuchungen beigetragen. Dem Schweizerischen Nationalfonds zur Förderung der Wissenschaften danken wir für die finanzielle Unterstützung des Projektes. Von der Schweizerischen Akademie für Naturwissenschaften (SANW) wurden die Druckkosten übernommen, wofür die SGK ihren grossen Dank ausspricht.

**Dipl. Ing. F. Jeanrichard**  
Bundesamt für Landestopographie  
Vizepräsident der SGK

**Prof. Dr. H.-G. Kahle**  
ETH Zürich  
Präsident der SGK

## PREFACE

En navigation aérienne, les approches posent des problèmes de précision, mais également de fiabilité, de disponibilité et de continuité. Le Dr M. Scaramuzza a pu évaluer, développer et analyser de manière scientifique le potentiel et les possibilités d'utilisation de méthodes d'approche assistées par GPS à l'aide de procédures appropriées destinées à tester leur faisabilité. Ce projet était intégré à un programme de coopération regroupant plusieurs partenaires. Outre l'Office fédéral de l'aviation civile qui assumait un rôle de coordination et le laboratoire de géodésie et de géodynamique (Geodäsie und Geodynamik Labor, GGL) de l'EPF Zurich, SWISSCONTROL, CROSSAIR, Telematica, Linden (D) et l'Office fédéral de topographie (S+T) y ont pris part. Que tous les participants soient ici chaleureusement remerciés pour leur contribution.

Le présent rapport contient des analyses et des simulations se référant à la méthode dite "Required Navigation Performance Parameter", les spécificités topographiques de la Suisse étant étudiées. Les virages critiques à basse altitude ont également été pris en compte et testés à l'occasion de vols réels. La question de la rapidité, de la qualité et de la fiabilité de la détection d'erreurs ainsi que de la communication d'avertissements correspondants a constitué un aspect central de l'étude. Des algorithmes du plus haut intérêt pour les applications ont été développés à cet effet. Un écart horizontal moyen par rapport à la trajectoire de vol prescrite atteignant 0,7% de l'écart permis a pu être mis en évidence. L'adjonction de capteurs supplémentaires tels que des altimètres devrait permettre au systèmes satellitaires de satisfaire aux normes futures pour la certification de nouveaux systèmes d'approche.

M. Scaramuzza a traité avec succès le problème complexe de la surveillance automatique de la fiabilité dans le cas d'approches assistées par GPS, exposé dans le présent volume de la Commission géodésique suisse (CGS). Il a accompli un travail scientifique important tant par les résultats obtenus que par le potentiel d'utilisation mis en évidence et a ainsi contribué à la conception de futures applications de navigation assistées par satellite en Suisse.

La navigation assistée par satellite offre la possibilité, en Suisse aussi, de répondre à des besoins existants en matière de procédures d'approche aux instruments que les moyens à disposition jusqu'à présent ne permettaient pas de couvrir. L'utilisation du GPS dans la circulation aérienne doit se traduire par un délestage des services actuels de contrôle aérien ainsi que par une simplification et une accélération des procédures d'approche. Le raccourcissement des trajectoires de vol y étant lié dans bien des cas, des avantages tant sur le plan économique qu'écologique en découlent.

La CGS adresse ses remerciements à M. Scaramuzza pour ses travaux qui apportent une nouvelle et importante contribution à la géodésie en Suisse. Le soutien du Dr A. Geiger du GGL, aussi bien au niveau scientifique que du point de vue de l'organisation, a constitué un élément essentiel dans la réussite de ce projet. Nous remercions le Fonds national suisse de promotion des sciences pour l'aide financière qu'il a apportée à ce projet. Enfin, les frais d'impression ont été pris en charge par l'Académie suisse des sciences naturelles (ASSN) à laquelle la CGS adresse ses plus vifs remerciements.

**Dipl. Ing. F. Jeanrichard**  
de l'Office fédéral de topographie  
Vice président de la CGS

**Prof. Dr. H.-G. Kahle**  
ETH Zurich  
Président de la CGS

## FOREWORD

In civil aviation navigation requirements for approach and landings include accuracy, reliability, availability, integrity and continuity. Dr. M. Scaramuzza has evaluated the feasibility of GPS- based landing approaches and studied the potential of applications on a scientific basis. The project was integrated in a common concept pursued by various partners. It was coordinated by the Swiss Federal Office of Civil Aviation (FOCA). Apart of the FOCA and the Geodesy and Geodynamics Lab (GGL) of ETH Zurich, Swisscontrol, Crossair, Telematica, and the Swiss Federal Office of Topography participated in the trials. All these institutions are thanked gratefully.

The volume presented includes analyses and simulations concerning the so-called 'Required Navigation Performance Parameter'. The effect of rugged terrain in Switzerland was studied, in particular. Also critical turns at low altitude were considered and tested during real flights. A central topic was the question, how fast, well and reliable errors could be detected and appropriate warnings be communicated. Corresponding algorithms were developed and applied successfully. A mean horizontal deviation of 0.7 % of the value allowed was achieved. In using additional sensors, such as altimeters, satellite systems could fulfil future navigation requirements for approach and landing, also in difficult topographic terrain, such as at the airport Lugano-Agno in Switzerland. Dr. Scaramuzza has successfully contributed to the problem of automatic reliability monitoring of GPS based landing approaches. With the results achieved he has provided a highly valuable scientific basis for developing concepts of future navigation applications in Switzerland.

Satellite based navigation provides the possibility to fill a gap in instrumental landing approaches which was up to now not available. GPS in civil aviation could help to ease up landing control procedures which would result in significant shortening of flight paths and thereby would be of ecological and economical advantage. The Swiss Geodetic Commission (SGC) thanks Dr. Scaramuzza for his pioneer work as a significant contribution to geodesy in Switzerland. Dr. A. Geiger's (GGL) continuing support both in scientific and practical aspects is also gratefully acknowledged. We also would like to thank Dr. W. Lechner, Telematica, Germany, for his help and advice during all stages of the project. The Swiss National Science Foundation (SNSF) has supported the work financially. Thanks are also due to the Swiss Academy of Sciences (SAS) for providing funds for printing this volume.

**Dipl. Ing. F. Jeanrichard**  
Swiss Federal Office of Topography  
Vice President of the SGC

**Prof. Dr. H.-G. Kahle**  
ETH Zurich  
President of the SGC





## Abstract

This work analyses the potential of the Global Positioning System (GPS) for navigation purposes in civil aviation, especially on approaches and landings in rugged terrain. This work is financed by the National Science Foundation (NF) and is part of the scientific analysis of a project borne by different partners, which aim is to gather insight and experiences into GPS based approach and landing systems. These aims are achieved by flying approaches and landings in Lugano-Agno and recording simultaneously relevant flight data. The Federal Office of Civil Aviation (FOCA) leads this project, where partners are the Crossair, Swisscontrol, Telematica and ETH Zürich.

Based on satellite measurements, GPS allows instantaneous positioning accuracy in the range of 50 - 100 meters. This accuracy is improved to the range of meters by applying the differential GPS mode. This mode is used for navigation purpose during the approach and landing flights. Further position accuracy improvement up to centimeter to decimeter level is achieved by applying carrier phase measurements. This positioning mode is used as reference.

The investigations are based on the coming standards on certification of approach and landing systems. The four Required Navigation Performance (RNP) parameters, accuracy, integrity, availability, and continuity are particularly analysed. These parameters cannot statistically meaningful be evaluated due to the small number of approaches flown up to now. Nevertheless these few approaches show a mean horizontal deviation from the desired course of 0.7% of the allowed deviation where the distribution ( $1\sigma$ ) is 6% of the allowed deviation. These results are promising for further test flights.

Theoretical analysis and simulations with respect to the RNP parameters including e.g. flight dynamic and topography show, that the number of visible satellites as well as its constellation can become critically at low altitude and during curved flight. Improvement of continuity can be shown theoretically when using additional satellite systems, especially with the Russian GLONASS and the planned European ENSS. Pseudolites improve the continuity mainly in the region of the critical parts of the final approach.

Two possible error sources, multipath and interference, are further investigated. A model describing the multipath of the GPS code signal is derived and verified with experiments. It is further shown, that the losses of the GPS signal detected during preliminary measurements at the airport of Lugano-Agno can be attributed to GPS carrier phase signal multipath.

A transmitter causing radio frequency interference was identified south of Lugano-Agno. A computer based technique for the identification of potential regions exposed to interference in the environment of a disturbing station is presented.

An enhanced algorithm to monitor the position accuracy by using only range measurements of GPS satellites (Receiver Autonomous Integrity Monitoring, RAIM) is finally developed and tested with simulations. The probability of false alarms is slightly larger than required, whereas the probability of missed detections fulfils the requirements. An improvement of these results can be achieved by integrating altimeter measurements into the algorithm (Aircraft Autonomous Integrity Monitoring, AAIM). By this way all requirements are fulfilled.

## Zusammenfassung

Die vorliegende Arbeit untersucht das Potential des Global Positioning System (GPS) im Bereich der Navigation in der zivilen Luftfahrt, insbesondere bei Landeanflügen in gebirgigem Gelände. Die Arbeit ist Teil der vom Schweizerischen Nationalfonds (NF) unterstützten wissenschaftlichen Auswertung eines von verschiedenen Partnern getragenen Projektes, das zum Ziel hat, Erkenntnisse und Erfahrungen im Gebiet von GPS-gestützten Landeanflügen zu sammeln. Diese Ziele sollen durch umfangreiche Landeanflüge im operationellen Betrieb in Lugano-Agno und gleichzeitigem Erfassen von flugrelevanten Daten erreicht werden. Die Leitung des Projektes untersteht dem Bundesamt für Zvilluftfahrt. Partner des Projektes sind die Crossair, Swisscontrol, Telematica und ETH Zürich.

Messungen zu GPS Satelliten ermöglichen eine momentane Positionsbestimmung mit einer Genauigkeit in der Grössenordnung von 50 - 100 Metern. Der Einbezug des differentiellen Modus erlaubt es, die Genauigkeit auf wenige Metern zu steigern. Dieser Modus wird für die Flugführung während den Anflügen verwendet. Eine weitere Steigerung der Positionsgenauigkeit auf Zentimeter bis Dezimeter kann durch den Einbezug von Träger-Phasenmessungen erreicht werden. Dieser Modus wird für die Bestimmung der Referenzposition verwendet.

Die Untersuchungen basieren auf den künftigen Standards zur Zertifizierung von neuen Anflugsystemen. Auf den vier Required Navigation Performance (RNP) Parameter, Genauigkeit, Zuverlässigkeit, Verfügbarkeit und Kontinuität wird im speziellen eingegangen. Da bis zum Abschluss dieser Arbeit nur wenige Anflüge vorliegen, können diese Parameter statistisch nicht aussagekräftig ausgewertet werden. Für diese Anflüge liegt die mittlere horizontale Abweichung vom vorgegebenen Flugweg bei 0.7% der erlaubten Abweichung und weist eine Streuung ( $1\sigma$ ) von 6% der erlaubten Abweichung auf, was als vielversprechend zu bewerten ist.

Theoretische Analysen und Simulationen bezüglich den vier RNP Parametern, insbesondere unter Berücksichtigung des Flugverhaltens und der Topographie, zeigen, dass bei geringer Flughöhe im Kurvenflug die Anzahl sichtbarer Satelliten sowie ihre Konstellationsgüte für die Navigation kritische Werte annehmen können. Die Steigerung der Kontinuität bei der Verwendung zusätzlicher Satellitensysteme, insbesondere des russischen GLONASS und des geplanten europäischen ENSS, kann gezeigt werden. Pseudolites steigern die Kontinuität insbesondere im Bereich von kritischen Stellen des Endanfluges.

Weiter werden die Signalmehrwegausbreitung und Interferenzen des GPS Signals untersucht. Ein Modell für die Mehrwegausbreitung des GPS Codesignals wird hergeleitet und anhand einer speziell angelegten Versuchsanordnung bestätigt. Die während den Vorversuchen auf dem Flughafen Lugano-Agno beobachteten Auslöschungen des GPS Signals können durch die Mehrwegausbreitung des GPS Träger-Phasensignals erklärt werden.

Südlich von Lugano-Agno konnte ein Sender identifiziert werden, der mit GPS Signale interferiert. Ein Computergestütztes Verfahren zur Identifizierung von möglichen Interferenzgebieten in der Umgebung eines bekannten Störsenders wird präsentiert.

Schliesslich wird ein verbesserter Algorithmus zur Überwachung der Positionsgenauigkeit ausschliesslich basierend auf Messungen der GPS Satelliten (Receiver Autonomous Integrity Monitoring, RAIM) entwickelt und mit Simulationen getestet. Die Wahrscheinlichkeit, dass ein Fehler fälschlicherweise gemeldet wird, liegt leicht über den Anforderungen. Diejenige, dass ein unerlaubter Positionsfehler nicht entdeckt wird, erfüllt die Anforderungen. Eine Verbesserung der Ergebnisse wird dadurch erreicht, dass Daten des barometrischen Höhenmessers in die Berechnungen einbezogen werden (Aircraft Autonomous Integrity Monitoring, AAIM). Dadurch können alle Anforderungen erfüllt werden.

# Contents

<b>1. Introduction</b>	<b>1</b>
1.1. Future of Civil Aviation Navigation . . . . .	1
1.2. Description and Objectives of the Project . . . . .	2
1.3. Description of the Work . . . . .	4
<b>2. The Lugano Trials</b>	<b>5</b>
2.1. Introduction . . . . .	5
2.2. Operational System . . . . .	8
2.2.1. Airborne Equipment . . . . .	8
2.2.2. Reference Station . . . . .	9
2.2.3. Data Link . . . . .	9
2.3. Measurement and Monitoring System . . . . .	9
2.3.1. ADARS . . . . .	9
2.3.2. GDARS . . . . .	10
2.3.3. Analysis Software Development . . . . .	10
2.4. Site Survey of Lugano-Agno Airport . . . . .	12
2.5. Schedule of Trials . . . . .	12
<b>3. Required Navigation Performance</b>	<b>14</b>
3.1. Introduction . . . . .	14
3.2. Error Propagation . . . . .	15
3.2.1. Systematic Errors . . . . .	15
3.2.2. Statistical Errors . . . . .	16
3.3. Accuracy . . . . .	17
3.3.1. Reference Track . . . . .	18
3.3.2. Navigation Error Characteristics . . . . .	18

3.3.3.	Approach Accuracy . . . . .	19
3.3.4.	Aircraft Position Accuracy . . . . .	21
3.3.5.	Pseudo Range Corrections (PRC) Accuracy . . . . .	24
3.3.6.	Probability Distribution of TSE . . . . .	28
3.3.7.	Control System and Approach Accuracy . . . . .	34
3.4.	Integrity . . . . .	37
3.5.	Availability and Continuity . . . . .	38
3.6.	Findings . . . . .	38
<b>4.</b>	<b>Satellite Visibility and Geometry</b>	<b>40</b>
4.1.	Introduction . . . . .	40
4.2.	Influences on Satellite Visibility and Geometry . . . . .	41
4.2.1.	Theoretical Satellite Visibility . . . . .	41
4.2.2.	Cut-Off Angle . . . . .	45
4.2.3.	Terrain . . . . .	50
4.2.4.	Aircraft Attitude . . . . .	55
4.2.5.	Aircraft Body Mask . . . . .	58
4.2.6.	Combination of Influences on Satellite Visibility and Geometry	59
4.3.	Supplemental Satellite Systems and Pseudolites . . . . .	63
4.3.1.	GPS and GLONASS . . . . .	63
4.3.2.	GPS and INMARSAT . . . . .	64
4.3.3.	GPS and ENSS . . . . .	64
4.3.4.	GPS and Pseudolites . . . . .	64
4.3.5.	Simulation Results . . . . .	65
4.4.	Comparison of Simulations with Real Flight Data . . . . .	67
4.5.	Findings . . . . .	69
<b>5.</b>	<b>Multipath and Interference</b>	<b>71</b>
5.1.	Multipath . . . . .	71
5.1.1.	Detecting Code Multipath with Code Minus Carrier Phase Measurements . . . . .	72
5.1.2.	Geometry of Multipath . . . . .	77
5.1.3.	Delay Lock Loop . . . . .	80
5.1.4.	Verification of the Multipath Model . . . . .	82

---

5.1.5. Signal Loss Caused by Carrier Phase Multipath . . . . .	84
5.2. Interference . . . . .	88
5.2.1. Introduction . . . . .	88
5.2.2. RFI in the Region of Lugano-Agno . . . . .	89
5.2.3. Use of Digital Terrain Models for Detection of Potentially Interfering Zones . . . . .	91
5.2.4. Lugano Field Tests August 1997 . . . . .	95
5.3. Findings . . . . .	98
<b>6. Integrity Monitoring</b>	<b>99</b>
6.1. Basics on Integrity Monitoring . . . . .	99
6.1.1. Introduction . . . . .	99
6.1.2. External Methods . . . . .	101
6.1.3. Internal methods (RAIM and AAIM) . . . . .	102
6.1.4. Combination of External and Internal Methods . . . . .	104
6.1.5. Test Variable Thresholds . . . . .	104
6.2. Derivation of a LSR Based RAIM Method for Single Failure . . . . .	105
6.2.1. Introduction . . . . .	105
6.2.2. Modeled Errors . . . . .	105
6.2.3. Relations between the Measurement Residuals . . . . .	107
6.2.4. Methods to Solve the Test Variable $\alpha$ . . . . .	109
6.2.5. Comparison of Measurement Residuals . . . . .	112
6.2.6. Time to Alarm $TtA$ . . . . .	113
6.2.7. Simulations . . . . .	113
6.2.8. Verification and Modification . . . . .	114
6.2.9. RAIM Quality Prediction . . . . .	118
6.2.10. Single Failure RAIM Overview . . . . .	121
6.2.11. RAIM Simulation Results . . . . .	121
6.3. RAIM Enhancements . . . . .	123
6.3.1. Dual Failure RAIM . . . . .	123
6.3.2. Barometric Aided Integrity Monitoring . . . . .	124
6.4. Findings . . . . .	126

---

<b>7. Summary and Conclusions</b>	<b>128</b>
7.1. The Lugano Trials . . . . .	128
7.2. Required Navigation Performance . . . . .	128
7.3. Satellite Visibility and Geometry . . . . .	129
7.4. Multipath and Interference . . . . .	130
7.5. Integrity Monitoring . . . . .	131
7.6. Final Remarks . . . . .	132
 <b>Bibliography</b>	 <b>135</b>
 <b>A. Abbreviations</b>	 <b>144</b>
 <b>B. Glossary</b>	 <b>147</b>
 <b>C. Recorded Labels</b>	 <b>152</b>
C.1. ADARS . . . . .	152
C.2. GDARS . . . . .	154



# 1. Introduction

## 1.1. Future of Civil Aviation Navigation

Different national and international radionavigation plans have foreseen to terminate the use of conventional navigation installations (e.g. VOR, NDB, ILS etc.) within the next decades and to replace them by satellite based navigation aids (e.g. [DoT and DoD, 1997, BMV, 1996]). The U.S. Departments of Transportation (DoT) and Defense (DoD), for example, propose to terminate the operations of nearly all conventional navigation facilities by the year 2010 (figure 1.1). It is expected, that satellite based navigation systems will be available as replacement by this date.

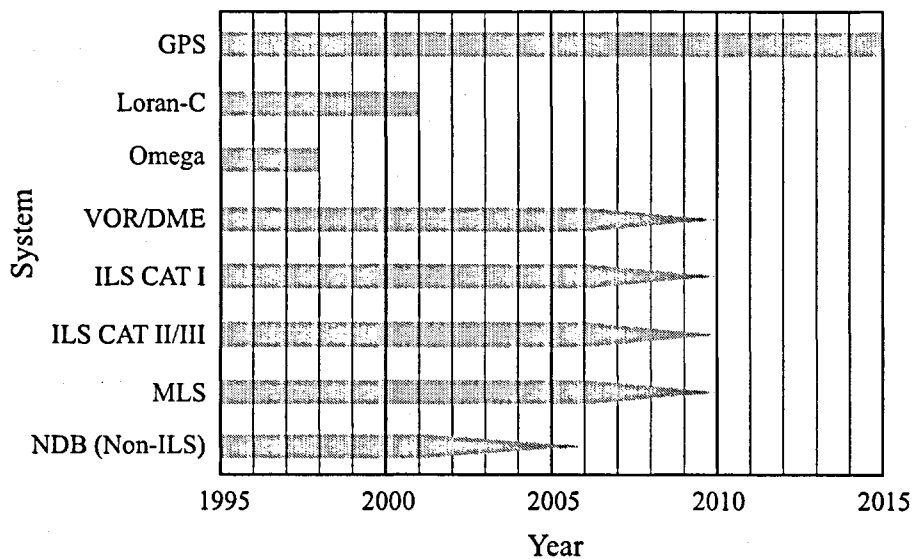


Figure 1.1.: Radionavigation system operating plan as proposed in 1996 by the U.S. Department of Transportation (DoT) and U.S. Department of Defense (DoD) [DoT and DoD, 1997]. It is planned, that most conventional radionavigation facilities will cease their operations by the year 2010.

Satellite based navigation provides the opportunity to perform a wide range of applications in civil aviation, which could not be realized with existing means up to the present day. These new possibilities can be applied to meet arising demands of the civil aviation community, including new navigation procedures, gate to gate navigation, air traffic surveillance, air traffic flow management, aircraft collision avoidance and more.

The advantages in navigation are mainly given by the increased independence from ground based navigation installations. Consequently only one navigation system has to be installed in the aircrafts. Such systems, which can be used globally, are called Global Navigation Satellite Systems (GNSS). Furthermore the flight routes can be selected more directly, as there are no requirements on overflying ground based stations (Area Navigation, RNAV). In many cases this will shorten the flight distances which would be advantageous both economically and ecologically.

The Swiss Federal Office for Civil Aviation (FOCA) is expected to support the use of GNSS. The following two items are subject to further investigations:

- The swiss airspace user should have the possibility to take advantage of satellite based navigation without reducing today's safety standards. The use of the Global Positioning System (GPS) should be allowed as additional navigation aid to the conventional navigation systems. GPS should be used in all phases of flight down to non-precision approach in overlay mode.
- The FOCA is interested in gathering more information on the possibilities of GPS-use for approach and landing with attention, among others, to the influence of the swiss topography to such flight procedures.

These aims are achieved by disseminating the required information on the needed equipment and its use as well as by initiating and leading appropriate projects.

The Swiss Radio Navigation Plan, which is being developed at the moment, has foreseen to gather GNSS CAT-I capability in the near future. CAT-II/III approach and landing capability will still be provided by the ILS as the needed standards for GNSS CAT-II/III are not expected to be available in the near future [CH-RNP, 1998].

## 1.2. Description and Objectives of the Project

Different GNSS approach and landing trials were carried out worldwide in the past years and showed promising results [Vallot *et al.*, 1991, Luftfartsverket, 1994]. Most of these trials were performed in a non-operational environment. As one of the first airliner, 'Continental Express' carried out operational GPS approaches and landings to the airport of Aspen, Colorado, but these flights did not comprise the collection of a large number of data for a systematic analysis of the system. Informal flight testing with the Honeywell/Pelorus Satellite Landing System (SLS-2000) at

Minneapolis/St. Paul International Airport has begun in 1996. Data recorded during these flights will be used for the Federal Aviation Administration (FAA) certification process.

To get own experience with this type of application, in 1993 the FOCA has initialized a GNSS approach and landing project, due to the missing of systematic investigations with a large number of flights under operational conditions in rugged terrain. The collection of data and its scientific analysis should finally give the needed know-how to the FOCA to make decisions on the certification of such procedures.

This project is lead by the FOCA and is carried out in cooperation with different national and international partners:

- the German Air Navigation Service 'Deutsche Flugsicherung' (DFS), the Institute of Flight Guidance of the Technical University of Braunschweig and Aerodata carried out preliminary investigations and supported the system design
- the regional airliner Crossair made available two SAAB 2000 and bought two GPS navigation systems and recording systems
- the swiss air navigation service Swisscontrol bought the reference stations, calculates the approach procedures and ensures the airspace safety for these operations
- the Swiss Air Force makes available its radar monitoring for the first part of the approach
- Telematica serves as consultant
- the Swiss Federal Office of Topography (L+T) carried out the site survey of the airport of Lugano-Agno
- the scientific analysis is carried out by the Geodesy and Geodynamics Laboratory (GGL) at the Swiss Federal Institute of Technology (ETH)

Different other partners contributed to this project by order of the FOCA. Contacts to Eurocontrol Experimental Centre (EEC) were maintained to arrange the data-transfer to their project SAPPHIRE.

This work is part of the scientific analysis, which is based on the four Required Navigation Performance (RNP) parameters, the accuracy, integrity, availability, and continuity as used by the aviation community. Further investigations are being done on possible error sources (multipath and interference). The objectives are to gather experience on the quality of the navigation system, to locate error sources and to find solutions to avoid quality degradation caused by these error sources.

It should be emphasized, that the aim of this work is not the certification of a GNSS approach and landing procedure, but to use geodetic techniques and methods to investigate the use of satellite navigation in civil aviation.

### 1.3. Description of the Work

The system used for the testflights is described in **Chapter 2** . Further an overview on the run of the trials is given.

The RNP parameters are discussed in **chapter 3**. The accuracy is dealt in depth in this chapter as it is the only of the four parameters, which can be determined directly with the available data up to now. Reasons of the limitation to estimate the other three parameters are specified at the end of the chapter. These remaining parameters are nevertheless discussed in further chapters.

**Chapter 4** investigates different influences on the number of visible satellites and on the Dilution Of Precision (DOP) under dynamic conditions. Simulations as well as investigations on real data are done. Sufficient satellite visibility and DOP values are conditional for the required availability and continuity of the system.

GPS is subject to a large number of error sources. Investigations on the effects of these errors are necessary. Two major error sources affecting the civil aviation, multipath and interference, are examined in **chapter 5**.

One of the major tasks is to ensure the integrity of the navigation system. Existing techniques to monitor the integrity are described in the first part of **chapter 6**. The second part presents the derivation of an enhanced Least Square Residuals (LSR) Receiver respectively Aircraft Autonomous Integrity Monitoring (RAIM respectively AAIM) algorithm. Extended simulations are done to test the quality of this technique. The RAIM and AAIM algorithms can be used to detect accuracy degradation.

## 2. The Lugano Trials

### 2.1. Introduction

The flight trials are carried out at the airport of Lugano-Agno, south of Switzerland, because its topographic conditions make special demands on the system (figure 2.1).

A conventional landing system is available for approaches from the south and several landings per day are performed by Crossair during regular operations. Most of these flights coming from the north of Switzerland have to overfly the airport first and then carry out the approach from the south (dotted line in figure 2.1). A straight in approach from the north would be a benefit for Crossair, but it is impossible with conventional systems mainly due to the topography. A satellite based approach and landing procedure, which allows among others to fly curves in this phase of flight, can solve this problem (black line in figure 2.1) and is used for the flight trials.

The entire approach and landing phase for the Lugano trials (the so-called North Approach) is based on Global Navigation Satellite System (GNSS) and whenever available on Differential GNSS (DGNSS). The Global Positioning System (GPS) is used as satellite system.

The North Approach was designed in 1995 as a 'Special Category I' (SCAT-I)-like non-precision approach procedure. SCAT-I means in this context an approach, which is based on the MLS/ILS CAT I procedure but with GNSS respectively DGNSS providing navigation guidance [RTCA, 1993]. A non-precision approach procedure is used, as the obstacle clearance does not fulfil the requirements for a precision approach at the airport of Lugano-Agno [ICAO, 1993].

As the approach is planned for flights coming from the north the first waypoint (LUKOM) is placed on the airway A9, about 35 NM north to Lugano-Agno (figure 2.2). This first waypoint has to be set at such a distance due to the surrounding mountains, which reach nearly 11'000 ft of altitude. A straight in approach is not possible due to the orientation of the runway and the surrounding topography. A curved approach was designed with heading changes at the waypoints of BIASC and SHARK. Also the glide slope angle changes at SODES, ISONE, and CHANG. These angles vary from 0° to 6.65°.

With this approach design and the Differential GPS-transmitter placed at the airport of Lugano-Agno the differential corrections are earliest available shortly before

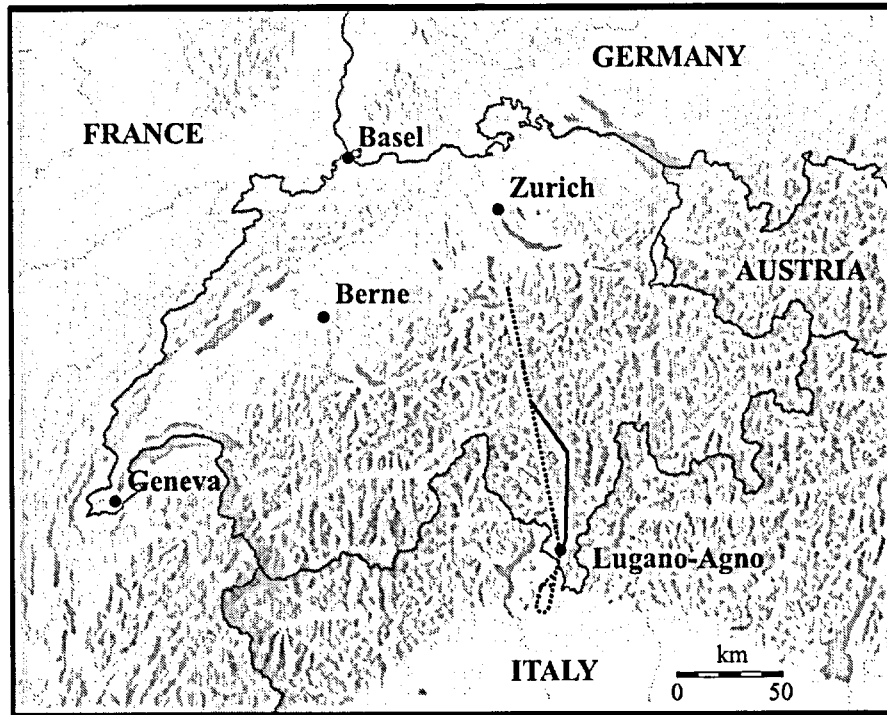


Figure 2.1.: The airport of Lugano-Agno is located in the south part of Switzerland, near to the Italian border. The topographic conditions can be deduced from the underlaid relief. The dotted line shows the actual approach and landing procedure for aircrafts coming from the north. The black line corresponds to the satellite based approach and landing procedure as used for the flight trials.

SODES. For this reason the entire approach is split into two parts. The first part uses the Flight Management System (FMS) overlay or back-up navigation and the second part the GPS navigation.

The approach is based on the Required Navigation Performance (RNP) tunnel concept for precision approach and landing [Laginja, 1993, Kelly and Davis, 1994]. The tunnel has at LUKOM a lateral limit of  $\pm 5$  NM, which narrows to  $\pm 0.3$  NM at SODES (Final Approach Fix, FAF). The vertical limit is  $\pm 560$  ft at SODES. The limits remain constant from SODES to TOUCH at the threshold of the runway (figure 2.3). These limits are used for the preliminary flights and will be adapted for the flight trials under operational conditions.

Due to the use of GPS as primary means of navigation from SODES onwards, the Federal Office of Civil Aviation requires, that trial flights have to be carried out only under Visual Meteorological Conditions (VMC) and during daytime [ICAO, 1990].

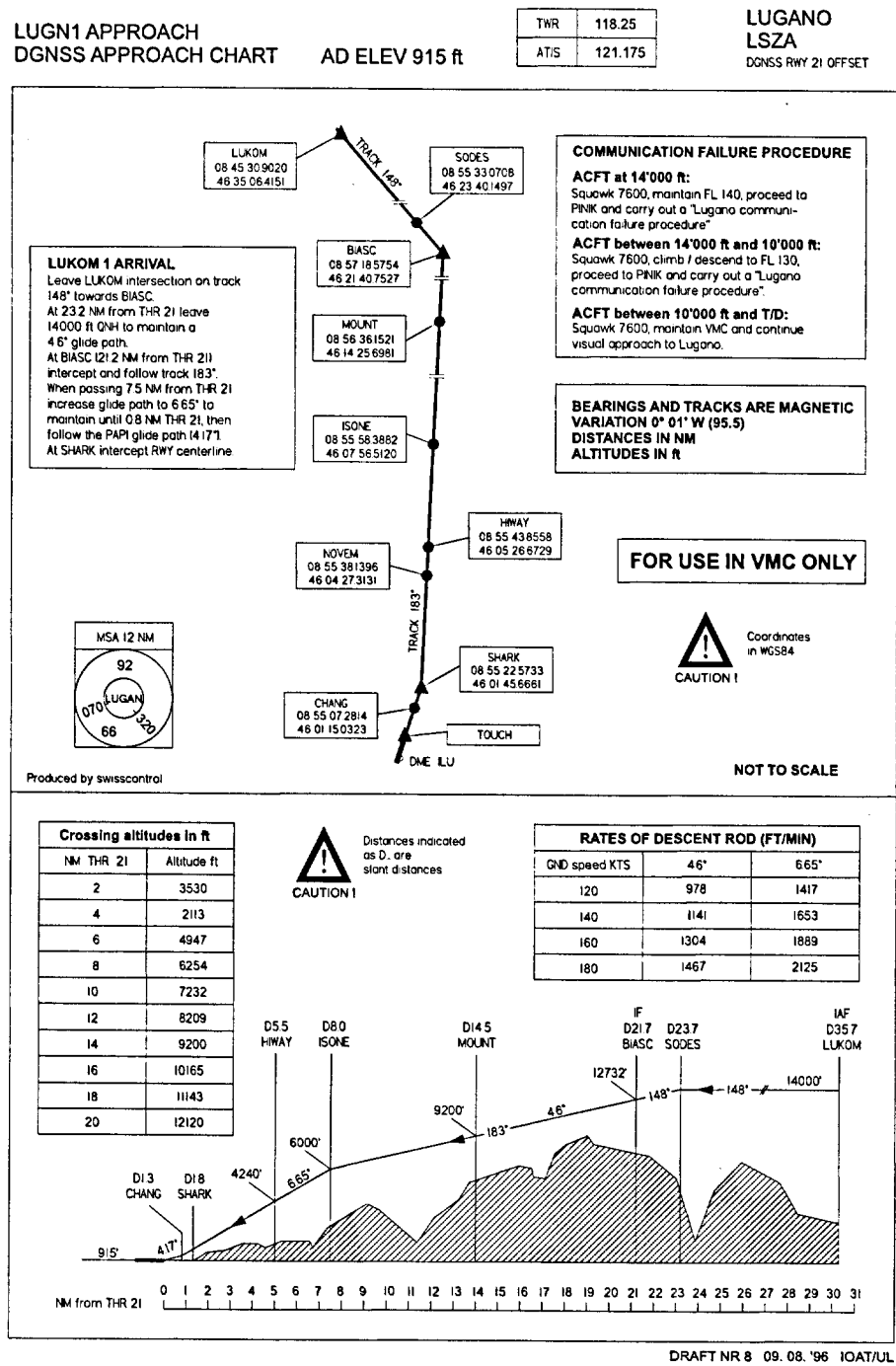


Figure 2.2.: DGNSS approach chart used for the Lugano trials. This chart shows among others the waypoints, ground- and vertical tracks and the terrain profile (courtesy of Swisscontrol).

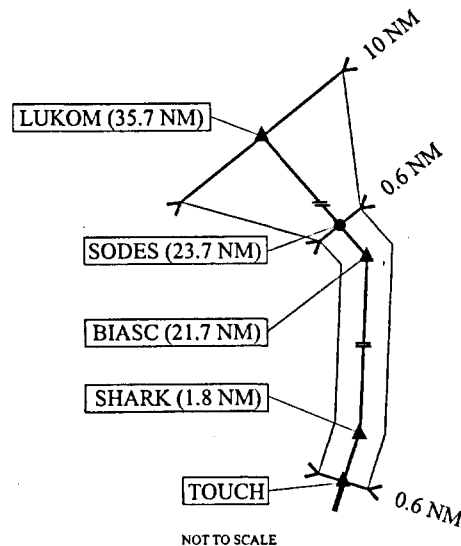


Figure 2.3.: The different tunnel widths are shown in this figure, which is not to scale. The values right of the waypoint names indicates the distance to waypoint TOUCH, where the values on the right side of the figure corresponds to the tunnel width.

## 2.2. Operational System

The operational system is used for the guidance of the aircraft during the GNSS approach in Lugano-Agno. It is composed of an airborne equipment, a GPS reference station, and a data link.

### 2.2.1. Airborne Equipment

Two SAAB 2000 were chosen as testbed for the flight trials (figure 2.4). This aircraft gives the options for installation of the airborne equipment and is also capable to fly steep approaches as required during the North Approach.

The GNSS airborne equipment comprises a single frequency GPS receiver (code). A VHF antenna mounted on the rear bottom fuselage of the aircraft enables to receive GPS correction values to achieve Differential GPS (DGPS) navigation.

The GPS data is transmitted together with other navigation and FMS data into the Electronic Flight Instrument System (EFIS), which is used for navigation.



### 2.2.2. Reference Station

The reference station used for the calculation of DGPS correction values is placed at the airport of Lugano-Agno. It consists of a single frequency GPS receiver (code). The antenna is mounted on top of the glide slope antenna, about 8 meters above the ground. A further receiver is planned to monitor the outgoing correction values.

### 2.2.3. Data Link

The data link antenna to broadcast the correction values calculated by the reference station is placed at the airport of Lugano-Agno, close to the ILU DME antenna (figure 2.2). No repeaters for data link support are installed at the moment. Site surveys were done to transfer the reference station to a mountain in the region of the airport to enhance the data link coverage, but none of the surveyed sites could fulfil the needed requirements.

The reference station used for the test flights in May and August 1996 was a provisional one and it is planned to replace it in the next phase of the project by a definitive one.

In the beginning the RTCM format was chosen for the correction values [RTCM SC-104, 1994]. This format will be replaced after the preliminary flights by the RTCA format [RTCA, 1993].

## 2.3. Measurement and Monitoring System

A measurement system was developed and built to monitor the operational system. Data of the airborne equipment is recorded by the Airborne Data Acquisition and Recording System (ADARS). The Ground Data Acquisition and Recording System (GDARS) records data at the reference station. The collected data are investigated with an analysis software package which was developed for this purpose.

### 2.3.1. ADARS

A single frequency GPS receiver (code and carrier phase) is part of the airborne measurement system. Further an Airborne Data Acquisition and Recording System (ADARS) (figure 2.5), which was developed and built for this purpose from the Swiss Aircraft Factory (SF) in Emmen, Switzerland, records the raw data from both airborne GPS receivers and about 70 different flight relevant parameters with a rate of 1 Hz up to 25 Hz. Table 2.1 gives an overview on the parameters, which are recorded by the ADARS.

Group	Parameters	Rate [Hz]
Navigation	Radio Height, LOC, GS, DME, Barometric Altitude	1 and 25
IRS Attitude	Ground Speed, Position, Angles, Angle Rates Accelerations	1 and 10
GPS	Pseudorange, Range Rate, Position, Time, DOP's, Measurement and Sensor Status of operational and measurement System	1
Meteorology	Wind, Temperature	1
Flight Technical Information	Runway Heading, Frequencies, Ground Station Identity	1
Hybrid Position	(for future expansion)	1

Table 2.1.: Summary of the parameters and rates recorded by the ADARS. More details are given in appendix C

The ADARS comprises a 486 CPU, SCSI card, 2.1 GB removable harddisk for data exchange, ARINC 429 and 717 cards and a GPS card of the measurement system. Post processing of the measurement system GPS receiver allows to calculate stand-alone code, differential code and carrier phase positions of the aircraft.

### 2.3.2. GDARS

The ground based measurement system includes a single frequency GPS receiver (code and carrier phase) and a Ground Data Acquisition and Recording System (GDARS) which records correction values from the operational system and the GPS raw data from the measurement system. The recording rates varies between 1 and 5 Hz. The GDARS consists mainly of a 486 CPU computer with a 2.1 GB removable harddisk for data transfer and the GPS of the measurement system.

### 2.3.3. Analysis Software Development

The harddisk with the recorded data of ADARS and GDARS can be used for data transfer to the analysis centre at the Federal Institute of Technology. A software package for data decoding and analysis was developed at GGL for this purpose. Most of the data decoding and analysis can be carried out automatically. This is advantageous to handle the large amount of data during the operational flights.

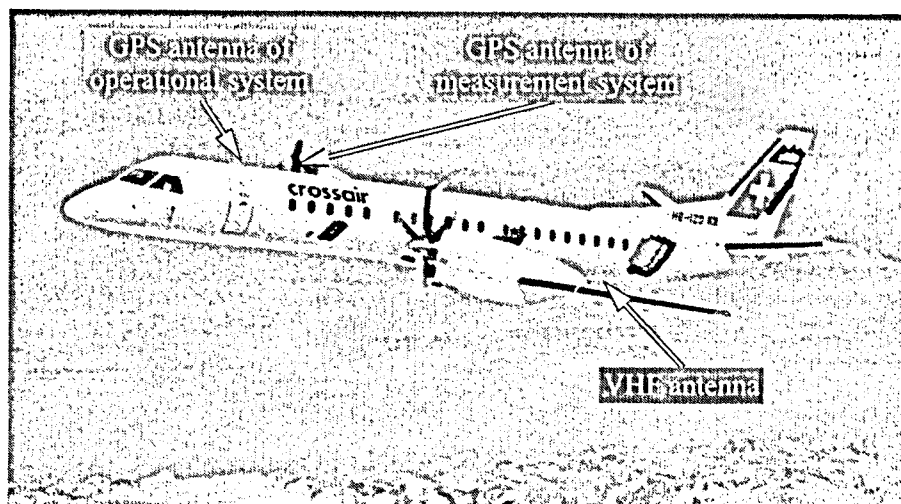


Figure 2.4.: Two SAAB 2000 of Crossair are used as testbed for the Lugano trials. Both GPS antennas of the operational and the measurement system are mounted on top of the fuselage whereas the VHF antenna for receiving the differential corrections is placed on bottom, aft fuselage (courtesy of Crossair).

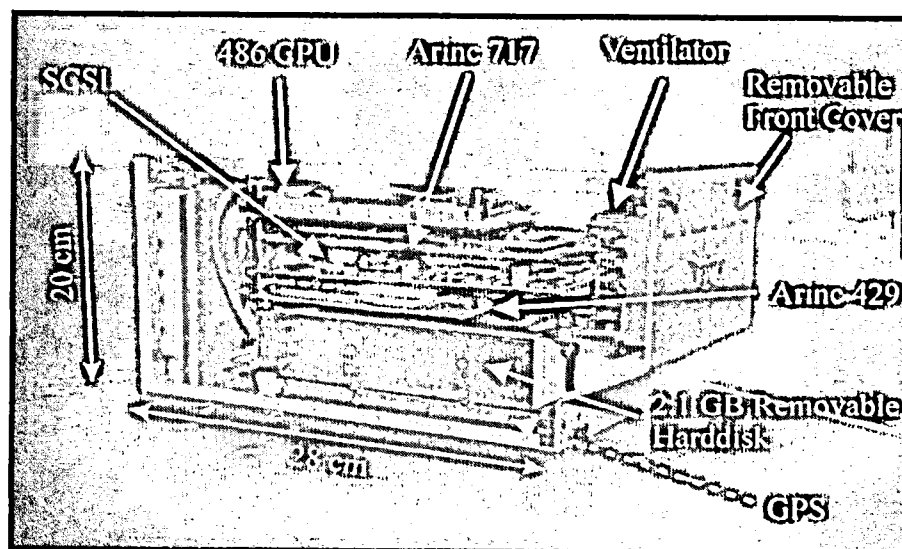


Figure 2.5.: Two Airborne Data Acquisition and Recording Systems (ADARS) were developed and built by Swiss Aircraft Factory (SF) in Emmen, Switzerland. The ADARS records the raw data of both airborne GPS receivers and about 70 different flight relevant parameters with a rate from 1 Hz up to 25 Hz.

## 2.4. Site Survey of Lugano-Agno Airport

Coordinates of ground reference points (receivers sites, runway thresholds etc.) at the Lugano-Agno airport are needed for the design of the GPS approach. The available coordinates are referred to CH1903. Transformation to WGS84 of this coordinate set is not possible with the accuracy requested as the integrity of the original coordinates is not given. Therefore a new site survey was carried out by L+T in order to determine the coordinates with an accuracy better than the required  $1\sigma$ -value = 3 cm [Wild and Santschi, 1995].

One GPS receiver was placed as main reference station during the entire campaign on a known triangulation point (LFP2). Two receivers were placed on two additional known points of the project 'Landesvermessung 1995' (LV95). Each point at the airport was surveyed twice with two receivers independently, with an occupation time of 20 minutes. The rapid static technique was applied. The Bernese Software of the Astronomical Institute of the University of Berne (AIUB) was used to calculate the coordinates. The resulting  $1\sigma$ -value of the accuracy is about 0.5 cm.

## 2.5. Schedule of Trials

The trial sequence is mainly divided into two phases:

- The first phase comprises preliminary flights for fine tuning of the approach procedure and the navigation system. These flights have experimental status and are carried out without passengers.
- The second phase comprises 500 to 1000 GPS guided north approaches under operational conditions. These approaches are only allowed if the conditions mentioned in chapter 2.1 are fulfilled. Transportation of passengers is allowed in this phase.

The time span for the planned flights depend strongly on the weather. Because the approach begins north of the Alps and ends south of them, meteorological conditions often vary. Clouds may be present on the one side of the ridge where on the other side Visual Meteorological Conditions (VMC) are given. Such a situation would not allow to fly the GPS north approach. A solution to shorten the time needed for the first phase was the selection of a second airport for part of the preliminary flights. The military air base of Interlaken was chosen for this purpose. Conditions are similar to the airport of Lugano-Agno. The air base is situated in a valley of the Alps, a curved approach with steep glide slopes is needed and a radar coverage is ensured by the military air traffic control. The main advantage is, that the entire approach is situated on the northern side of the Alps, thus reducing meteorological problems. Site surveys were carried out, mainly for the selection of the site for the reference ground station. A definitive location has not been selected until now.

Test flight series to Lugano-Agno were carried out on May, 15<sup>th</sup> and August, 23<sup>rd</sup> 1996. The aircraft departed both times from Basel-Mulhouse, carried out the approaches at Lugano-Agno and flew back to Basel-Mulhouse.

### **First test flights on May, 15<sup>th</sup> 1996**

The approaches of the first flight were flown in an overlay mode. This means, that the aircraft followed the lateral guidance, but maintained a constant altitude. This procedure was necessary as VMC was not available on lower altitudes. Two GPS north approaches of this kind were carried out, followed by a south approach with conventional navigation and a full stop landing at Lugano-Agno. The aircraft departed later for a third overlay approach and flew directly back to Basel-Mulhouse. Only part of the system worked properly at this time. IRS and hybrid data were not recorded. The reason was an incompatibility of the used data bus and the recording unit. No data from the operational GPS was recorded during the return flight. The reason for this outage was either a malfunction of the receiver or a wrong manipulation of the receiver. Some time tag problems were also detected. All other data buses worked properly. Interference problems were identified south of the Lugano-Agno airport (see chapter 5.2). The course direction indicator (CDI) did not work properly during the curved flight. Vertical guidance was not available but did not influence the guidance of the aircraft as the pilot maintained a constant altitude.

### **Second test flights on August, 23<sup>rd</sup> 1996**

Six approaches were carried out during the second flight. Some of them were deliberately flown with lateral offsets. One approach was flown with the best possible accuracy. All data buses worked properly. The CDI and the vertical guidance were still unusable. The interference problems were still present. An alarm signal appeared on the Ground Proximity Warning System (GPWS) when the aircraft overflew a certain mountain (Cima dell'Uomo). The minimum height was complied to but the approach rate was too high.

Further flights are not planned at the moment. The trials will proceed, when the problems of the CDI and vertical guidance will be solved. A new approach procedure is also needed to avoid the alarm of the GPWS.

## 3. Required Navigation Performance (RNP)

### 3.1. Introduction

The Federal Aviation Administration (FAA) requested the Radio Technical Commission for Aeronautics (RTCA) to prepare a civil Minimum Aviation System Performance Standard (MASPS) for the use of the Global Positioning System (GPS). Special Committee 159 (SC-159) was formed to prepare this standard and an 'Integrity Working Group' was appointed to investigate and report civil integrity problems related to GPS. Following documents, among others, were published by the SC-159:

- Report of Special Committee 159 on Minimum Aviation System Performance Standard (MASPS) for the Global Positioning System (GPS), DO-202, [RTCA, 1988]
- Minimum Operational Performance Standards (MOPS) for Airborne Supplemental Navigation Equipment Using Global Positioning System (GPS), DO-208, [RTCA, 1991]
- Minimum Aviation System Performance Standards DGNSS Instrument Approach System: Special Category I (SCAT-I), DO-217, [RTCA, 1993]
- Minimum Operational Performance Standards for Global Navigation Satellite Systems (GNSS) Airborne Antenna Equipment, DO-228, [RTCA, 1995]
- Minimum Operational Performance Standards for Global Positioning System / Wide Area Augmentation System Airborne Equipment, DO-229, [RTCA, 1996b]

The RTCA document DO-217 refers to SCAT-I procedures, as it is used in the Lugano trials, and defines the following four parameters as essential: Accuracy, Integrity, Availability, and Continuity. These parameters are defined by the ICAO All-Weather Operations Panel (AWOP) 14 as the Required Navigation Performance (RNP) parameters and were developed by the Special Committee on Future Air Navigation Systems (FANS). The RNP concept [ICAO, 1994b] should replace the methods commonly used to indicate required navigation capability for certain equipment. This change was imperative with the development of new navigation systems.

Further explanations are given in [Kelly and Davis, 1994]. It is noted, that further requirements for equipments and approach procedures as used in the Lugano trials are also given in [FAA, 1992, FAA, 1994].

The following investigations are based on the requirements given in the documents mentioned above.

## 3.2. Error Propagation

Error propagations will be of importance in the coming investigations and therefore be discussed briefly at this point.

### 3.2.1. Systematic Errors

The basic linearized GPS measurement equation is:

$$(\mathbf{A}^T \mathbf{P} \mathbf{A}) \vec{x} = \mathbf{A}^T \mathbf{P} \vec{f}, \quad (3.1)$$

where

- $\mathbf{A}$  = linearized observation equation matrix
- $\mathbf{P}$  = weight matrix
- $\vec{f}$  = vector of ranges or range errors
- $\vec{x}$  = vector of unknown position or position shift.

The matrix  $\mathbf{A}$  can be written as:

$$\mathbf{A} = \begin{pmatrix} e_{1_1} & e_{2_1} & e_{3_1} & -1 \\ e_{1_2} & e_{2_2} & e_{3_2} & -1 \\ \vdots & \vdots & \vdots & \vdots \\ e_{1_n} & e_{2_n} & e_{3_n} & -1 \end{pmatrix} \quad (3.2)$$

with

$$\begin{aligned} e_{1_s} &= -\sin(\lambda_s) \cdot \cos(\varphi_s) \\ e_{2_s} &= -\cos(\lambda_s) \cdot \cos(\varphi_s) \\ e_{3_s} &= -\sin(\varphi_s), \end{aligned}$$

where

$$\begin{aligned} e_{i_s} &= \text{unit vector from antenna to satellite in the topocentric system} \\ \lambda_s &= \text{azimuth of satellite} \end{aligned}$$

- $\varphi_s$  = elevation of satellite  
 $i$  = axis ( $i = 1 \dots 3$ )  
 $s$  = satellite number ( $s = 1 \dots n$ )  
 $n$  = number of tracked satellites.

The normal equation matrix  $\mathbf{N}$  is equal to  $\mathbf{A}^T \mathbf{P} \mathbf{A}$  and can be written with the weight matrix  $\mathbf{P}$  set equal to the unit matrix as:

$$\mathbf{N} = \begin{pmatrix} [e_{1,s}^2] & [e_{1,s}e_{2,s}] & [e_{1,s}e_{3,s}] & [-e_{1,s}] \\ [e_{1,s}e_{2,s}] & [e_{2,s}^2] & [e_{2,s}e_{3,s}] & [-e_{2,s}] \\ [e_{1,s}e_{3,s}] & [e_{2,s}e_{3,s}] & [e_{3,s}^2] & [-e_{3,s}] \\ [-e_{1,s}] & [-e_{2,s}] & [-e_{3,s}] & [n] \end{pmatrix}. \quad (3.3)$$

The squared brackets indicate a sum for  $s = 1 \dots n$

$$[x_s] = \sum_{s=1}^n x_s. \quad (3.4)$$

Formula (3.1) can now be written as

$$\mathbf{N} \vec{x} = \mathbf{A}^T \vec{f}. \quad (3.5)$$

The unknown vector  $\vec{x}$  is:

$$\vec{x} = \mathbf{N}^{-1} \mathbf{A}^T \vec{f}. \quad (3.6)$$

The vector  $\vec{f}$  can be constructed with ranges or range errors. The solution  $\vec{x}$  is then the position or the position displacement.

### 3.2.2. Statistical Errors

The covariance of  $\vec{x}$  is:

$$\text{Cov}(\vec{x}) = (\mathbf{N}^{-1} \mathbf{A}^T) \cdot \text{Cov}(\vec{f}) \cdot (\mathbf{N}^{-1} \mathbf{A})^T. \quad (3.7)$$



By setting

$$\text{Cov}(\vec{f}) = \mathbf{P}^{-1} = \mathbf{I} \quad (3.8)$$

it follows

$$\text{Cov}(\vec{x}) = \mathbf{N}^{-1} \mathbf{A}^T \mathbf{A} \mathbf{N}^{-1T} = \mathbf{N}^{-1}. \quad (3.9)$$

The Dilutions Of Precision (DOP) can be derived with  $\mathbf{N}^{-1}$  and gives a quantitative estimation of the satellite constellation geometry, which has a direct influence to the position quality. The DOP can be calculated as follows (e.g.[Bauer, 1992]):

$$\begin{aligned} HDOP &= \sqrt{N_{11}^{-1} + N_{22}^{-1}} \\ VDOP &= \sqrt{N_{33}^{-1}} \\ PDOP &= \sqrt{N_{11}^{-1} + N_{22}^{-1} + N_{33}^{-1}} \\ GDOP &= \sqrt{N_{11}^{-1} + N_{22}^{-1} + N_{33}^{-1} + N_{44}^{-1}} \end{aligned} \quad (3.10)$$

where

$HDOP$  = Horizontal DOP  
 $VDOP$  = Vertical DOP  
 $PDOP$  = Position DOP  
 $GDOP$  = Geometrical DOP.

### 3.3. Accuracy

Accuracy is defined in the context of the approach phase of flight as the ability of the total system to maintain the aircraft position within a Total System Error (TSE) with a 95% probability (inner tunnel) and to stay within a specified aircraft containment surface (outer tunnel) which defines the obstacle clearance and terrain avoidance [RTCA, 1995].

The inner tunnel defined for the Lugano trials corresponds to the tunnel described in chapter 2.1. The outer tunnel has to be defined by the Federal Office of Civil Aviation (FOCA). The 95% inner tunnel incident probability was redefined as follows: 95% of the flown approaches should not show an inner tunnel incident [BAZL AG OPS, 1995].

### 3.3.1. Reference Track

A true or reference position is used to determine the accuracy of the navigation system. For this purpose the GPS carrier phase solution from the measurement system was chosen, as its accuracy is an order of magnitude better than the GPS differential-code and GPS stand-alone solution used for the navigation system [Cocard, 1994]. Nevertheless the reference position has a smaller error of  $1\sigma$ -value = 20cm. As this position is used as reference it will be set as 'error-free' in further investigations.

### 3.3.2. Navigation Error Characteristics

The following descriptions are based on 'Manual on Required Navigation Performance (RNP)' [ICAO, 1994b]. Three errors, the Total System Error (TSE), the Navigation System Error (NSE), and the Flight Technical Error (FTE) are of interest when discussing the accuracy of a navigation system (figure 3.1). The errors are assumed to be random and independent in a first step. It will be shown later, that these assumptions are only partially valid.

The TSE corresponds to the distance between the true position and the desired course. The desired course can be calculated with the waypoints used for navigation. It is assumed that the desired course is calculated error free.

The NSE is the difference between the true position and the position used for navigation purpose. This error in the GPS stand-alone mode is a combination of the navigation sensor error, airborne receiver error and reference position error. The navigation sensor error comprises navigation data transfer times, computation errors, display errors, sensor noise etc. Error components of the ground station receiver have to be added when using the DGPS mode.

Note that the difference between the GPS positions of operational and measurement system represents only one part of the NSE, which will further be named  $NSE_{GPS}$ .

The FTE refers to the accuracy with which the aircraft is controlled. This corresponds to the distance between the position used for navigation purpose and the desired course.

It is understood that the coordinates of the waypoints and both GPS positions have to refer to the same system. Any applied correction (e.g. implementation of geoidal undulation) to a position has to be coordinated with the other positions to avoid further errors.

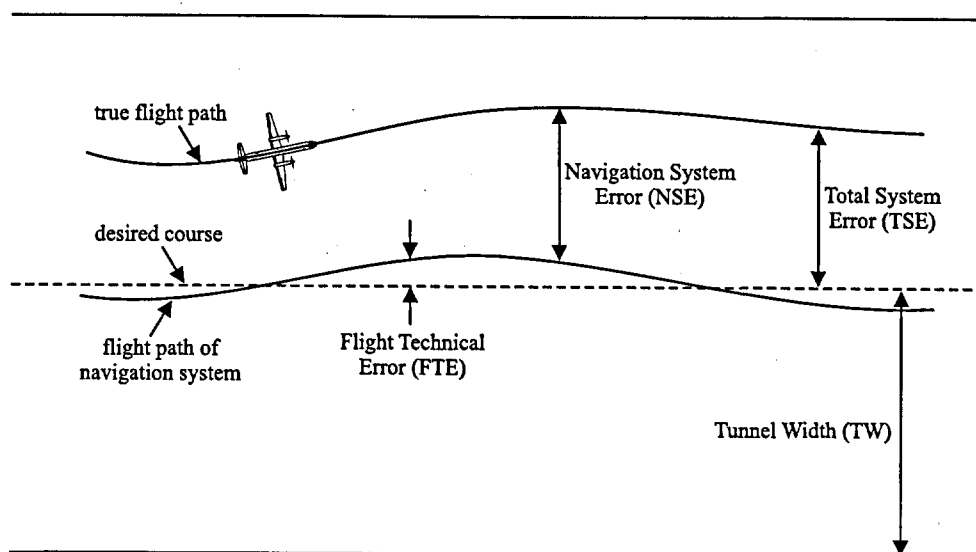


Figure 3.1.: Navigation error characteristics as defined by the ICAO.

### 3.3.3. Approach Accuracy

The three errors TSE, FTE and NSE are determined for parts of the approach. It is not reasonable to make any statements about the vertical accuracy as the vertical guidance was not available at this time. The longitudinal accuracy is not computable as there were no time conditions to maintain. Additionally the pilot did not have a proper course indication during the curved flight. All these facts restrict the investigations to the lateral accuracy for the parts of the approach from LUKOM to SODES and from BIASC to SHARK. Four flights were available for the first part of the approach, which navigation is based on absolute GPS and three for the second part with differential GPS (DGPS). The other flights comprise intended offsets and are not considered in the accuracy investigation. Figure 3.2 shows the lateral track and the error distribution where table 3.1 contains its mean values and standard deviations.

It is seen, that the *TSE* is small compared to the tunnel width, but this fact does not allow to make any final statements on the quality of the system as the number of approaches is far too small.

The reception of the pseudo range corrections before the waypoint SODES is a condition to meet the accuracy requirements to enter into the tunnel with a width of 0.3 NM. This requirement could not be fulfilled. Contact to the ground station was only available between SODES and BIASC onwards.

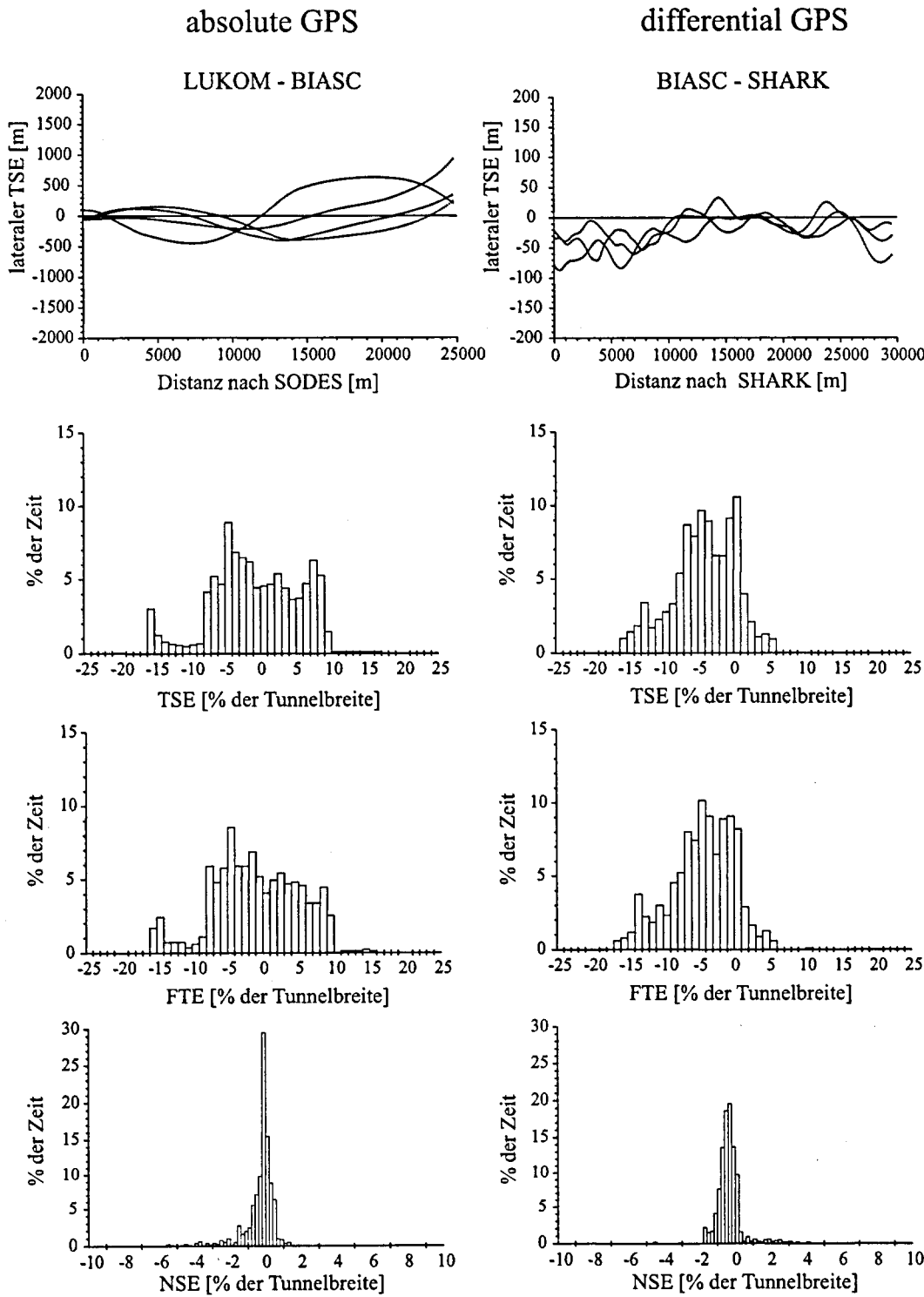


Figure 3.2.: Distributions of the TSE, FTE and NSE between the waypoints LUKOM and SODES, respectively BIASC and SHARK.

	LUKOM - SODES	BIASC - SHARK
$\overline{TSE}$	-0.67 %	-4.16 %
$\sigma_{TSE}$	6.22 %	4.46 %
$\overline{FTE}$	-0.97 %	-4.48 %
$\sigma_{FTE}$	6.07 %	4.51 %
$\overline{NSE}$	-0.30 m	-0.32 m
$\sigma_{NSE}$	0.86 m	0.96 m

Table 3.1.: Mean and standard deviation of the TSE, FTE and NSE between the waypoints LUKOM and SODES, respectively BIASC and SHARK. The values for TSE and FTE are given in percent of the tunnel width.

### 3.3.4. Aircraft Position Accuracy

Only part of the Navigation System Error (NSE) can be determined determined with the data recorded as the navigation sensor errors are not known (see chapter 3.3.2). The difference between the GPS positions from the operational and measurement system can be compared and leads to  $NSE_{GPS}$ . This value is split into a cross-track, an along-track and a vertical component for both GPS modes (stand-alone GPS and DGPS). Figure 3.3 shows the distribution of these six values, whereas table 3.2 contains the mean values and its standard deviations.

The GPS service supplier assures, that the horizontal position error will be less than 100 m and the vertical position error less than 159 m during 95% of time [Department of Defence, 1993] for single frequency receivers with Selected Availability (SA) switched on. The standard deviations in table 3.2 are much smaller than expected.

	stand-alone GPS	differential-code GPS
$\overline{NSE_{GPS}^{lon}}$	0.61 m	0.58 m
$\sigma_{ops}^{lon}$	22.89 m	12.51 m
$\overline{NSE_{GPS}^{lat}}$	1.50 m	-0.63 m
$\sigma_{ops}^{lat}$	23.74 m	15.30 m
$\overline{NSE_{GPS}^{ver}}$	-47.72 m	-6.44 m
$\sigma_{ops}^{ver}$	40.63 m	18.78 m

Table 3.2.: Mean and standard deviations of cross-track, along-track and vertical GPS position differences between the measurement and operational system for the stand-alone and differential GPS mode.

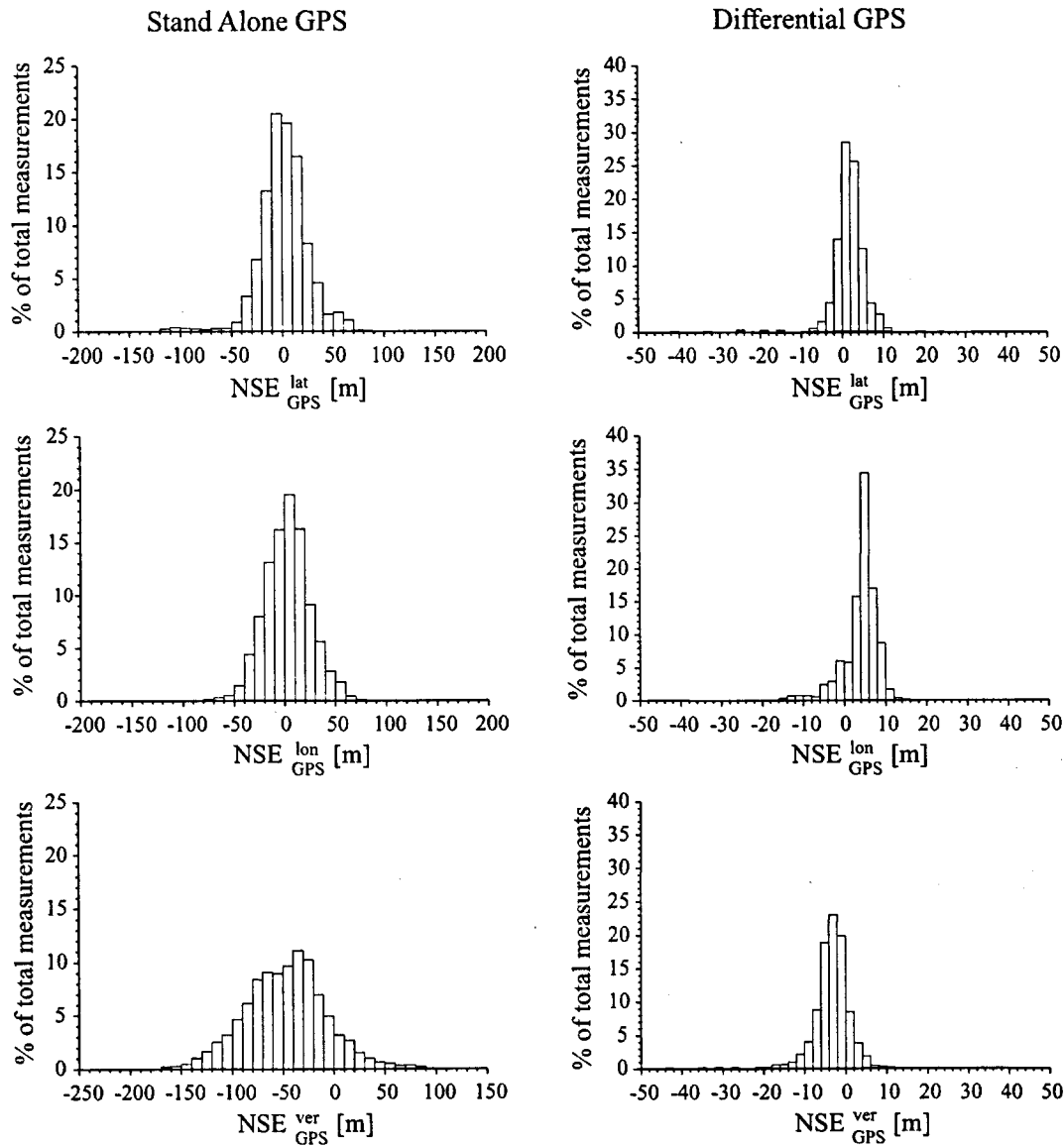


Figure 3.3.: Distributions of cross-track, along-track and vertical GPS position differences between the measurement and operational system for the stand-alone and differential GPS mode.

The mean values of the horizontal position in the stand-alone mode as in the differential mode are close to zero. A time delay caused by data transfer from the GPS to the navigation system or clock synchronization errors between GPS clock and navigation system clock would mainly appear in the longitudinal *NSE*. Such an error seems not to be present.

The vertical mean value in the stand-alone mode has a shift of nearly 50 m, which exceeds the expected range. It is assumed that the operational GPS receiver corrects its altitude with a geoid to achieve an orthometric altitude. The GPS of the measurement system instead delivers ellipsoidal altitudes. The vertical difference should then correspond to the geoidal undulation referred to WGS84 ellipsoid.

Investigations to confirm this assumption are done with the Swiss geoid of [Geiger, 1990]. Figure 3.4 shows the geoidal undulation referred to the WGS84 ellipsoid. Its values vary between 46 m and 54 m. The flight track is overlaid in this figure and it is visible, that the geoidal undulation varies about 2 m during the North Approach.

The mean geoidal undulation correction calculated for the entire flight with the help of the geoid is -51.47 m and differs 3.75 m from the detected vertical error. This difference may be caused by using different geoids and by errors in the position solution of the operational GPS. The main part of the vertical shift disappears, when differential mode is used, but it is still large.

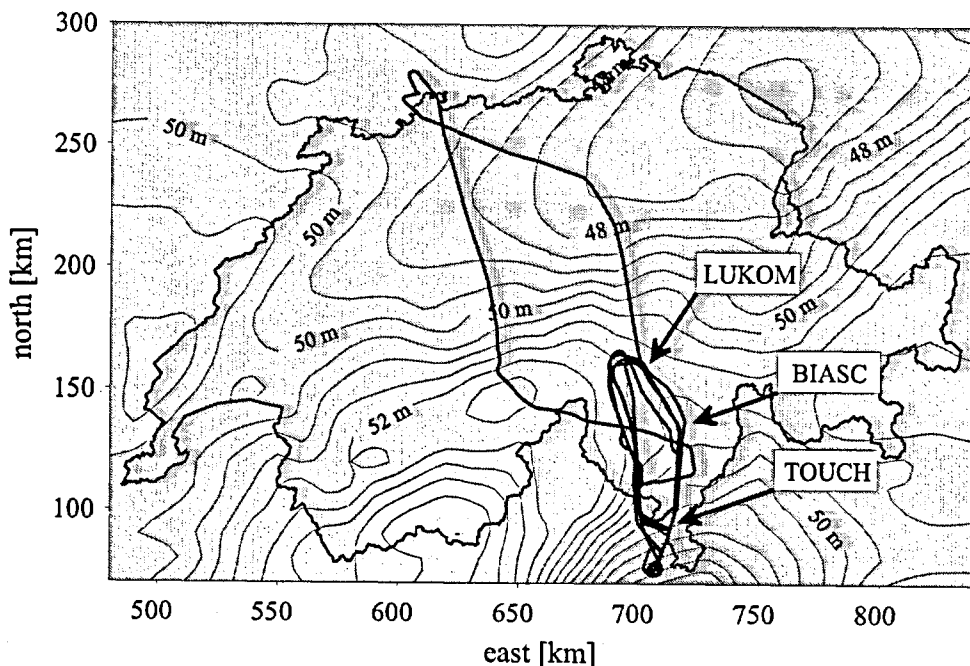


Figure 3.4.: Geoidal undulation in Switzerland referred to WGS84 with the flight track of the test flights overlaid.

### 3.3.5. Pseudo Range Corrections (PRC) Accuracy

The accuracy of the Pseudo Range Corrections (PRC) broadcasted by the ground station has a direct influence on the accuracy of the aircraft position when using the DGPS mode. The error of a faulty PRC would cause the same error in the 'corrected' pseudo ranges of the aircraft receiver and consequently a position shift.

Pseudo range corrections of the operational ground station ( $PRC_{op}$ ) were recorded by GDARS. The raw data and the algorithm used for determination of  $PRC_{op}$  are not available. The measurement system provides instead all raw data which allows to calculate the pseudo range corrections of the measurement system ( $PRC_{me}$ ) as a reference. The algorithm used for the determination of the PRC differs in both systems as it will be shown later.

The calculation of  $PRC_{me}$  is based on the equation for code measurements :

$$\begin{aligned}\rho^i(t_R) &= d_i + c \cdot cl_R - c \cdot cl^i + d(Ion)^i + d(Trp)^i + \delta^i \\ &= |\vec{x}^i(t_T) - \vec{x}_R(t_R)| + c \cdot cl_R - c \cdot cl^i + \\ &\quad d(Ion)^i + d(Trp)^i + \delta^i,\end{aligned}\tag{3.11}$$

where

$\rho^i$	= pseudo range of satellite $i$
$t_R$	= receiving time in GPS time
$t_T$	= transmitting time in GPS time
$c$	= speed of light in vacuum
$cl^i$	= clock bias of satellite $i$
$cl_R$	= clock bias of receiver $R$ on ground station
$d^i =  \vec{x}^i(t_T) - \vec{x}_R(t_R) $	= slant range between satellite $i$ and receiver
$\vec{x}^i(t_T)$	= coordinates of satellite $i$
$\vec{x}_R(t_R)$	= coordinates of receiver $R$ on ground station
$d(Trp)^i$	= path delay due troposphere of satellite $i$
$d(Ion)^i$	= path delay due ionosphere of satellite $i$
$\delta^i$	= other systematic errors and noise of satellite $i$ .

The position  $\vec{x}_R$  of the ground station is known (see chapter 2.4). The path delays caused by the ionosphere as well as the remaining systematic errors and noise  $\delta^i$  are disregarded in a first step. The tropospheric path delay is based on [Saastamoinen, 1973]. Consequently the pseudo range depends on the slant range only, the tropospheric path delay and the clock biases. The total amount of clock errors can be distributed uniformly to all pseudo ranges of one measurement epoch using its mean value  $\overline{cl}$  [RTCA, 1998]:



$$\overline{cl} = \frac{1}{N} \sum_{i=1}^N (cl_R - cl^i). \quad (3.12)$$

The pseudo range correction  $PRC_{me}^i$  of satellite  $i$  corresponds now to :

$$PRC_{me}^i = \rho^i - d^i - d(Trp)^i - c \cdot \overline{cl}. \quad (3.13)$$

Using of a mean clock bias  $\overline{cl}$  has the effect that the sum of all  $PRC_{me}^i$  of one measurement epoch is equal to zero:

$$\sum_{i=1}^N PRC_{me}^i = 0. \quad (3.14)$$

The sum of  $PRC_{op}^i$  is not equal to zero. This means, that the estimation of the clock biases on the operational system was done with another algorithm.

The differences  $\Delta^i$  between the pseudo range corrections of the operational and measurement system are of interest:

$$\Delta^i = PRC_{op}^i - PRC_{me}^i. \quad (3.15)$$

A mean difference  $\overline{\Delta^i}$

$$\overline{\Delta^i} = \frac{1}{N} \sum_{i=1}^N \Delta^i \quad (3.16)$$

is subtracted from every single difference  $\Delta^i$  during one measurement epoch to center the  $\Delta^i$  around zero. The corrected difference  $\Delta^{\prime i}$  is calculated as follows:

$$\Delta^{\prime i} = \Delta^i - \overline{\Delta^i}. \quad (3.17)$$

The sum of the  $\Delta^{\prime i}$  is equal to zero.

Such differences were calculated for a period of 28 days during 16 hours a day. This corresponds to an amount of  $1.37 \cdot 10^6$  values. Figure 3.5 shows the distribution of the  $\Delta^{\prime i}$ .

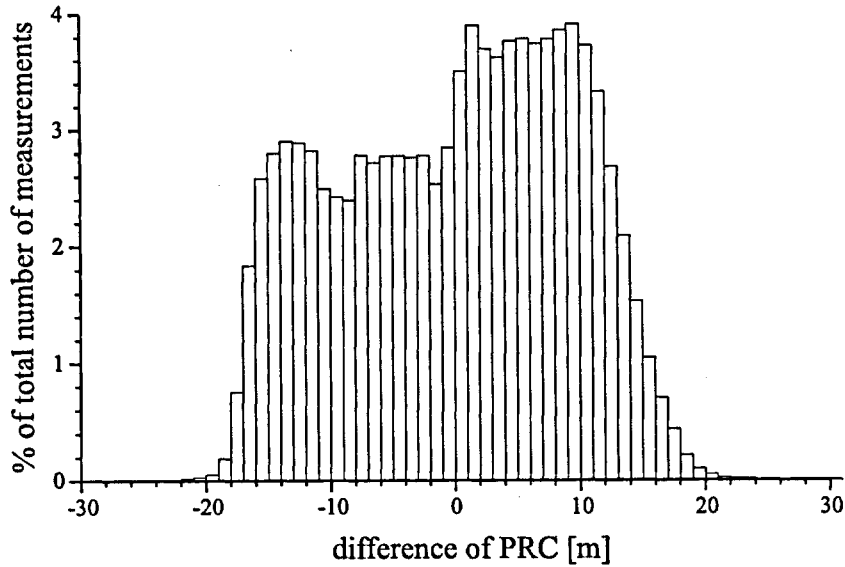


Figure 3.5.: Distribution of differences between the Pseudo Range Corrections of the operational and the measurement system of the ground station. It is noted, that the differences cover a range from  $-3375\text{ m}$  to  $1142\text{ m}$ , which leads to a large standard deviation.

The mean value of the  $\Delta^i$  is, as expected, nearly zero ( $6.6 \cdot 10^{-8}\text{ m}$ ) and the standard deviation  $63.4\text{ m}$ . The main part lie in the range of  $-25\text{ m}$  to  $25\text{ m}$ , where about  $0.2\%$  of the differences lie outside this range and can reach values of  $-3375\text{ m}$  and  $1142\text{ m}$ , respectively, which leads to the large standard deviation. The range of  $50\text{ m}$  for the main part of the differences is very large and may be caused by the use of:

- wrong coordinates of the ground station position
- different geoid models
- different tropospheric and ionospheric models.

The first two items were checked by using formula 3.6, where  $\vec{f}$  is constructed with the  $\Delta^i$  for each measurement epoch. A constant  $\vec{x}$  would be expected if wrong coordinates or different geoid models were used but this effect was not noted.

It is more probable that different atmospheric models were used. Figure 3.6 shows the differences  $\Delta^i$  depending on the satellite elevation. A systematic error is clearly visible, as the differences are negative for high elevations and become positive for small elevations.

The bandwidth of this differences does not correspond to the noise. The ionosphere depends, for example, also on the azimuth of the satellite, which is not differentiated in figure 3.6. For this reason the differences of pseudo range corrections of one satellite during one day are plotted in figure 3.7. The impact of other parameters

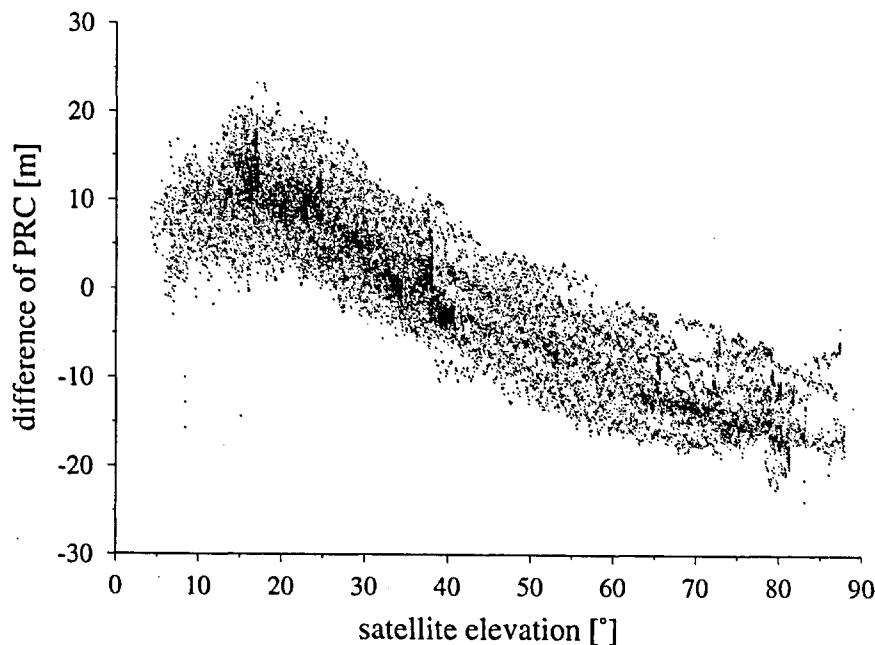


Figure 3.6.: Differences between the Pseudo Range Corrections of the operational and the measurement system depending on the satellite elevation during one day.

is visible, as the differences differ from five to ten meters depending on the ascent, respectively, descent and consequently from the azimuth of the satellite.

This comparison shows clearly, that the atmospheric corrections used have to be coordinated between reference stations and rover. [RTCA, 1996b] determines the models which have to be implemented in the navigation system. The tropospheric correction depends on the satellite elevation, the rover's altitude, day of the year (season) and the rover's absolute latitude. This algorithm is under review and may be revised further. The ionospheric correction uses a vertical path delay grid, which will be broadcasted. The rover is able to estimate an ionospheric correction depending on its position with the knowledge of the grid. This grid is essential as the ionosphere varies at different locations. The reference station did not use such data at the moment of the trials. It is possible, that ionospheric corrections transmitted in the broadcast message were used in the operational system, where the measurement system did not use a ionospheric model.

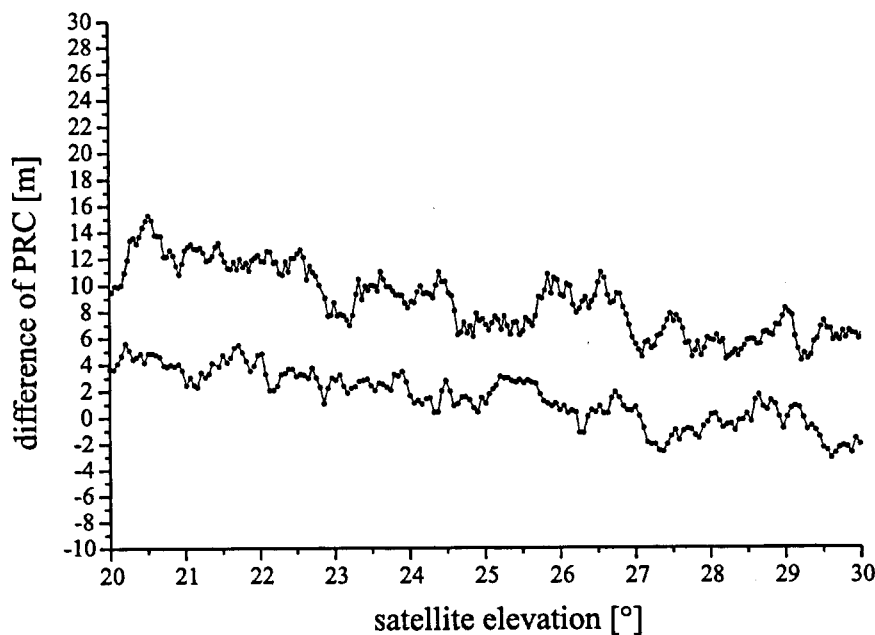


Figure 3.7.: Differences between the Pseudo Range Corrections of the operational and the measurement system depending on the satellite elevation for one satellite during one day.

3.3.6. Probability Distribution of TSE

The assumption of random and not coupled errors was made at the beginning of chapter 3.3.2. It should be expected, that the errors are normal distributed. Figure 3.8 shows the lateral *TSE* of the six<sup>th</sup> approach between BIASC and SHARK.

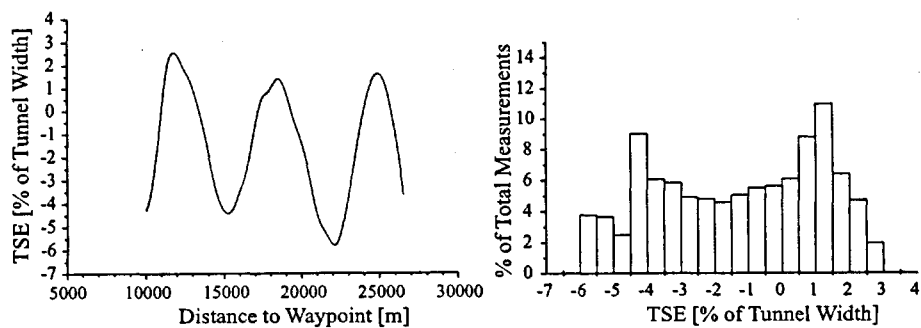


Figure 3.8.: TSE depending on distance to waypoint MOUNT (left) and the corresponding distribution (right) for the six<sup>th</sup> approach.

The distribution has a kurtosis of  $K = -1.38$  (fourth moment of the distribution), where

$$K = \left( \frac{1}{N} \sum_{j=1}^N \left[ \frac{x_j - \bar{x}}{\sigma} \right]^4 \right) - 3. \quad (3.18)$$

The term  $-3$  makes the value zero for a Gaussian distribution [Press *et al.*, 1990]. The kurtosis is a non-dimensional value, describing the peakedness or flatness relative to a normal distribution. A negative value describes a distribution like camel humps.

A random error would mean, that the aircraft would jump from one position to the other. In reality the errors depend on the precedent errors and would change continuously. A function

$$E = f(t) \quad \text{or} \quad E = f(d), \quad (3.19)$$

where

- $E$  = error (e.g.  $TSE$ )
- $t$  = time
- $d$  = distance from or to a waypoint

describing the error can help to gather a better insight into the expected distribution. The function  $f(t)$  will be used for further investigations, but also  $f(d)$  would lead to the same result. The inverse function of (3.19) is:

$$t = f^{-1}(E). \quad (3.20)$$

The error distribution  $v(E)$  of (3.20) can now be calculated as follow:

$$v(E) = \frac{d}{dE} f^{-1}(E) \quad (3.21)$$

The accumulated probability of all possible errors has to be equal to 1. The function  $v(E)$  has consequently to be normalized by dividing it through

$$A_v = \int_{E_{min}}^{E_{max}} v(E) dE. \quad (3.22)$$

The normalized error distribution  $v_n(E)$  is:

$$v_n(E) = \frac{v(E)}{A_v}. \quad (3.23)$$

Following two examples illustrate error distributions, which could be expected for the *TSE*.

### Example 1

A sine curve with constant frequency and amplitude is chosen to describe an aircraft oscillating around the desired course without gathering a better accuracy:

$$E = f(t) = A \cdot \sin(\omega t + \varphi), \quad (3.24)$$

where

- $\omega$  = frequency
- $A$  = amplitude
- $\varphi$  = phase-shift.

Equation (3.24) in (3.20) to (3.23) gives:

$$v_n(E) = \frac{1}{\pi \sqrt{A^2 - E^2}} \quad (3.25)$$

for the range of  $[-A, A]$ .

This distribution does not depend on the frequency  $\omega$  and the phase-shift  $\varphi$  for intervals  $[0 \dots 2N\pi]$  with  $N$  as an integer. Figure 3.9 shows on the left side the modeled cross-track and on the right side the cross-track error distribution.

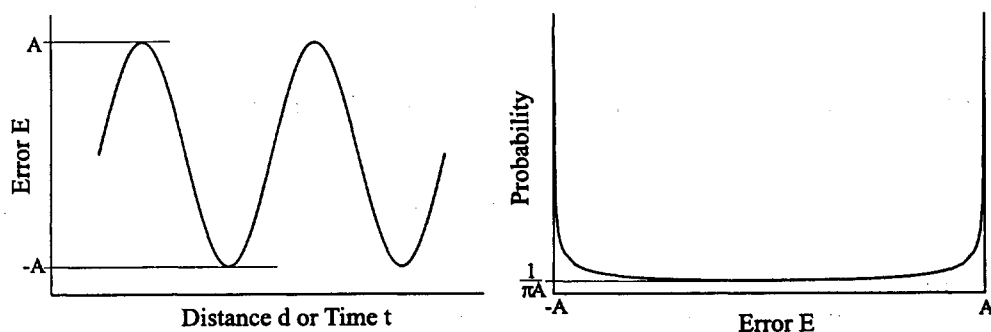


Figure 3.9.: Sine curve describing a modeled error depending on time or distance (left) and corresponding error distribution (right).

Following error probabilities can be derived:

$$\begin{aligned} v_n(-A) &= \infty \\ v_n(0) &= \frac{1}{\pi A} \\ v_n(A) &= \infty. \end{aligned}$$

The expectation value  $E^*$  of  $E$  is

$$E^*(E) = \int_{-A}^A E v_n(E) dE = \int_{-A}^A \frac{E}{\pi \sqrt{A^2 - E^2}} dE = \frac{1}{\pi} \left[ -\sqrt{A^2 - E^2} \right]_{-A}^A = 0 \quad (3.26)$$

and the variance  $D^*$  of  $E$  is

$$\begin{aligned} D^*(E) &= \int_{-A}^A (E - E^*(E))^2 v_n(E) dE = \int_{-A}^A \frac{E^2}{\pi \sqrt{A^2 - E^2}} dE \\ &= \frac{1}{\pi} \left[ -\frac{E}{2} \sqrt{A^2 - E^2} + \frac{A^2}{2} \arcsin \left( \frac{E}{A} \right) \right]_{-A}^A = \frac{A^2}{2}. \end{aligned} \quad (3.27)$$

The standard deviation is defined as

$$\sigma = \sqrt{D^*}. \quad (3.28)$$

Equation (3.27) in (3.28) gives a standard deviation of

$$\sigma = \frac{A}{\sqrt{2}} \quad (3.29)$$

for the function given in (3.24).

The amount of time  $T_\sigma$ , in which the error  $E$  is smaller than  $\sigma$  can be calculated as follow:

$$T_\sigma = \frac{1}{\pi} \int_{-\frac{A}{\sqrt{2}}}^{\frac{A}{\sqrt{2}}} \frac{1}{\sqrt{A^2 - E^2}} dE = \frac{1}{\pi} \left[ \arcsin \frac{E}{A} \right]_{-\frac{A}{\sqrt{2}}}^{\frac{A}{\sqrt{2}}} = 0.5, \quad (3.30)$$

which means, that during 50% of time the aircraft would be expected to be within a range of  $\pm \frac{A}{\sqrt{2}}$ .

The following equation

$$\int_{-b}^b v_n(E) dE = T_P, \quad (3.31)$$

where

$b$  = searched containment boundary

$T_P$  = total time, in which  $E < b$ ,

can be solved for  $b$ . This boundary  $b$  is with equation (3.19) in (3.31)

$$b = A \cdot \sin\left(\frac{T_P \pi}{2}\right). \quad (3.32)$$

Table 3.3 lists the  $T_P$  and the corresponding boundary  $b$  depending on  $\sigma$  and  $A$ .

$T_P$	$b(\sigma)$	$b(A)$
50.0%	$1.000 \cdot \sigma$	$0.707 \cdot A$
68.3%	$1.242 \cdot \sigma$	$0.879 \cdot A$
95.0%	$1.410 \cdot \sigma$	$0.997 \cdot A$
100.0%	$1.414 \cdot \sigma$	$1.000 \cdot A$

Table 3.3.: Comparison between the confidence intervals of a normal distribution and a distribution based on a sine curve.

The  $\sigma$  in a normal distribution corresponds to a containment of 68.3% of the random values, where  $2 \cdot \sigma$  corresponds to 95.5% and  $3 \cdot \sigma$  to 99.7%. The  $2 \cdot \sigma$  in the sine distribution of this example contains already all values  $E$ . Therefore statements on the confidence interval have to be done carefully, when errors of this kind are present.

### Example 2

An increasing accuracy during an approach is normally expected. The amplitude  $A$  is assumed to decrease with increasing time  $t$ . Such a behaviour can be described by a damped oscillation:

$$E = f(t) = A \cdot e^{-\delta t} \cdot \sin(\omega t + \varphi), \quad (3.33)$$



where

$\delta$  = decay of amplitude  $A$ .

It should be shown, that it is not possible to find the inverse function of (3.33) in a closed form. Consequently it will be shown, how the distribution of this function is characterized. Figure 3.10 shows on the left side the track modeled and on the right side the track error  $E$  distribution for given initial values  $A, \delta, \omega$  and  $\varphi$ , which leads the system to a damped oscillation.

The distribution contains some peaks, which are analogous to the ones on the border of the distribution of the sine curve. These peaks are caused, when the first derivative of  $f(t)$  is equal zero. These local maximums converge to  $E = 0$  when  $t$  increases to infinity, due to

$$\lim_{t \rightarrow \infty} A = 0. \quad (3.34)$$

The characteristics of the distribution depends on the selected initial values and can differ from the example shown in figure 3.10, especially when the system does not oscillate.

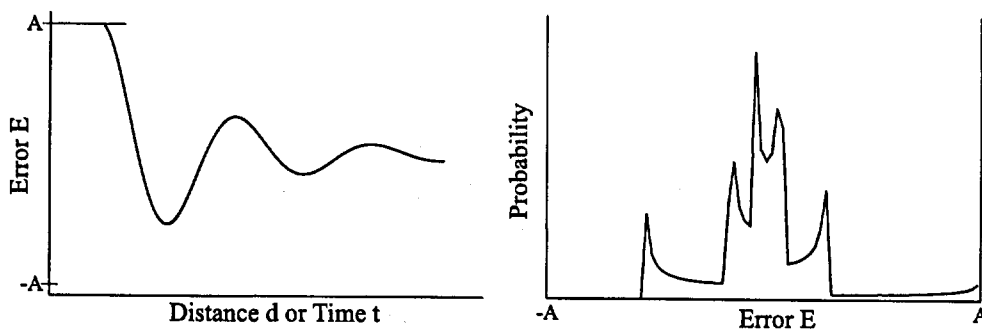


Figure 3.10.: Damped oscillation describing a modeled error depending on time or distance (left) and corresponding error distribution (right).

These two examples show, that assumptions on the error distributions have to be done carefully.

### 3.3.7. Control System and Approach Accuracy

The control system of an aircraft, respectively the pilot, has an influence on the accuracy of the aircraft, which oscillates around the desired course. The algorithms used in the control systems are not known and might be very complex to discuss at this point. A simplified control system based on [Brockhaus, 1994] will be derived for further investigations and shows its possible impact on the accuracy.

Following forces are assumed to be active:

$$F_1 = -c \cdot E, \quad (3.35)$$

where

$F_1$  = 'restoring force'  
 $c$  = linear factor quantifying  $F_1$  depending on  $E$ .

This is the main force to reduce the cross-track error  $E$ . This force increases linearly with  $E$ , but could also be chosen as a constant or other function depending on  $E$ .

A force  $F_2$  is used to reduce the amplitude of an oscillating cross-track error  $E$ :

$$F_2 = -b \cdot \frac{dE}{dt}, \quad (3.36)$$

where

$F_2$  = 'friction force'  
 $b$  = linear factor quantifying  $F_2$  depending from the cross-track velocity of the aircraft.

A force  $F_3$  describing the aircraft inertia is defined as following:

$$F_3 = m \cdot \frac{d^2E}{dt^2}, \quad (3.37)$$

where

$F_3$  = aircrafts inertia  
 $m$  = mass.

A perturbation force  $F_0$ , which disturbs the control, is defined:

$$F_0 = A_P \cdot \sin(\omega t), \quad (3.38)$$

where

- $F_0$  = describes a perturbation with a sine function (e.g. SA)
- $A_P$  = amplitude of perturbation
- $\omega$  = frequency of perturbation.

$F_0$  can, for example, describe the SA. A sine function is chosen in this case for reasons of simplification. A sum of sine curves would comply better with SA. Furthermore it is assumed that  $F_0$  affects the control system directly.

These forces are linked together as follow:

$$\begin{aligned} F_3 + F_2 + F_1 &= F_0 \\ m \cdot \frac{d^2 E}{dt^2} - b \cdot \frac{dE}{dt} - c \cdot E &= A_P \cdot \sin(\omega t) \\ \frac{d^2 E}{dt^2} + 2\delta \cdot \frac{dE}{dt} + \omega_0^2 E &= K_P \cdot \sin(\omega t) \end{aligned} \quad (3.39)$$

with

$$\delta = \frac{b}{2m}, \quad \omega_0 = \sqrt{\frac{c}{m}}, \quad \text{and} \quad K_P = \frac{A_P}{m},$$

which corresponds to an inhomogeneous linear differential equation of second order with constant coefficients. This equation can be solved by finding a general solution  $f_0(t)$  and a particular solution  $f_p(t)$  and forming the sum of both solutions

$$f(t) = f_0(t) + f_p(t), \quad (3.40)$$

The general solution of the homogeneous differential equation has three cases:

$$\delta < \omega, \quad \delta = \omega, \quad \delta > \omega. \quad (3.41)$$

The first case corresponds to a damped oscillation, which will be further investigated. Its solution is

$$f_0(t) = C_0 \cdot e^{-\delta t} \cdot \sin(\omega_d t + \varphi_d) \quad (3.42)$$

with

$$\omega_d = \sqrt{\omega_0^2 - \delta^2}.$$

The parameters  $C_0$  and  $\varphi_d$  can be found by using initial values  $E(0)$  and  $\frac{dE(0)}{dt}$ .

The particular solution of the inhomogeneous differential equation is

$$f_P(t) = C_P \cdot \sin(\omega t - \varphi) \quad (3.43)$$

with

$$C_P = \frac{K_P}{\sqrt{(\omega_0^2 - \omega^2)^2 + 4\delta^2\omega^2}}$$

and

$$\begin{aligned} \varphi &= \arctan\left(\frac{2\delta\omega}{\omega_0^2 - \omega^2}\right) & \text{for } \omega < \omega_0 \\ \varphi &= \frac{\pi}{2} & \text{for } \omega = \omega_0 \\ \varphi &= \arctan\left(\frac{2\delta\omega}{\omega_0^2 - \omega^2}\right) + \frac{\pi}{2} & \text{for } \omega > \omega_0. \end{aligned}$$

Equation (3.42) and (3.43) in (3.40) gives

$$f(t) = C_0 \cdot e^{-\delta t} \cdot \sin(\omega_d t + \varphi_d) + C_P \cdot \sin(\omega t - \varphi) \quad (3.44)$$

which corresponds to two superposed sine curves. The first term in (3.44) disappears after a while, depending on the parameter  $\delta$ . After this level off, the system will continue to oscillate depending on the second term in equation (3.44).

A critical situation appears, when the control system enters in resonance with the perturbation force. The resonance frequency  $\omega_r$  can be calculated for the particular solution by finding the maximum value for  $C_P$ . The first derivative of  $C_P$  is zero for  $\omega_r$

$$\frac{dC_P(\omega_r)}{d\omega} = 0. \quad (3.45)$$

From this it follows

$$\omega_r = \sqrt{\omega_0^2 - 2\delta^2}. \quad (3.46)$$

The maximum cross-track error caused by the perturbation function to the control system can be found with equation (3.46) in (3.44):

$$C_{P_{max}} = \frac{K_P}{2\delta} \cdot \frac{1}{\sqrt{\omega_0^2 - \delta^2}}. \quad (3.47)$$

Figure 3.11 shows the progression of the amplitude  $C_P$  depending on the perturbation frequency  $\omega$ . The peak of  $C_P$  can be a multiple of the values in the neighborhood.

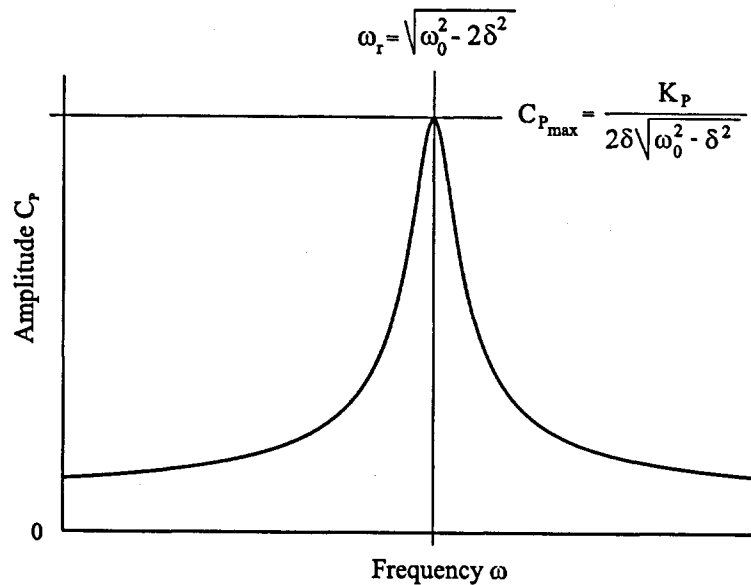


Figure 3.11.: Resonance of a simplified aircraft control system caused by a perturbation function with a sine form.

This simple example shows, that the *TSE* of an aircraft becomes critical, when the control system of an aircraft and the SA are in resonance. It is evident, that a large number of different and complex control systems are in use. Nevertheless it should be tested, if SA could affect a control system by the way of resonance or not.

### 3.4. Integrity

The system integrity refers to the ability of the system to provide timely warnings to the user when the system should not be used for navigation [RTCA, 1991].

An integrity warning flag was not recorded by the ADARS during the first two test flights due to technical problems. Therefore it is not possible to make any statements about the system integrity used.

Safeguards are also carried out by the GPS service supplier. Nevertheless it cannot be excluded, that degraded signals are transmitted unintentionally or intentionally. Further degraded signals (e.g. multipath) can only be detected at the aircraft itself. Two distinct methods of assuring GPS integrity have evolved as the civil use of GPS has progressed. One is the GPS Integrity Channel (GIC), which uses a ground monitoring station network to estimate the GPS integrity and disseminates the GPS state via data links. Another method is the Receiver Autonomous Integrity Monitoring (RAIM). An enhanced RAIM algorithm is developed and discussed in chapter 6.

### 3.5. Availability and Continuity

Availability is defined as the ability of the total system to perform its function at the initiation of the intended operation [Lössner *et al.*, 1996]. This means, that the aircraft has to track the minimum required number of satellites at the beginning of the approach at the waypoint LUKOM. These are four satellites for a position estimation or more for the use of integrity monitoring algorithms. Further the integrity of the tracked signals have to be warranted at this point.

Continuity is defined as the ability of the total system to perform its function without interruption during the intended operation [Lössner *et al.*, 1996]. This means, that the availability requirements (minimum number of tracked satellites and integrity) can be transferred to the entire approach, from the waypoint LUKOM to the waypoint TOUCH.

As the system integrity flag is not recorded, it is also not possible to make any statements about the availability and continuity. Nevertheless investigations on availability and continuity are done in chapter 4.

### 3.6. Findings

The accuracy of the Pseudo Range Corrections (PRC), the GPS position of the aircraft operational system and the approach flights are analysed in this chapter.

The PRC of the operational and the measurement system shows very large differences, most of them lying in the range of  $\pm 20$  m. A systematic error, depending on the satellite elevation, is revealed. It is assumed, that these errors are caused by the use of different atmospheric models for path delay reduction. This does not create problems, when ground reference and airborne equipment uses both the same atmospheric reduction models. These models would have to be prescribed for all receivers to avoid an accuracy degradation.

The accuracy of the aircraft position (Navigation System Error, NSE) is estimated for the stand-alone and differential GPS (DGPS) mode separately by comparing

the positions of the operational system with the GPS carrier phase positions of the measurement system. The mean cross-track and along-track position differences are in the range of 0.5 to 1.5 *m*. The  $1\sigma$ -value is for the stand-alone mode in the range of 23 *m* and in the DGPS about 13 *m*. The mean vertical position difference is nearly 48 *m* in the stand-alone mode. It can be shown, that this difference corresponds to the geoidal undulation. It is assumed, that the operational system corrects its altitude with a geoidal undulation, where the measurement system does not make this corrections. Similar to the atmospheric models, the geoid model has to be prescribed for all receivers to avoid accuracy degradation. This degradation is eliminated when operating in the DGPS mode. Nevertheless, the mean vertical difference is still more than 6 *m*.

The investigations on the Total System Error (TSE) of the approaches have to be restricted to the lateral fraction and on straight approach legs only due to the problems with the vertical guidance and the CDI. Reasonable investigations are possible on three, respectively four, approaches. This small number of approaches does not allow to make any statistical significant statement on the system accuracy. Nevertheless it gives an idea on the accuracy performance of the navigation system. The examined approaches are divided into a GPS stand-alone and a DGPS part. The mean Total System Error (TSE) in the stand-alone mode is -0.67% and the  $1\sigma$ -value 6.22% of the tunnel width. The corresponding values for the DGPS mode are -4.16% and 4.46%, respectively. These values shows the accuracy potential of satellite based navigation systems.

Investigations on the TSE probability distributions show, that these errors are not normal distributed. Attention has to be given, when statistics is carried out on such data.

Finally, the influence of the Selective Availability (SA) on the aircraft control system and consequently the accuracy is analysed. For this purpose a simple control system algorithm and modeled SA is chosen. It is seen, that control systems can enter in resonance with the SA causing an accuracy degradation.

Technical problems did not allow to record the system integrity flag, so that statements on integrity, availability and continuity are not possible. These parameters are nevertheless treated theoretically in the following chapters.

## 4. Satellite Visibility and Geometry

### 4.1. Introduction

Four tracked GPS satellites with a good constellation geometry are at least required to calculate a three-dimensional position (three for each geometrical dimension and one for the unknown clock error). This constellation allows to navigate with GPS. Each additional tracked satellite over-determines the equation system for position calculation, which results in a better solution. RAIM algorithms use at least five tracked satellites for an error detection. At minimum six tracked satellites are required for the isolation and exclusion of an erroneous satellite without losing the RAIM capacity. More tracked satellites could be needed depending on the required accuracy. The number of available satellites in the DGPS mode depends on the intersection of the tracked satellites of the rover and the reference station.

The following terms used in this chapter are defined as following:

'tracked satellite' : a satellite, whose signal is properly tracked by a receiver

'visible satellite' : a satellite, whose line of sight to a receiver antenna is not obstructed

The number of visible satellites and the Dilution Of Precision (DOP) resulting from the satellite constellation are conditional for the availability and continuity of the navigation system. Therefore the different influences on the satellite visibility have to be investigated.

The number of tracked satellites depends mainly on:

1. satellite constellation
2. aircraft altitude
3. the selected cut off angle
4. terrain obstructions
5. aircraft attitude
6. aircraft body shielding



7. interference
8. multipath effects
9. receiver performance
10. antenna characteristic

The first six parameters depend directly from the 'line of sight' between receiver antenna and satellite. These influences can be predicted and used for satellite visibility simulations. The last four parameters are difficult to predict and depend strongly on receiver and antenna performance. These problems will be discussed at the end of this chapter as well as in chapter 5.

Simulations can be conducted to study the influence of the first six parameters mentioned above. Comparison of the simulations with real flights gives an idea of the quality of the models used and may indicate additional problems related to satellite tracking.

Availability and continuity of satellite visibility can be studied with theoretical approaches, simulations and collected data of real flights. Investigations of this kind were conducted by Eurocontrol Experimental Centre (EEC) in collaboration with the Civil Aviation Authority of United Kingdom (UK CAA) and Defence Research Agency (DRA) [EEC, 1994a, EEC, 1994b]. One of the main scopes was to determine the limits of coverage of geostationary and GPS satellite signals. Simulations were compared with real data from flight trials including approaches and landings. The simulations did not include terrain, aircraft attitude and aircraft body shielding. Analysis of the trials showed among other things, that aircraft attitude, aircraft tail, fin and fuselage significantly affected the signal received. Terrain had an impact on the satellite signal during approaches and landings in mountainous area.

## 4.2. Influences on Satellite Visibility and Geometry

### 4.2.1. Theoretical Satellite Visibility

The positions of satellites are first calculated in a geocentric Cartesian coordinate system for a given time, based either on broadcast ephemeris or on precise-ephemeris downloaded via the internet (e.g. <ftp://cddis.gsfc.nasa.gov>, <ftp://igs.ifag.de>, <ftp://igs.ensg.ign.fr>). In a second step a transformation of the satellite position into a topocentric system (azimuth, elevation and distance) is performed with the knowledge of the receiver's position.

First we will consider the ideal case: no obstructions as well as no restrictions from antenna characteristics. In this case even satellites with negative elevation are in view from an aircraft flying at an altitude  $h_A$  (figure 4.1). The minimal elevation angle assuming a spherical earth is:

$$\delta_H = -\arccos\left(\frac{R_E}{R_E + h_A}\right), \quad (4.1)$$

where

$R_E$  = earth radius = 6379 km.

E.g. an aircraft flying at an altitude of 10'000m would be able to 'see' a satellite within an elevation of  $-3.2^\circ$  according to equation (4.1). This effect will be taken into account for simulations.

Tropospheric refraction bends the signal path slightly towards the earth (figure 4.1). An approximation can be calculated with a constant curvature of the signal in the troposphere [Chaperon, 1988]. The angle between the tangent to the earth and the tangent to the line of sight to the satellite at the entrance in to the atmosphere is approximately:

$$\delta_R = 2 \cdot \delta_S + \delta_A, \quad (4.2)$$

where

$\delta_R$  = total refraction angle  
 $\delta_S$  = half refraction angle of inbound signal  
 $\delta_A$  = half refraction angle of outbound signal.

The relation  $\delta_S \geq \delta_A$  is always valid. The term  $\delta_S$  can be calculated with the triangle  $\triangle(C_E, C_R, T)$ , where each side length is known (figure 4.1):

$$\delta_S = \frac{1}{2} \arcsin\left(\frac{(R_E + h_T)^2 - R_R^2 - (R_R - R_E)^2}{2R_R(R_R - R_E)}\right), \quad (4.3)$$

where

$R_R$  = radius of curvature of refracted signal path in troposphere  
 $h_T$  = maximum altitude of troposphere ( $\approx 15'000m$ )  
 $C_E$  = earth centre  
 $E_R$  = centre of the circle of the refracted signal path  
 $T$  = beginning of inbound signal refraction.

The refraction radius  $R_R$  can be written as

$$R_R = \frac{R_E}{\kappa}, \quad (4.4)$$

where

$\kappa$  = refraction coefficient.

$\delta_S$  is  $0.26^\circ$  with  $\kappa = 0.13$  in equation (4.3).  $\delta_R$  would be at maximum  $3 \cdot \delta_S \leq 0.78^\circ$  due to equation (4.2) with  $\delta_S \geq \delta_A$ , which is small and will not be taken into consideration for simulations. Therefore, in an idealized case, satellites can be seen beyond the horizon at a minimal elevation of  $-\delta_H - \delta_R \sim -4^\circ$ .

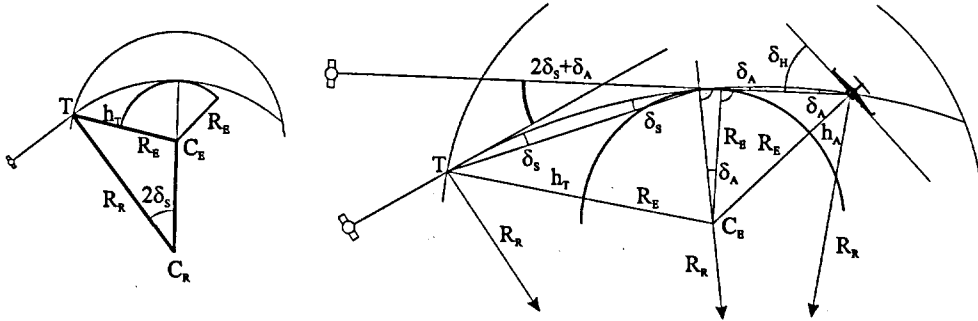


Figure 4.1.: Visible satellites with negative elevation are possible due to the geometry of aircraft, satellite and earth. The signal refraction in the troposphere augments this effect, but it can be neglected for altitudes as used in civil aviation.

Figure 4.2 shows the result of a simulation for the Lugano North Approach for August, 23<sup>th</sup> 1996. The number of theoretically visible satellites was calculated for about every 200 m along the approach path and every 5 minutes during 24 hours. These values are used as reference for further investigations. During this day six approaches were flown from the north to Lugano-Agno airport.

The simulation comprises 99128 calculations of satellite positions and their resulting visibility. During this time seven to twelve satellites are visible. Figure 4.3 shows the distribution of visible satellites for the simulation. The y-axis indicates the amount of time in percent of day depending on the number of visible satellites (x-axis).

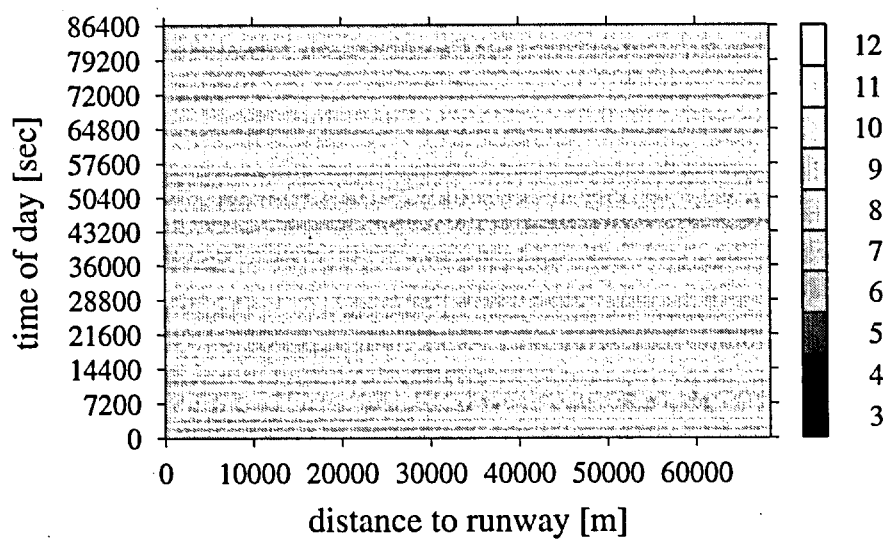


Figure 4.2.: Results of a simulation for the Lugano North Approach showing the number of theoretically visible satellites on-board the aircraft when no obstructions are taken into account. The x-axis indicates the distance to runway in meters, where the y-axis represents the time in seconds of day. The colours correspond to the amount of visible satellites. It can be seen, that at least seven satellites are always visible in this case.

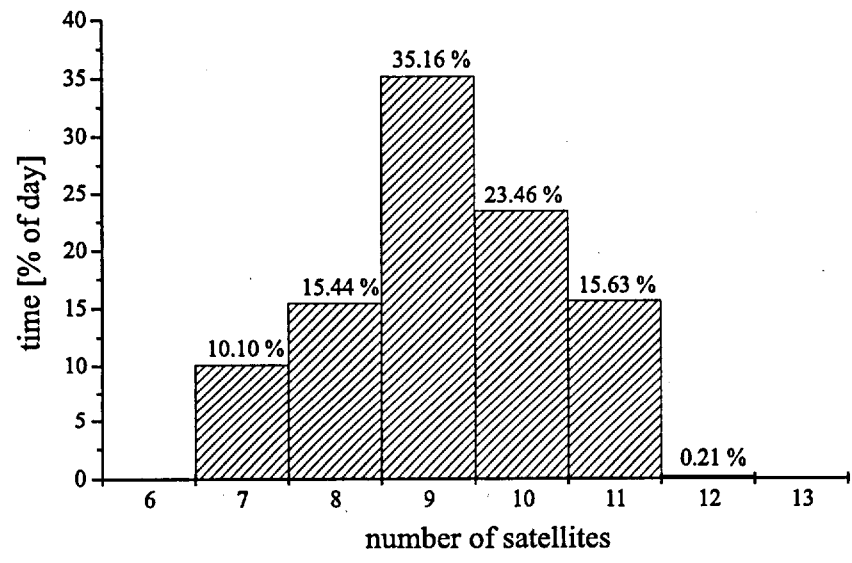


Figure 4.3.: Distribution of number of visible satellites on-board the aircraft of the simulation shown in figure 4.2.

### 4.2.2. Cut-Off Angle

Cut off angles are used in connection with GPS in order to eliminate measurements of satellites tracked at low elevation. The signal of such satellites travel a longer path in the atmosphere than signals from satellites with higher elevation. Consequently the path delay, which is mainly produced by the troposphere and ionosphere, increases with lower satellite elevation. The introduction of a cut off angle is a simple way to reduce these effects. Negative effect in using a cut off angle is the loss of satellites and in consequence a reduced satellite constellation quality. Investigations have to be done on the selection of the size of cut off angle.

The main part of the tropospheric path delay can be eliminated with tropospheric measurement techniques, tropospheric models, or differential GPS. Several techniques for the measurement of the wet path delay like radiometers [Bürki *et al.*, 1992] or solar spectrography [Sierk *et al.*, 1997] have been developed. However they are not suitable for operational use in aviation at the moment. Tropospheric induced path delay models are sometimes used in receivers and eliminate a part of the error. DGPS eliminates most parts of this error, depending on the distance and difference of the altitude between reference station and rover.

The impact of the troposphere on the position accuracy will be studied depending on the satellite constellation and the antenna position for the area of the Lugano North Approach. A simplified standard atmosphere model is used for this purpose. [CCIR, 1986] gives the dependence of the refractive index of the atmosphere at radio frequencies as a function of height:

$$n(h) = 1 + 315 \cdot 10^{-6} \cdot e^{-0.136h}, \quad (4.5)$$

where

$n$  = refractive index  
 $h$  = height in kilometers.

The zenith path delay (path delay for a signal coming from the zenith) is:

$$\Delta_t^z = \int_{h_u}^{h_t} (n(h) - 1) dh, \quad (4.6)$$

where

$\Delta_t^z$  = zenith path delay  
 $h_u$  = actual height of receiver antenna  
 $h_t$  = maximum height of troposphere.

Equation (4.5) in (4.6) gives:

$$\Delta_t^z = \int_{h_u}^{h_t} (315 \cdot 10^{-6} \cdot e^{-0.136h}) dh = -2.32 \cdot 10^{-3} \cdot [e^{-0.136h}]_{h_u}^{h_t}. \quad (4.7)$$

The path delay for inclined paths at an elevation  $\varphi$  can be calculated by multiplying a 'mapping function' with the zenith path delay [Höflinger, 1993]:

$$\Delta_t = \frac{\sqrt{R_E^2 \cdot \cos^2\left(\frac{\pi}{2} - \varphi\right) + 2R_E h_t + h_t^2} - R_E \cdot \cos\left(\frac{\pi}{2} - \varphi\right)}{h_t} \cdot \Delta_t^z, \quad (4.8)$$

where

$\Delta_t$  = path delay for a given satellite elevation  
 $\varphi$  = satellite elevation.

This mapping function takes the earth curvature into consideration, which is needed for small  $\varphi$ . More accurate mapping function are given by e.g. [Herring, 1992, Niell, 1996]

The impact of the path delay on the horizontal and vertical position accuracy is of interest and can be calculated with equation (3.6). The  $i^{th}$  element of the vector  $\vec{f}$  corresponds to the path delay  $\Delta_t$  of the  $i^{th}$  satellite.

Figure 4.4 bottom shows the horizontal (grey line) and vertical (black line) position shift caused by the troposphere in a GPS stand alone mode. The vertical error is usually larger than the horizontal error. This error characteristic is caused by the satellite constellation and the larger path delays for lower satellites. It is also visible that the vertical error is always positive which is due to the time variable in the measurement equation. The horizontal error is also constantly positive as it is a square sum of the east-west and north-south component of the position shift.

Figure 4.4 top shows the GDOP and the number of visible satellites. A correlation of larger GDOP with fewer satellites and vice versa can be observed. There is also a correlation between GDOP and position shift. A better GDOP leads to a larger position shift, which normally would not be expected. This is due to better satellite constellation when low elevation satellites are taken into account, but much worse range error due to the troposphere. The GDOP and all other DOP's do not contain systematic errors like path delays. Consequently a better DOP does not always mean a better position accuracy.

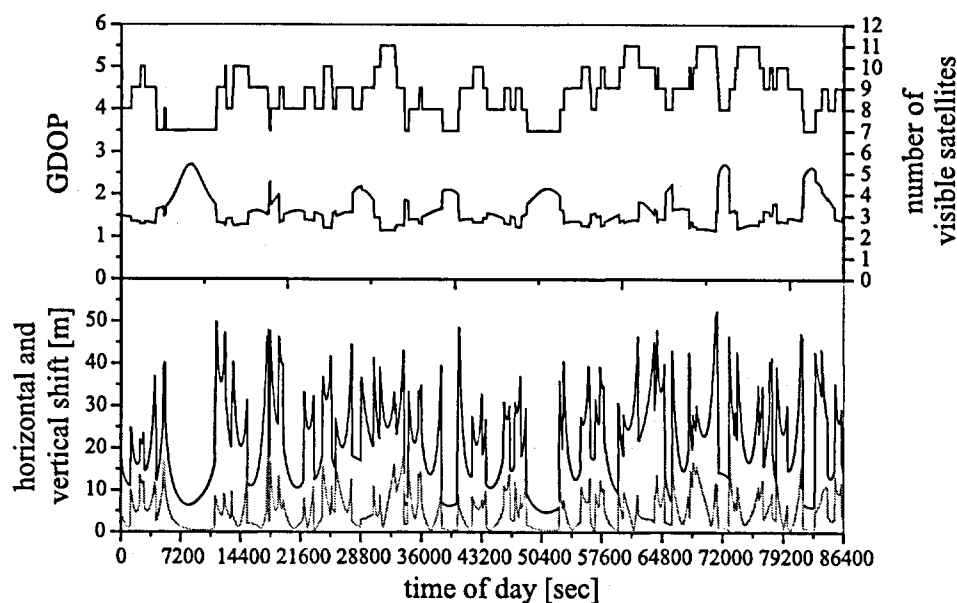


Figure 4.4.: The number of visible satellites and the GDOP depending on the time of day are shown on top of this figure. The bottom of the figure shows the horizontal (grey line) and vertical (black line) position shift caused by the tropospheric path delay.

The use of a cut off angle reduces the position shift, but at the expense of satellite visibility and reduced constellation quality. Figure 4.5 bottom shows the mean tropospheric induced horizontal and vertical shift and its standard deviation (grey area) during one day depending on the cut off angle. Figure 4.5 top shows the mean GDOP and its minimum and maximum values (grey area) as well as the minimally available number of satellites. A cut off angle of  $12.5^\circ$  leads to a minimal availability of 4 satellites. Cut off angles of  $10^\circ$  or smaller are recommended, pointing out, that neither terrain nor aircraft attitude are taken into consideration in this diagram. On the other hand the mean vertical shift is  $7.3\text{ m}$  at a cut off angle of  $10^\circ$ .

All calculations were done for a sea level situation, which is the worst case for the stand alone GPS mode in a standard atmospheric model. The tropospheric path delay decreases with augmenting altitude and vanishes at the troposphere maximal altitude, in this case set to  $15000\text{ m}$ .

The DGPS mode eliminates the major part of tropospheric path delay, if rover and reference receiver are close enough together. The error increases with larger altitude differences but remains small for horizontal displacement between the rover and the reference station. Maximal position shift is reached for a rover position at the troposphere maximum altitude and a reference station at sea level. This position shift is comparable with the shift at sea level for a GPS stand alone mode.

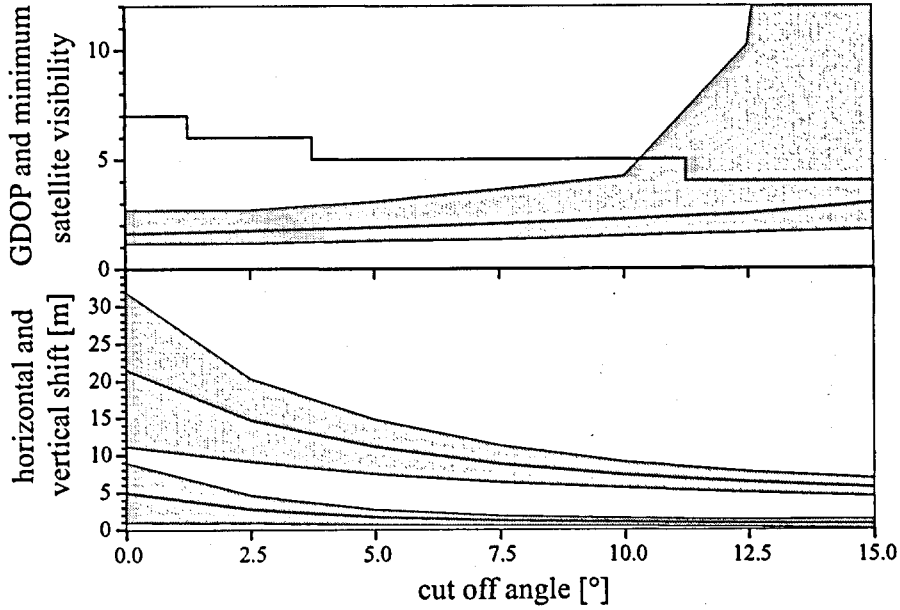


Figure 4.5.: The grey area on top of this figure represents the minimum and maximum GDOP depending on the cut off angle. The line included in this area is the mean GDOP. The stepped line represents the minimum number of visible satellites. The grey areas on the bottom shows the minimum and maximum horizontal (lower area) and vertical (upper area) position shift. The line included in the area represents the mean position shift.

The selection of the cut off angle has to be a trade off on position shift and GDOP. Square sum of these two values gives an estimate for the cut off angle:

$$TO(co) = \sqrt{GDOP^2(co) + \overline{d_h}^2(co) + \overline{d_v}^2(co)}, \quad (4.9)$$

where

$co$	= cut off angle
$TO$	= trade off value
$\overline{GDOP}(co)$	= mean GDOP depending on cut off angle
$\overline{d_h}(co)$	= mean horizontal position shift depending on cut off angle
$\overline{d_v}(co)$	= mean vertical position shift depending on cut off angle.

The minimum  $TO$ -value is decisive for the selection of the cut off angle. Common GPS receivers use tropospheric models which eliminates about  $\frac{2}{3}$  of the tropospheric path delay in the stand alone mode. Figure 4.6 shows the  $TO$ -value for uncorrected



(grey line) and corrected (black line) measurements. The minimum  $TO$ -value lies beyond  $15^\circ$  for uncorrected and in the range of  $7.5^\circ$  to  $10^\circ$  for corrected measurements. As expected, the needed cut off angle decreases by correcting the measurements. It follows, that better models requires smaller cut off angles. Figure 4.5 shows further, that only five satellites are visible with a cut off angle of  $7.5^\circ$  to  $10^\circ$ . A cut off angle of  $2.5^\circ$  would be more appropriated when taking the minimum number of visible satellites into account. As mentioned above, the major part of the tropospheric path delay can be eliminated by using the DGPS mode. Smaller cut off angles can be selected in this case.

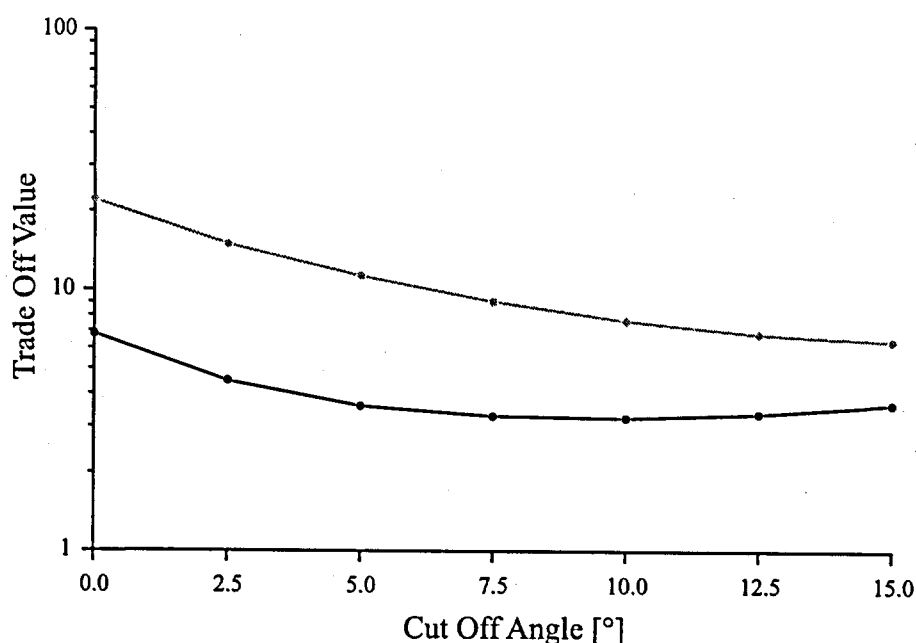


Figure 4.6.: The trade off value is shown for measurements with uncorrected (grey line) and corrected (black line) tropospheric path delay. The minimum  $TO$ -value lies beyond  $15^\circ$  for uncorrected and in the range of  $7.5^\circ$  to  $10^\circ$  for corrected measurements.

It is noted that the tropospheric model used in these investigations is standardized with a constant refractive index for a defined altitude. Reality is more complicated as the atmosphere changes with the meteorological situation. Therefore the results shown above give just an order of magnitude of the tropospheric effect on the GPS position solution. Further investigations on the influence of the troposphere to GPS-based precision approaches are given in [Blomenhofer and Hein, 1995].

The error characteristics caused by the ionosphere has some similarities to the errors caused by the troposphere and will therefore be treated only briefly. The ionosphere can be considered as a dielectric medium which causes a path delay to the code pseudo range measurements. This error increases with lower satellite elevation. Additionally it depends also on daytime, season, position of the sun relative to

satellite and the solar activity. The ionosphere is at an altitude of 50 *km* to 250 *km* so that the path delay changes only slightly at altitudes used for civil aviation. The consequence is, that the ionospheric path delay can be eliminated in the DGPS mode, even when the altitude difference between rover and reference station is large.

The calculations for the troposphere can mainly be used. The vector  $\vec{f}$  in equation 3.1 has to be constructed with the ionospheric path delays. Such values can mostly be estimated with models given in e.g. [Wells *et al.*, 1986, Höflinger *et al.*, 1992]. The resulting position shifts are normally slightly larger than those caused by troposphere refraction. Top of figure 4.5 remains the same, as it depends only on the geometrical constellation of the satellites.

### 4.2.3. Terrain

Satellite coverage studies were mainly conducted with the assumption of an unobstructed view of the sky (e.g. [Green *et al.*, 1989]). Analysis on PDOP for a GPS receiver in an idealized valley were done by [Duerr, 1992]. He shows that PDOP varies significantly with time of day and latitude. Best results were obtained for latitudes between 30° and 60°. The airport of Lugano-Agno is at a latitude of 46°. Nevertheless the PDOP may vary significantly during a day. Loss of satellite signals during approaches and landings in mountainous area due to terrain masking were also reported by [EEC, 1994a].

Problems in Lugano-Agno arise during the final part of the approach. The mountains around the waypoint SHARK reach 12° of elevation (figure 4.7 top) and on waypoint TOUCH up to 18° (figure 4.7 bottom).

The use of a Digital Terrain Model (DTM) allows to calculate the impact of the terrain onto satellite visibility. A DTM with a grid resolution of 25 *m* is available for Switzerland and was generated at the Swiss Federal Office of Topography (L+T)[L+T, 1993]. Wood or buildings are not taken into account. The grid nodes and heights are given in the Swiss Coordinate System. Heights of points, which are not located at grid nodes have to be interpolated. A bilinear interpolation is used for this purpose (figure 4.8) :

$$h_P = \frac{y_P - y_1}{y_3 - y_1} \cdot (H_2 - H_1) + H_1 \quad (4.10)$$

with

$$H_1 = h_1 + \frac{x_P - x_1}{x_2 - x_1} \cdot (h_2 - h_1) \text{ and } H_2 = h_3 + \frac{x_P - x_3}{x_4 - x_3} \cdot (h_4 - h_3),$$

where

- $h_P$  = unknown height of point  $P$
- $x_P, y_P$  = x-y coordinates of point  $P$
- $x_i, y_i, h_i$  = known coordinates of points  $P_i (i = 1 \dots 4)$  around point  $P$ .

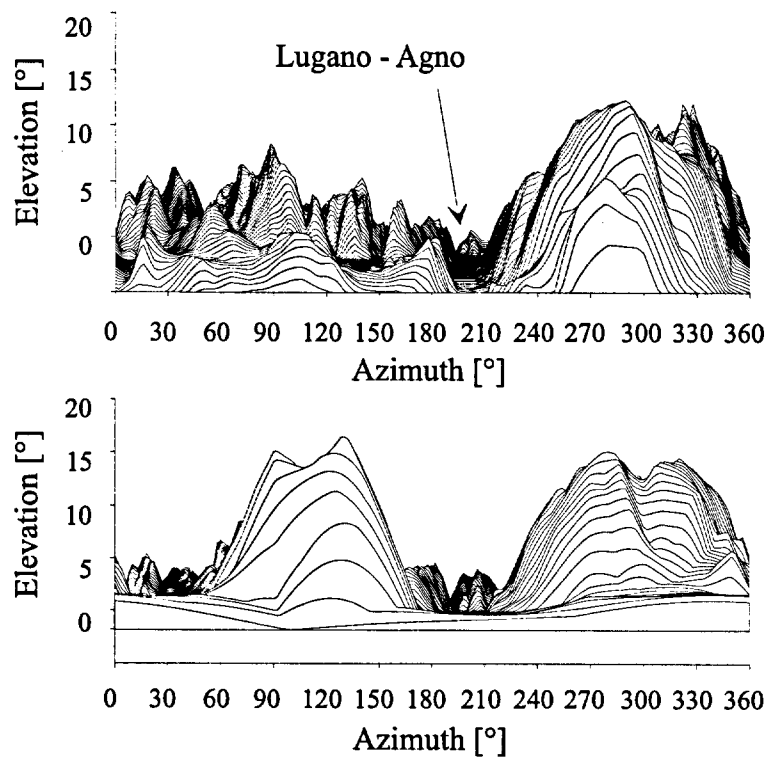


Figure 4.7.: The terrain surrounding the waypoints SHARK (top) and TOUCH (bottom) are shown in an azimuth-elevation diagram. These terrain views are extracted from a Digital Terrain Model (DTM).

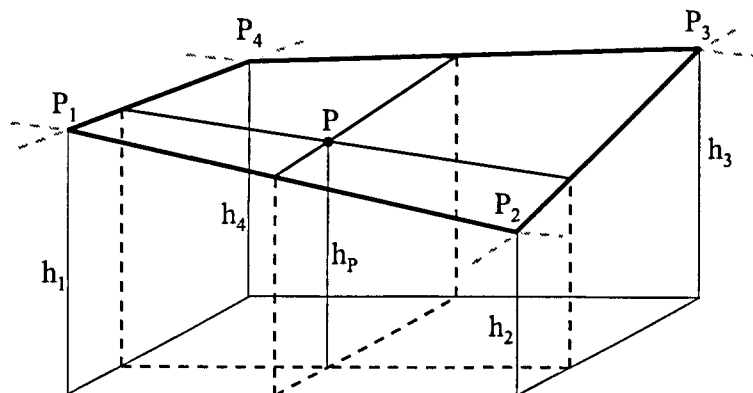


Figure 4.8.: Heights of points ( $P$ ), which are not located at grid nodes ( $P_1 \dots P_4$ ) have to be interpolated. A bilinear interpolation is used for this purpose.

Due to the amount of data of such a DTM an approach to keep reading of data and calculation time low is to filter the DTM to a lower resolution (e.g. 100 m or 250 m) and then to operate with the bilinear interpolation (4.10) to find the needed altitude. The altitude accuracy decreases by using such filters. Figure 4.9 shows the accuracy of the interpolation for three locations with a typical topography for Switzerland (Alps, Jura, and Midland). A DTM of  $6 \times 6$  km with 25 m grid resolution is filtered to 50, 75, 100, 125, 150, 200, and 250 m grid resolution. The interpolation is then applied to the points, where the altitude is known in the original grid. The difference between interpolated and original altitude corresponds to the error caused by the filter at this point. The standard deviation (1 sigma) is calculated for every filtered grid and plotted in figure 4.9. The error seems to increase linearly with the grid resolution. All three correlation coefficients are greater than 0.99. It is also clearly visible, that the error increases, where topography becomes more rugged. This is mainly the effect of 'cutting' mountain peaks and 'filling' valleys when interpolation is used.

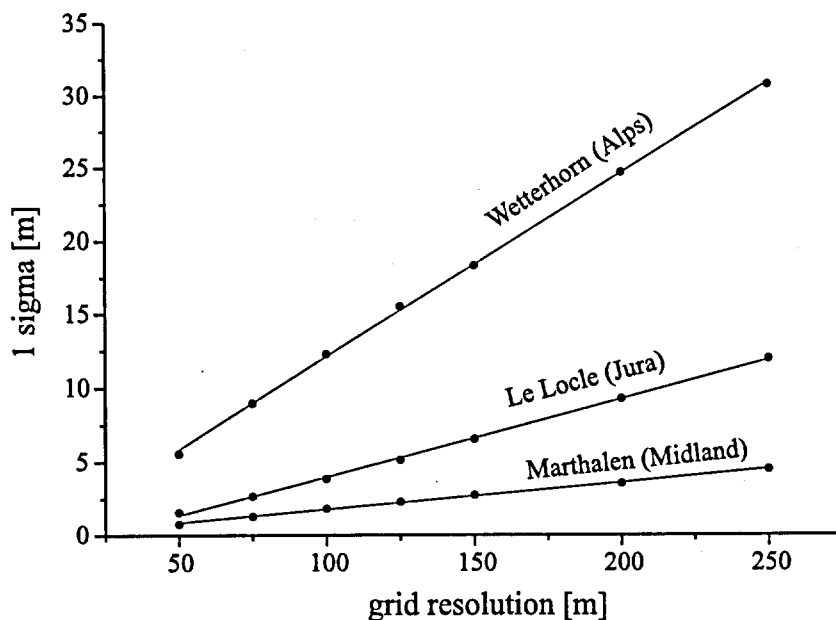


Figure 4.9.: The accuracy of the bilinear interpolation is ascertained by comparing interpolated altitudes of a filtered DTM with the altitudes in the original, non-filtered DTM. It is seen, that the accuracy decreases with reduced DTM resolution and in more rugged terrain.

Furthermore the earth curvature has to be taken into consideration. An approximation uses the assumption that the earth is a sphere:

$$E = \frac{R}{\cos \gamma} - R \approx \frac{R}{1 - \frac{\gamma^2}{2}} - R \approx \frac{\gamma^2 R}{2} = \frac{d_0^2}{2R} \quad (4.11)$$

with

$$\begin{aligned} \cos \gamma &= 1 - \frac{\gamma^2}{2!} \left( + \frac{\gamma^4}{4!} - \dots \right) \text{ for the first approximation,} \\ \frac{1}{1-x} &= 1 + x \left( +x^2 + x^3 + \dots \right) \text{ for the second approximation,} \\ \gamma &= \frac{d_0}{R}, \end{aligned}$$

where

- $E$  = height difference between planar and spherical view
- $R$  = 6379km = earth radius (earth assumed to be a sphere)
- $\gamma$  = earth central angle
- $d_0$  = distance formed by  $\gamma$  projected to earth surface on height 0.

A terrain horizon has to be calculated for every investigated point to get the effect of the terrain on satellite visibility. The grid resolution and the radius of the area, which is taken into account for the calculations have to be selected in a way to keep calculation time reasonable and to allow sufficiently accurate results. The radius will subsequently be set to 50 km and the grid resolution to 100 m.

Simulation are done for the entire Lugano North Approach. The amount of lost visible satellites due to terrain masking is shown in figure 4.10 in percent of time of one day.

Figure 4.11 shows the amount of visible satellites during on day on the whole approach. It is seen, that less than six satellites are visible during a short period. RAIM would not be available during this time. The terrain affects the satellite visibility only during the last part of the approach when the aircraft is flying at low altitude.

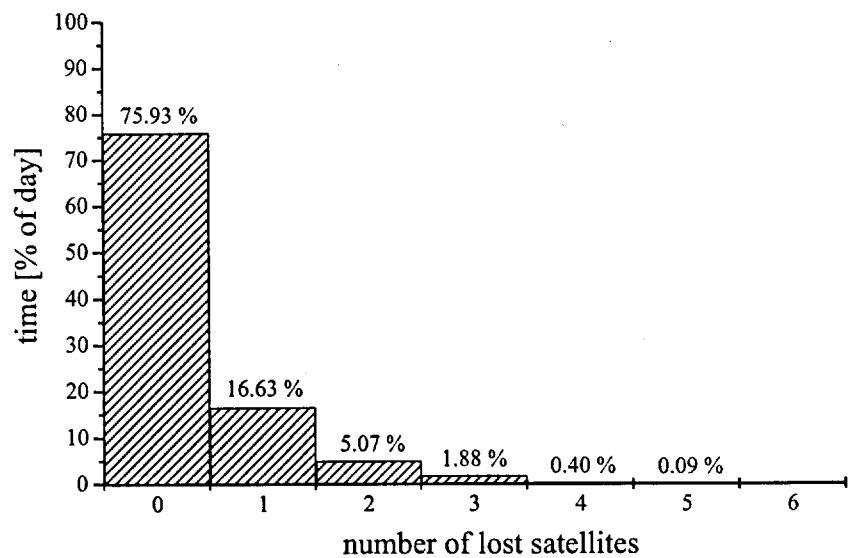


Figure 4.10.: Distribution of lost satellites due to terrain masking resulting from simulations during an entire day on the whole North Approach.

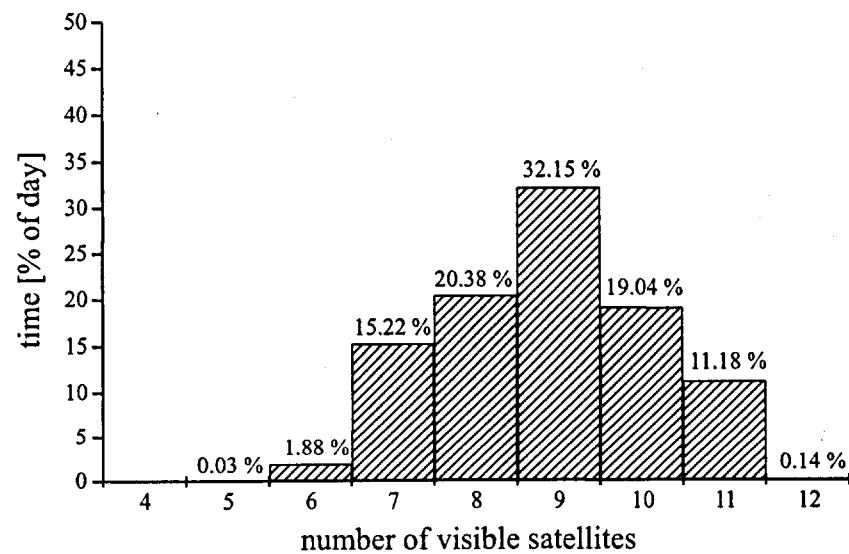


Figure 4.11.: Distribution of total number of visible satellites from simulations during an entire day on the whole North Approach when taking terrain masking into consideration.

#### 4.2.4. Aircraft Attitude

The attitude of the aircraft has an impact on satellite visibility, especially when flying curves or steep approaches or departures. In these cases the satellites can be masked by the antenna horizon. This effect can be estimated by transforming the satellite positions from the topocentric system to the fixed aircraft system. This can be done with the knowledge of roll, pitch and yaw angles. The yaw angle will further be set equal to the heading. The rotation matrices for each axis of the aircraft are:

$$\mathbf{R}_{\Phi} = \begin{pmatrix} 1 & 0 & 0 \\ 0 & \cos \Phi & \sin \Phi \\ 0 & -\sin \Phi & \cos \Phi \end{pmatrix}, \quad (4.12)$$

$$\mathbf{R}_{\Theta} = \begin{pmatrix} \cos \Theta & 0 & -\sin \Theta \\ 0 & 1 & 0 \\ \sin \Theta & 0 & \cos \Theta \end{pmatrix},$$

$$\mathbf{R}_{\Psi} = \begin{pmatrix} \cos \Psi & \sin \Psi & 0 \\ -\sin \Psi & \cos \Psi & 0 \\ 0 & 0 & 1 \end{pmatrix},$$

where

- $\Phi$  = roll angle
- $\Theta$  = pitch angle
- $\Psi$  = yaw angle  $\approx$  heading.

The transformation matrix from the topocentric system to the fixed aircraft system is:

$$\mathbf{R}_{TA} = \mathbf{R}_{\Phi} \cdot \mathbf{R}_{\Theta} \cdot \mathbf{R}_{\Psi} \quad (4.13)$$

The unit vector  $\vec{e}_T$  in the topocentric system, which points from the antenna to the satellite can now be transformed to the unit vector  $\vec{e}_A$  in the aircraft system:

$$\vec{e}_A = \mathbf{R}_{TA} \cdot \vec{e}_T \quad (4.14)$$

Azimuth and elevation of the satellite in the fixed aircraft system can be calculated with  $\vec{e}_A$ . The inverse transformation from the fixed aircraft to the topocentric system is:

$$\mathbf{R}_{AT} = \mathbf{R}_{TA}^T \quad (4.15)$$

due to the orthogonality of  $\mathbf{R}_{TA}$ .

Simulations are done to estimate the influence of the attitude of the aircraft on satellite visibility during the North Approach. The two track angles at BIASC and SHARK are replaced by curves with a constant radius of 5000 m. Curved flight in this case lasts during about 6% of the approach distance. The roll angle is set to 20° during curved flight and to 0° on straight legs. The pitch angle corresponds to the glide slope angle, and the yaw angle is set equal to the heading of the aircraft. The loss of satellites due to the attitude is shown in figure 4.12 in percent of one day. Loss of five satellites is possible. This result seems extreme but it has to be pointed out, that sometimes eleven to twelve satellites are visible. So it is important to check also the minimal number of visible satellites (figure 4.13). There are a short period, where only five satellites are in the field of view. RAIM would not be available during this time.

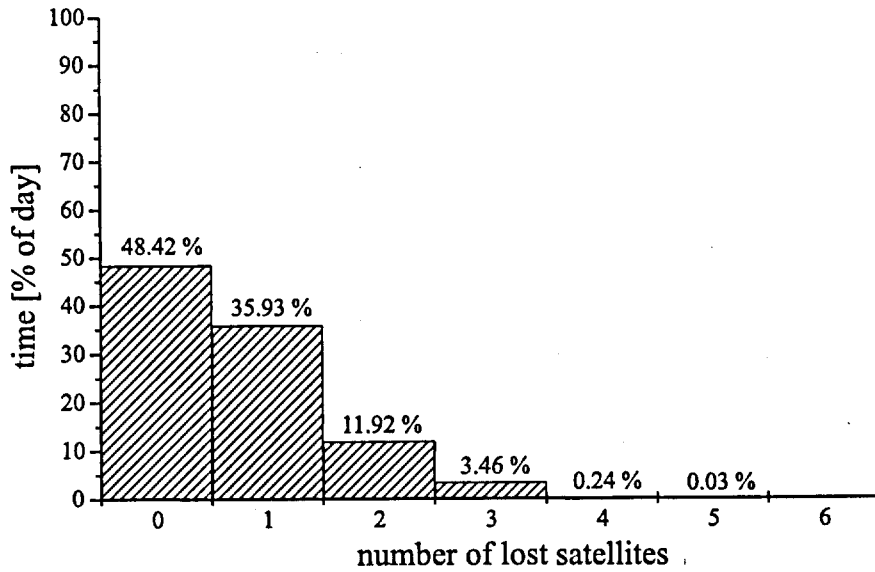


Figure 4.12.: Distribution of lost satellites due to aircraft attitude resulting from simulations during an entire day on the whole North Approach.

A more general simulation can be done by fixing the position of the aircraft and rotating its heading from 0° to 360° with different angles  $\zeta$ , where  $\zeta$  is defined as the angle between the zenith direction of the topocentric system and the zenith direction of the fixed aircraft system. The angle  $\zeta$  can be calculated with the rotation matrices:

$$\vec{z}_A = \mathbf{R}_\Phi \cdot \mathbf{R}_\Theta \cdot \vec{z}_T \quad (4.16)$$

where

$\vec{z}_T = [0, 0, 1]^T$  = zenith vector in the topocentric system

$\vec{z}_A$  = zenith vector in the fixed aircraft system.



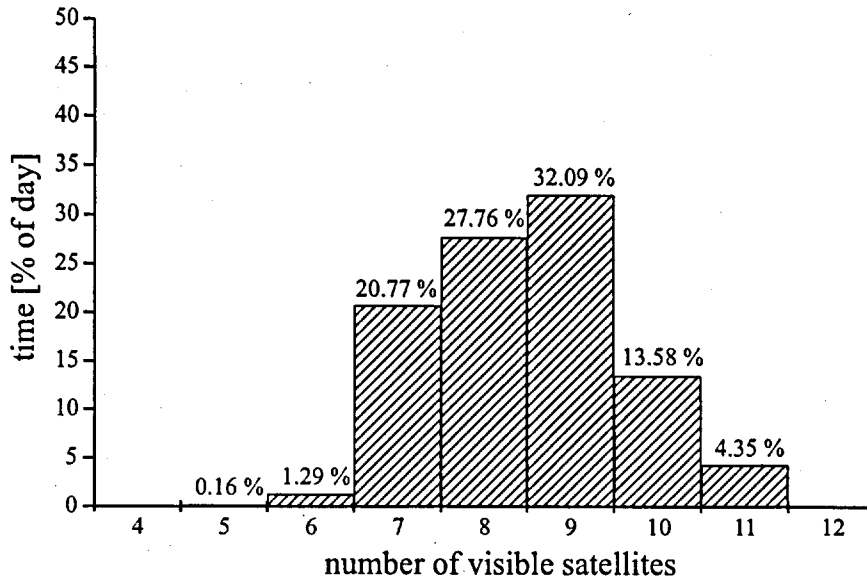


Figure 4.13.: Distribution of total number of visible satellites from simulations during an entire day on the whole North Approach when taking the aircraft dynamic into consideration.

The angle  $\zeta$  is independent of the yaw angle, so that the rotation matrix  $\mathbf{R}_\Theta$  is not taken into consideration in equation (4.16).  $\zeta$  depends only on  $\vec{z}_A$  and can be calculated as following:

$$\zeta = \arctan \left( \frac{\sqrt{(\sin \Theta)^2 + (\sin \Phi \cdot \cos \Theta)^2}}{\cos \Phi \cdot \cos \Theta} \right). \quad (4.17)$$

The amount of lost satellite visibility during one day depending on the angle  $\zeta$  is shown in figure 4.14. The angle of  $0^\circ$  is not represented, as there are no outages. Roll angles usually do not exceed  $20^\circ$  during a normal flight. Nevertheless an angle of  $30^\circ$  is represented, as such high roll angles were reached for short times during the test flights. Loss of five satellites is possible for  $\zeta$  equal  $30^\circ$ , which is not visible in the diagram. It can be seen, that the attitude has a strong influence on satellite visibility. An angle of only  $10^\circ$  leads to loss of at least one satellite during more than 50% of time.

There is also a correlation between loss of satellites and the zenith direction of the aircraft system in the topocentric system. It can be expected that more satellites are lost if the direction points to the north than to the south due to constellation.

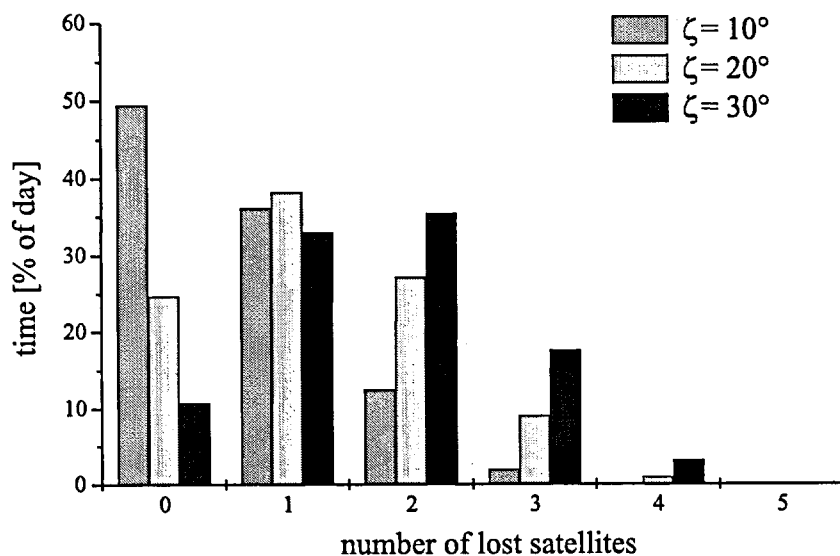


Figure 4.14.: Number of lost satellites depending on the angle  $\zeta$ .

#### 4.2.5. Aircraft Body Mask

Aircraft body masking means that parts of the aircraft may shadow satellites. Figure 4.15 shows the aircraft horizon as seen from the GPS antenna. The centre of the polar plot corresponds to the antenna position in the highlighted aircraft drawing. As the antenna is mounted on top of the fuselage, only the horizontal and vertical stabilizer define the aircraft horizon at an azimuth around  $180^\circ$ . The elevation of the horizontal stabilizer is very small. The vertical stabilizer reaches  $12^\circ$ , but it is very thin in its horizontal extension. Such masking areas can be neglected compared to terrain or attitude masking.

The propeller areas at the azimuths of  $120^\circ$  and  $240^\circ$  would allow the signal to pass through, but some disturbances have to be expected.

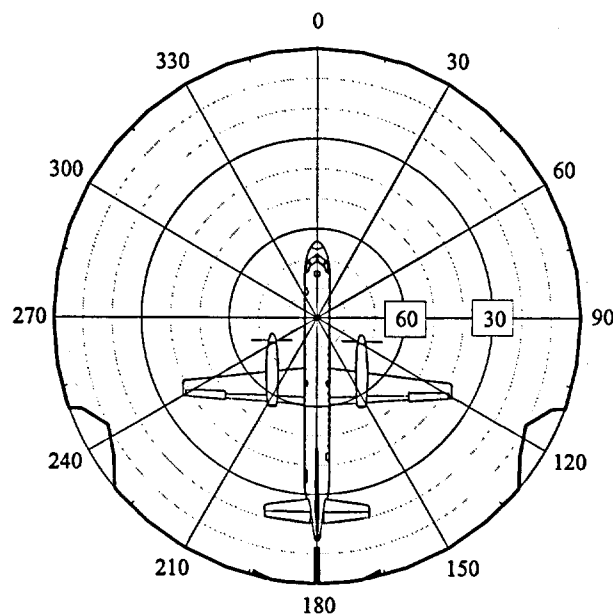


Figure 4.15.: Polar plot of the aircraft body horizon as seen from the GPS antenna.

#### 4.2.6. Combination of Influences on Satellite Visibility and Geometry

The total amount of lost satellites visibility is not the sum of lost satellites by single causes (e.g. terrain, attitude). A single satellite may for example be shadowed by the terrain and the aircraft attitude. For this reason each single satellite has to be treated separately for each influence. A simulation is done for the North Approach, where the terrain, the attitude, and the cut off angle is taken into account. The cut off angle is set in this case to  $0^\circ$  and has only a minimal impact.

The results are shown in figure 4.16, represented in the same way as in figure 4.2. Top of figure 4.16 represents the stand-alone GPS mode, where it is noticeable, that the terrain affects only the last part of the approach, beginning at 20000 *m* in front of runway. The impact of the roll angle is also clearly visible at both curves at 40000 *m* and 2000 *m*. The pitch angle has only a small influence, but its changes can be detected at about 43000 *m* and 14000 *m*. Three satellites only are available during 10 seconds a day at 40000 *m* and 2000 *m* on x-axis and 14500 seconds at y-axis. The flight through these areas would last about 15 seconds each. A minimum of four satellites are available during 2 minutes and 10 seconds a day and a flight through this time window lasts about 15 to 20 seconds.

The bottom of figure 4.16 represents the differential GPS mode beginning at waypoint SODES, about 43000*m* in front of the runway. The sudden loss of satellite

visibility at this point is due to the intersection of satellite visibility of the ground station and aircraft required for differential GPS. Loss of satellite visibility due to terrain is of minor importance, because the ground station is already masked by terrain and decisive for the number of visible satellites. The roll angle effects are still visible. Three satellites only are available during 35 seconds a day at 40000 *m* and 2000 *m* on x-axis and 14500 seconds at y-axis. The flight through these areas would last about 15 seconds each. A minimum of four satellites are available during 7 minutes a day, and a flight through this time window lasts about 15 to 20 seconds.

Figure 4.17 on top shows the distribution of the available satellites during the approach including the DGPS mode. The corresponding available GDOP is shown on the bottom of this figure, where it is seen, that larger DOP's are possible.

Solutions have to be found to avoid or bridge such critical time gaps. One possibility is to omit approaches during periods of problematic satellite constellations. The constellation repeats daily with a time shift of 4 minutes per day. This time drift would interfere with the stringent traffic flow needed nowadays. Another solution can be achieved by combining the GPS with Inertial Navigation Systems (INS). The INS should then be able to navigate alone during a short period with the needed accuracy and integrity. Investigations and development of such systems are in progress (e.g. [Vallot *et al.*, 1991, Vieweg *et al.*, 1995]).

Furthermore five or six satellites are needed for common RAIM algorithms. This condition may create additional critical constellations. The use of additional instruments to support integrity monitoring (Aircraft Autonomous Integrity Monitoring, AAIM) can help to solve the problem created by the number of satellites (see chapter 6 and e.g. [Butzmühlen, 1996]).

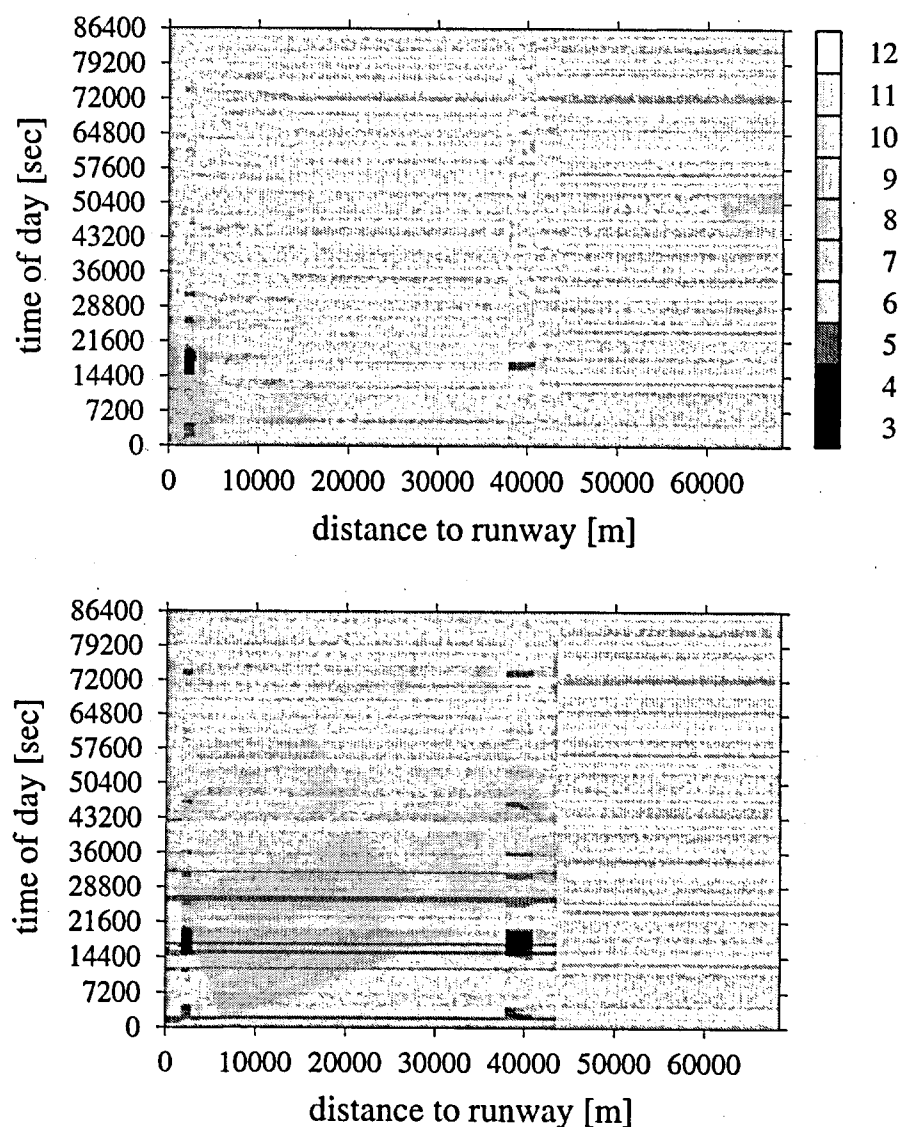


Figure 4.16.: Results of a simulation for the Lugano North Approach showing the number of theoretically visible satellites when obstructions are taken into account. The figure on top represents the GPS stand-alone mode where the figure on bottom includes the differential GPS mode from SODES onwards. The representation is the same as in figure 4.2.

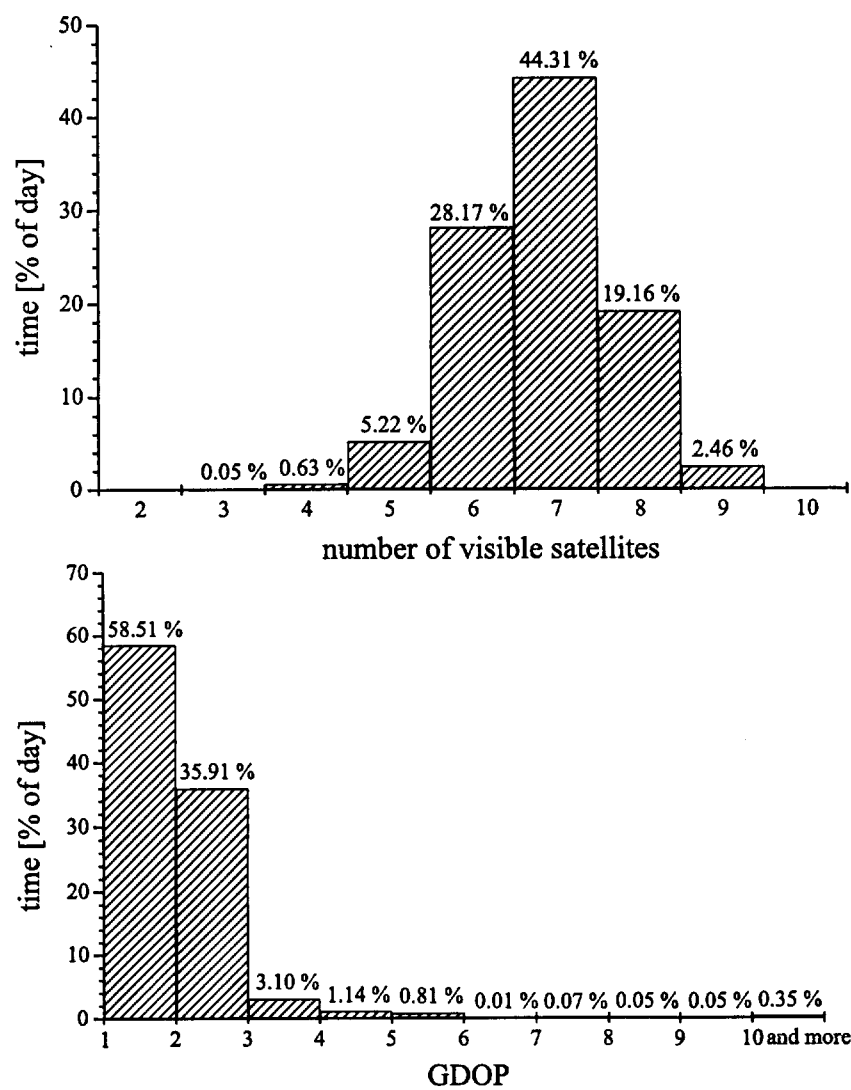


Figure 4.17.: Distribution of number of visible satellites (top) respectively the GDOP (bottom) during an entire day on the whole North Approach.

### 4.3. Supplemental Satellite Systems and Pseudolites

The use of supplemental satellite systems, respectively pseudolites, would help to minimize availability and continuity gaps as mentioned in the previous chapter. Following hybrid systems will be compared with the GPS alone mode:

- GPS and the Russian GLObal Navigation Satellite System (GLONASS)
- GPS and three geostationary satellites (INMARSAT)
- GPS and the proposed European Navigation Satellite System (ENSS)
- GPS and Pseudolites

The first three combinations were repeatedly proposed as contribution to the Global Navigation Satellite System of the first and second generation (GNSS-I and GNSS-II).

#### 4.3.1. GPS and GLONASS

The augmentation of GPS with GLONASS could be used to meet the needed GNSS-I, respectively EGNOS performance (e.g. [Flament and Pieplu, 1997]), and flight trials with combined GPS/GLONASS receivers were already performed (e.g. [Vieweg and Lechner, 1994, Lowe *et al.*, 1997]). It is assumed, that the full GLONASS constellation with 24 operational satellites is available, which is rather an optimistic scenario [Marchal and Carle, 1997]. This situation is chosen, as the employment of GLONASS for aviation duty would require the full operability of this system.

The NORAD two line orbit elements are used to determine the GLONASS satellite positions. These elements are based on the SGP4 and SDP4 orbit models [Hoots and Roehrich, 1980]. Computer program units of [Kelso, 1992a, Kelso, 1992b] are implemented in the program for satellite position estimation.

Further the observation matrix  $A$  has to be modified due to the non-synchronized clocks of GPS and GLONASS. This modification is needed for the correct determination of the DOP's. The design matrix  $A$  has the following form:

$$A = \begin{bmatrix} e_{1_1} & e_{2_1} & e_{3_1} & -1 & 0 \\ \vdots & \vdots & \vdots & \vdots & \vdots \\ e_{1_m} & e_{2_m} & e_{3_m} & -1 & 0 \\ e_{1_{m+1}} & e_{2_{m+1}} & e_{3_{m+1}} & 0 & -1 \\ \vdots & \vdots & \vdots & \vdots & \vdots \\ e_{1_n} & e_{2_n} & e_{3_n} & 0 & -1 \end{bmatrix}, \quad (4.18)$$

where the indices  $1 \dots m$  represents the GPS satellites and  $m+1 \dots n$  represents the GLONASS satellites.

The DOP's can then be calculated with equation (3.10), where the weight matrix  $P$  has to be modified, if needed, depending on the range accuracy of the different systems. The following investigations are simplified by setting  $P$  equal to the unit matrix.

#### 4.3.2. GPS and INMARSAT

Geostationary satellites can contribute to GNSS-I with integrity channels and range signals [Bellen and Naerlich, 1997, Peckham, 1997]. Three INMARSAT-2 satellites with locations at longitudes of  $54.5^\circ\text{W}$ ,  $15.5^\circ\text{W}$  and  $64^\circ\text{E}$  are selected for the simulations. The NORAD orbit elements are used for the satellite position estimations, which shows a small motion with a period of 24 hours.

The design matrix  $A$  has to be modified analogous to equation (4.18), assuming that the clocks of the three INMARSAT are synchronized with each other.

#### 4.3.3. GPS and ENSS

The European Navigation Satellite System (ENSS) is proposed as an European contribution to GNSS-II [Lautenbach, 1997]. A definitive constellation does not yet exist, but proposals use 12 satellites in Inclined Geosynchronous Orbits (IGSO) (inclination =  $63.4^\circ$ ) distributed on two orbital planes. Additional three geostationary satellites are used [Wlaka, 1997, Hein *et al.*, 1997].

The observation matrix  $A$  has to be modified analogous to equation (4.18), assuming that the clocks of the geostationary satellites are synchronized with those of the ENSS.

#### 4.3.4. GPS and Pseudolites

A pseudolite is a ground based transmitter, configured to emit a GPS-like signal for GPS augmentation [Seybold *et al.*, 1997]. The pseudolites do not have a large transmission range. Consequently they have to be placed near the critical approach parts. In the case of Lugano-Agno it would be appropriate to place them in the region of the waypoint SHARK. The pseudolite clocks are synchronized with GPS [Seybold *et al.*, 1997]. Nevertheless two or more pseudolites would be appropriate in the region of SHARK, due to the critical number of visible satellites during some periods of the day. The use of two pseudolites is assumed for the availability simulations.

A GPS receiver can track pseudolites and satellites signals simultaneously only in an intermediate zone where both signals have approximately the same strength



[Cobb and O'Connor, 1998]. This characteristics is known as the near-far problem. The radius ratio of the inner boundary to the outer boundary of this zone can be assumed to be about  $\frac{1}{9}$  for an omnidirectional transmitting pseudolite [Weiser, 1997]. The location and the power of the pseudolite transmitter have consequently to be coordinated.

#### 4.3.5. Simulation Results

Simulations regarding the satellite visibility is done for GPS and the described hybrid systems. These calculations cover the entire approach during one entire day, including terrain masking, aircraft attitude, and cut off angle. These simulations are valid for stand-alone modes, which means, that the ground station does not have an influence on the number of visible satellites. Table 4.1 shows the amount of time in percent of day for a specific number of visible satellites. The improvements of the different systems are clearly visible in the table 4.2 with the mean, minimum and maximum number of visible satellites. GLONASS and ENSS shows improvements either concerning the mean as well as the minimal number of visible satellites. INMARSAT shows an improvement of the expected three satellites for the mean and maximum number of satellites, but the minimum number increases only by one satellite. This is due to the low elevation of the INMARSAT, which cannot support enough the GPS during the last phase of flight, where terrain masking and aircraft attitude are relevant. The improvement of pseudolites seems to be minimal concerning the mean number of visible satellites, but especially the minimum number can be increased by two in the critical phase of flight.

Table 4.3 shows the amount of GDOP's in percent of all GDOP's subdivided in ranges of the size of one. It is seen, that the addition of GLONASS, ENSS or pseudolites helps to avoid large GDOP's. The INMARSAT shows nevertheless large GDOP's due to the problem of low elevations. Table 4.4 shows an enhancement of the mean GDOP of over 60% for large satellite systems like GLONASS and ENSS.

num of sats	GPS [% of day]	GPS + GLONASS [% of day]	GPS + INMARSAT [% of day]	GPS + ENSS [% of day]	GPS + Pseudolites [% of day]
3	0.01	0.00	0.00	0.00	0.00
4	0.13	0.00	0.01	0.00	0.00
5	0.25	0.00	0.08	0.00	0.08
6	3.35	0.00	0.10	0.00	1.43
7	22.17	0.00	0.33	0.00	19.22
8	28.22	0.00	1.69	0.00	26.32
9	29.58	0.02	4.10	0.00	31.01
10	12.01	0.12	20.94	0.00	15.07
11	4.29	0.26	27.11	0.01	6.36
12	0.00	0.94	29.35	0.05	0.49
13	0.00	2.83	11.99	0.12	0.01
14	0.00	5.49	4.29	0.28	0.00
15	0.00	12.33	0.00	0.95	0.00
16	0.00	17.42	0.00	2.40	0.00
17	0.00	20.50	0.00	9.12	0.00
18	0.00	19.33	0.00	10.06	0.00
19	0.00	14.42	0.00	30.08	0.00
20	0.00	5.22	0.00	26.64	0.00
21	0.00	1.11	0.00	14.28	0.00
22	0.00	0.00	0.00	6.03	0.00

Table 4.1.: Time, given in percent of a day, of the number of visible satellites for the GPS stand-alone mode and hybrid systems during an entire day on the whole approach.

	GPS	GPS + GLONASS	GPS + INMARSAT	GPS + ENSS	GPS + Pseudolites
Mean	8.4	16.9	11.3	19.3	8.6
Min	3	9	4	11	5
Max	11	21	14	22	13

Table 4.2.: Mean, minimum and maximum number of visible satellites during an entire day on the whole approach for the GPS stand-alone mode and hybrid systems.

GDOP	GPS [% of day]	GPS + GLONASS [% of day]	GPS + INMARSAT [% of day]	GPS + ENSS [% of day]	GPS + Pseudolites [% of day]
0 - 1	0.00	19.80	0.00	25.69	0.02
1 - 2	76.45	80.11	86.88	74.29	80.49
2 - 3	22.70	0.08	12.73	0.01	19.23
3 - 4	0.66	0.00	0.27	0.00	0.23
4 - 5	0.10	0.00	0.05	0.00	0.02
5 - 6	0.02	0.00	0.02	0.00	0.00
6 +	0.04	0.00	0.04	0.00	0.00

Table 4.3.: Time, given in percent of a day, of the GDOP for the GPS stand alone mode and hybrid systems during an entire day on the whole approach.

	GPS	GPS + GLONASS	GPS + INMARSAT	GPS + ENSS	GPS + Pseudolites
Mean	1.73	1.12	1.59	1.08	1.65

Table 4.4.: Mean GDOP during an entire day on the whole approach for the GPS stand alone mode and hybrid systems.

## 4.4. Comparison of Simulations with Real Flight Data

Time, position and attitude are known for the real flights. So it is possible to compare the derived satellite visibility model with the reality. Figure 4.18 represents such a comparison for two approaches. The maximum of the coloured area on bottom of the figure is the total amount of visible satellites without any masking taken into account (10 to 11 satellites). The dark grey area represents the loss of satellite visibility due to the terrain and the light grey area due to the attitude. The white line indicates the real number of tracked satellites during the test flights. In the middle part of the figure, the angle  $\zeta$  is represented to indicate the attitude state. The altitude of the aircraft is shown at the top of the figure to give an idea about the terrain impact.

It is clearly visible, that the terrain affects the satellite visibility during low altitude parts of flight (dark grey area). There is also a strong correlation between  $\zeta$  and the loss of satellites (light grey area).

The number of satellites tracked is mostly lower than the number of visible satellites calculated. The model matches the reality better, when the aircraft is flying at low altitude. A main reason would be the exclusion of the unknown antenna characteristics in the calculations, which is compensated by terrain effects.

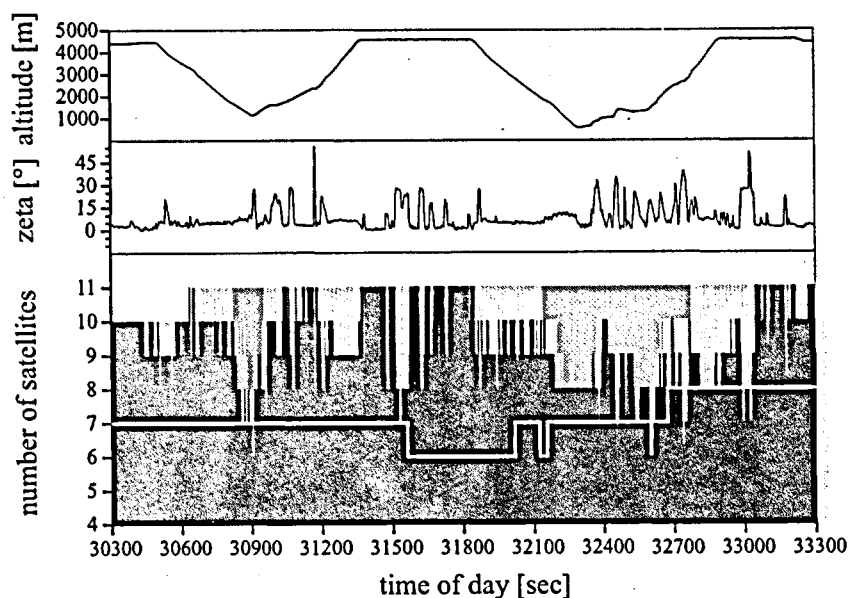


Figure 4.18.: Comparison of simulations on number of visible satellites with the number of tracked satellites during two landings of a real flight. The top part of the figure represent the altitude of the aircraft and the middle part the angle  $\zeta$ . The white line on bottom shows the number of tracked satellites. The dark grey area shows the number of calculated lost satellites due terrain and the light grey area due to aircraft attitude. The black area shows the calculated number of visible satellites.

Satellites with elevations down to  $-37^\circ$  in the fixed aircraft system were tracked during the flight. Figure 4.19 shows an azimuth-elevation diagram of the tracked satellites in the fixed aircraft system. The solid line indicates the minimum elevation of tracked satellites for a given azimuth. This line decreases at azimuths of  $90^\circ$  and  $270^\circ$ . It can be excluded with the method described in chapter 5.1, that these signals are tracked due to multipath effects. It is more likely, that the signals are conducted through the shell of the lateral, curved fuselage of the aircraft to the antenna. It is to point out, that this effect can produce uncontrolled range measurement errors. Use of cut off angle in the topocentric system does not avoid this effect. It is recommended to use additionally a small cut off angle in the fixed aircraft system to avoid the tracking of such satellites.

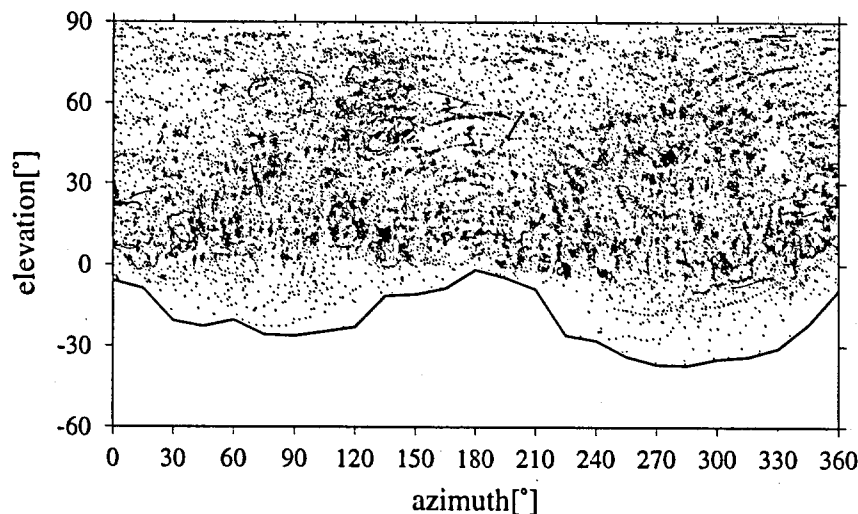


Figure 4.19.: The dots in the azimuth-elevation diagram show the position of the tracked satellites in the fixed aircraft system during the test flights. The line represents the minimum elevation of tracked satellites for a given azimuth.

## 4.5. Findings

The availability and continuity depends, among others, on the number of visible satellites and their constellation. Six visible satellites at minimum are mandatory to provide navigation and Receiver Autonomous Integrity Monitoring (RAIM) capability. Sufficient satellite visibility and resulting Dilution Of Precision (DOP) is conditional for the availability and continuity of the navigation system. Approach simulations with real satellite constellations are carried out including cut off angle, terrain masking extracted from a Digital Terrain Model (DTM), modeled flight dynamics (roll, pitch and heading of aircraft), and aircraft body masking. The first three mentioned influences can sometimes have a large impact on satellite visibility. Contrary to expectation, the aircraft body does nearly not affect the satellite visibility as the antenna is mounted on top of the fuselage where the obstructions are negligible. The simulations shows, that the influences of terrain, aircraft attitude and cut off angle together can reduce the number of visible satellites during short periods to three. Six or less satellites are visible during 5.9 % of a day where a GDOP larger than 5 occurs during 1.34 % of a day. The flight through the gaps with less than six satellites would last 20 to 30sec. The GDOP reaches partially large values, which would make the navigation system unusable.

Additional satellites and/or pseudolites would give the possibility to bridge such critical situations. Simulations with GPS and additionally the Russian GLObal NAVigation Satellite System (GLONASS), three geostationary INMARSATs, the planned European Navigation Satellite System (ENSS), and two pseudolites placed

2.5km in front of the runway showed significant improvements. The addition of GLONASS, respectively ENSS, can solve the problems. The pseudolites could enhance the continuity, but three at minimum are needed. The INMARSATs can contribute only to a slight improvement.

Comparison of the number of tracked satellites during the flights with the predicted number of visible satellites using the real aircrafts position and attitude occasionally shows up to four non-tracked satellites. This is mainly caused by the unknown receiver antenna characteristics. It is also noted, that sometimes more satellites than expected are tracked. It can be shown, that these satellites lie down to  $-37^\circ$  beneath the antenna horizon. Multipath and refraction can be excluded as cause. It is assumed, that the GPS signal is conducted via the aircraft fuselage shell to the antenna, which can provoke uncontrolled effects on the range measurements and consequently also on the GPS position. For this reason it would be reasonable to use a small cut off angle in the aircraft fixed coordinate system.

## 5. Multipath and Interference

The GPS range measurement is affected by different error sources like ephemeris errors, clock errors, selective availability, tropo- and ionosphere, noise, multipath and interference. Investigations on the last two mentioned error sources are done in this chapter. These two errors are of main importance as they cannot be detected by a ground based integrity monitoring system (see chapter 6).

### 5.1. Multipath

Multipath is caused by reflection or diffraction of the L-band signal on the aircraft, terrain, buildings etc. That means, that the signal travels from the satellite to the receiver antenna via multiple paths [Kee and Parkinson, 1994, Townsend and Fenton, 1994] as shown in figure 5.1. The consequence is an error in the estimated ranges or the obliteration of the GPS signal.

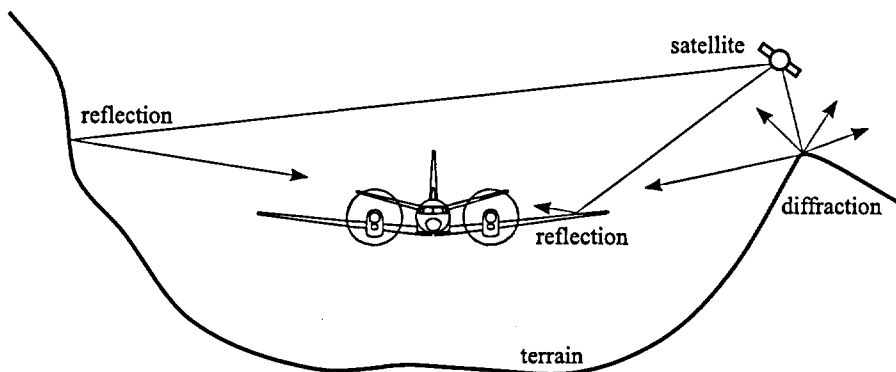


Figure 5.1.: Multipath of GPS signal can be generated by reflected or diffracted signals on the terrain or artificial objects (aircraft, buildings, etc.)

The following investigations will only take the reflection part of multipath into consideration, assuming that diffraction multipath is much weaker than refraction multipath and therefore the main part of this error source [Townsend and Fenton, 1994].

Multipath shows the following effects among others:

- The multipath signal has always a time delay with respect to the direct signal due to the longer propagation path. The estimated ranges are consequently larger than ranges measured with the direct signal.
- Multipath is usually weaker than the direct signal due to power loss on the reflector and affects the signal to noise ratio [Auber *et al.*, 1994]. Exceptions occur when the direct signal is prevented of reaching the receiver antenna or when multipath is caused by multiple or rough surfaces [van Nee, 1992].
- Polarization of the direct signal changes on the reflector from left-handed to right-handed [Braasch, 1994, van Nee, 1992].
- Cross correlation of multipath signal with internal generated signal will be negligible, if the delay is greater than two Pseudo Range Noise (PRN) chips length [Proakis, 1983].
- The error is not eliminated by using the Differential GPS (DGPS) mode and is the dominating error source in this mode [Hurrass and Hickmann, 1997].
- Multipath effects on carrier phase measurements are negligible compared to those of the pseudorange [Braasch, 1994].
- The reflected signal has a phase shift and normally a smaller amplitude, but the same frequency compared to the direct signal. The resulting signal on the receiver is composed of the direct and superimposed reflected signal [Hurrass and Hickmann, 1997].

[Auber *et al.*, 1994] distinguishes two types of reflection, a specular and a diffuse one. This difference can be applied to reflectors with a sinusoidal surface (e.g. water surface). A specular reflection can be strong when several reflected signals are accumulated to one signal.

### 5.1.1. Detecting Code Multipath with Code Minus Carrier Phase Measurements

Different methods, electrically or by using the received data, were derived to identify multipath. An approach by using received data only is to compare code with carrier phase measurements [Braasch, 1994]. The code and carrier phase observation equations are

$$d_{code} = d_s + SA + c \cdot t_{rec} + c \cdot t_{sat} + d_{trp} + d_{ion} + d_{code-mp} + d_{code-noise} \quad (5.1)$$

$$d_{phase} = d_s + SA + c \cdot t_{rec} + c \cdot t_{sat} + d_{trp} - d_{ion} + d_{phase-mp} + d_{phase-noise} + \Delta, \quad (5.2)$$



where

$d_{code}$	= code range measurement
$d_{phase}$	= carrier phase integrated doppler measurement
$d_s$	= true range from satellite to receiver
$SA$	= Selective Availability
$c \cdot t_{rec}$	= receiver clock error
$c \cdot t_{sat}$	= satellite clock error
$d_{trp}$	= tropospheric delay
$d_{ion}$	= ionospheric delay
$d_{code-mp}$	= code multipath
$d_{code-noise}$	= code noise
$d_{phase-mp}$	= carrier phase multipath
$d_{phase-noise}$	= carrier phase noise
$\Delta$	= unknown integer ambiguity of carrier phase .

The true range  $d_s$ , Selective Availability  $SA$ , tropospheric delay  $d_{trp}$  and clock errors  $c \cdot t_{rec}$  and  $c \cdot t_{sat}$  can be assumed to be identical for code and carrier phase measurements. The ionospheric delay  $d_{ion}$  has also the same size, but different sign due to different velocities of the code (group velocity) and carrier phase signal (phase velocity) in dispersive medium. Noise and multipath can be assumed to be much smaller for carrier phase than for code measurements. The difference of code and carrier phase measurements is then

$$\begin{aligned} d' &= d_{code} - d_{phase} \\ &\approx 2 \cdot d_{ion} + d_{code-mp} + d_{code-noise} - \Delta. \end{aligned} \quad (5.3)$$

The unknown integer ambiguity  $\Delta$  of the integrated doppler measurements remains constant for a period without cycle slips. This bias is eliminated by estimating and subtracting out the mean of  $d'$  over a period without cycle slips. This operation can only be done in the post processing as all the data has first to be screened for cycle slips.

The ionospheric effect can be eliminated by using a dual frequency receiver as the ionosphere is a dispersive medium in the GPS L-bands. However, the measurement system in the Lugano trials uses a single frequency receiver. In this case the elimination of the ionospheric delay is achieved by subtracting a fitted polynomial function. A function of second degree

$$d_{ion}(T) = a \cdot T^2 + b \cdot T + c, \quad (5.4)$$

where

$T$  = time of day  
 $a, b, c$  = parameter of polynom

gives satisfactory results for a stationary receiver and during a period of one to two hours.

The remaining residual  $D$  is approximately the code noise and code multipath error

$$D \approx d_{\text{code-mp}} + d_{\text{code-noise}}. \quad (5.5)$$

Figure 5.2 shows the residual  $D$  of one satellite for two consecutive days measured at the Lugano ground station. The receiver is stationary at the airfield, where it can be expected, that the near environs (building, vehicles etc.) do not change from day to day. The antenna is fitted with choke rings to suppress multipath effects.

Since the satellite constellation repeats from day to day, multipath effects will also show similar repetition characteristics. Thus day to day cross correlation  $r$  (equation (5.6)) of the residuals  $D$  reveals the presence of multipath.

$$r = \frac{\sum_{i=1}^n (D_i^{(1)} - \bar{D}^{(1)}) (D_i^{(2)} - \bar{D}^{(2)})}{\sqrt{\sum_{i=1}^n (D_i^{(1)} - \bar{D}^{(1)})^2 \sum_{i=1}^n (D_i^{(2)} - \bar{D}^{(2)})^2}}, \quad (5.6)$$

where

$$\bar{D}^{(1)} = \frac{1}{n} \sum_{i=1}^n D_i^{(1)}$$

$$\bar{D}^{(2)} = \frac{1}{n} \sum_{i=1}^n D_i^{(2)}.$$

Figure 5.3 represents the cross correlation of both curves of figure 5.2. The correlation reaches a maximum at the time offset of about 4 minutes. This offset is caused by the 4-minutes early day by day repetition of the satellite constellation.

These residuals can further be partially split into a multipath and noise term by smoothing the residuals with a adjacent averaging. The smoothed residuals are now closer to the multipath errors. The noise can be achieved by subtracting the smoothed residuals from the original ones. Figure 5.4 shows on top the original residuals, in the middle the smoothed ones and on bottom the difference of both residuals above. The abrupt increase of the noise on the right side may have a connection with the fact, that the satellite was disappearing behind the horizon at an elevation of  $10^\circ$ . The smoothed residual can be characterized by a non stochastic, sinusoidal signal.

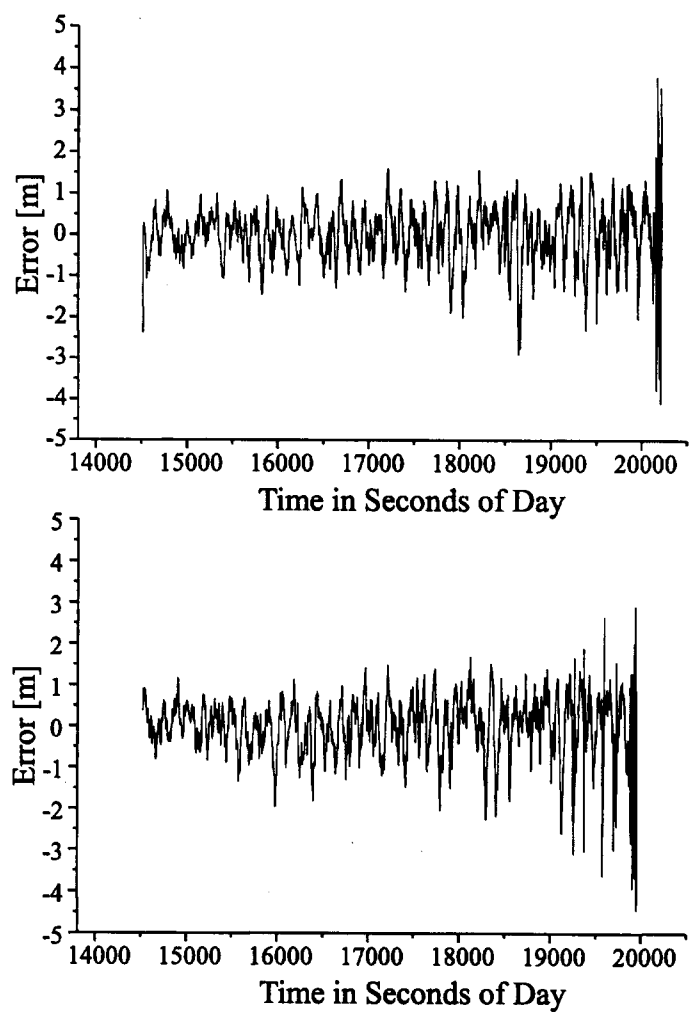


Figure 5.2.: Noise and multipath of one satellite for two consecutive days.

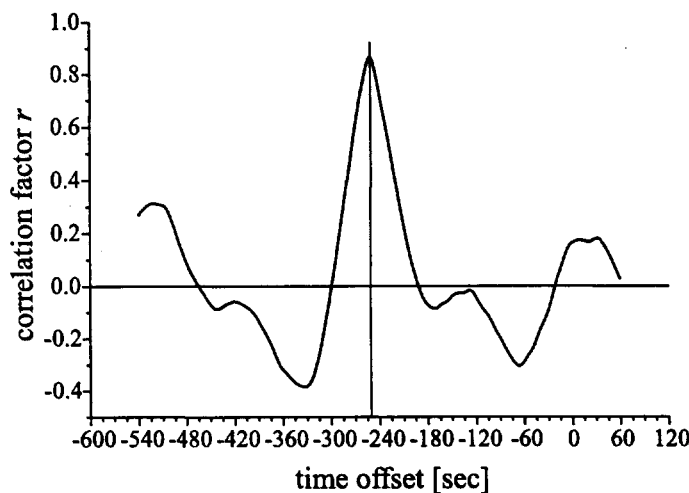


Figure 5.3.: Cross-correlation  $r$  of the two curves in figure 5.2. The correlation is high at a time offset of about four minutes, caused by early day by day repetition of satellite constellation.

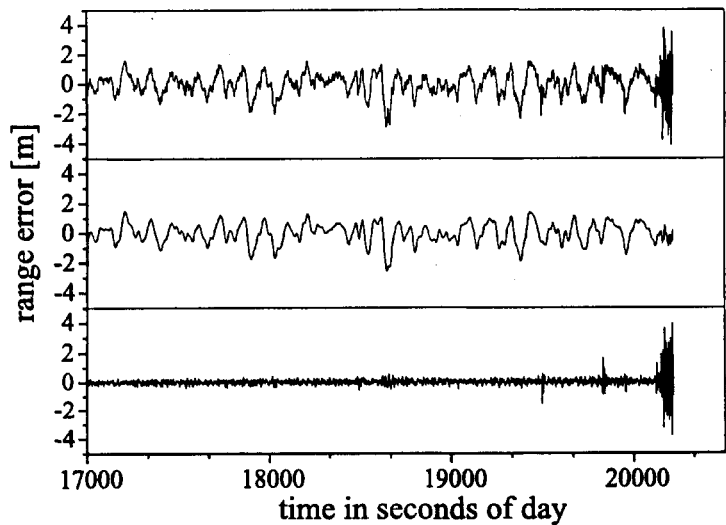


Figure 5.4.: Residuals, smoothed residuals and noise (from top to bottom) of code minus carrier phase ranges.

### 5.1.2. Geometry of Multipath

As shown in figure 5.3 it is expected, that multipath effects are present. Nevertheless it can not be excluded, that other systematic and repeatable errors are involved. The modeling of multipath would help in the decision of the presence of multipath.

The range elongation induced by multipath depends only on the relative positions of satellite, antenna and reflectors. Figure 5.5 shows these relations for the case of one reflector. It is noted, that all vectors lie in one plane, formed by  $\vec{n}$  and  $\vec{e}_R$ .

The angle  $\gamma$  follows from figure 5.5:

$$\begin{aligned}\gamma &= \frac{\pi}{2} - \arccos\left(\frac{\vec{e}_0^T \vec{n}}{|\vec{e}_0||\vec{n}|}\right) \\ &= \frac{\pi}{2} - \arccos(\vec{e}_0^T \vec{n}).\end{aligned}\quad (5.7)$$

The value  $h'$  is calculated with  $h'_1$  and  $h'_2$ :

$$\begin{aligned}h'_1 &= |\vec{a}| \cdot \cos \alpha \\ &= |\vec{a}| \cdot \frac{\vec{n}^T \vec{a}}{|\vec{n}||\vec{a}|} \\ &= \vec{n}^T \vec{a}\end{aligned}$$

$$\begin{aligned}h'_2 &= -|\vec{p}| \cdot \cos \beta \\ &= -|\vec{p}| \cdot \frac{\vec{n}^T \vec{p}}{|\vec{n}||\vec{p}|} \\ &= -\vec{n}^T \vec{p}\end{aligned}$$

$$\begin{aligned}h' &= h'_1 + h'_2 \\ &= \vec{n}^T \vec{a} - \vec{n}^T \vec{p}.\end{aligned}\quad (5.8)$$

It follows for the range elongation  $\delta d$

$$\delta d = 2h' \sin \gamma. \quad (5.9)$$

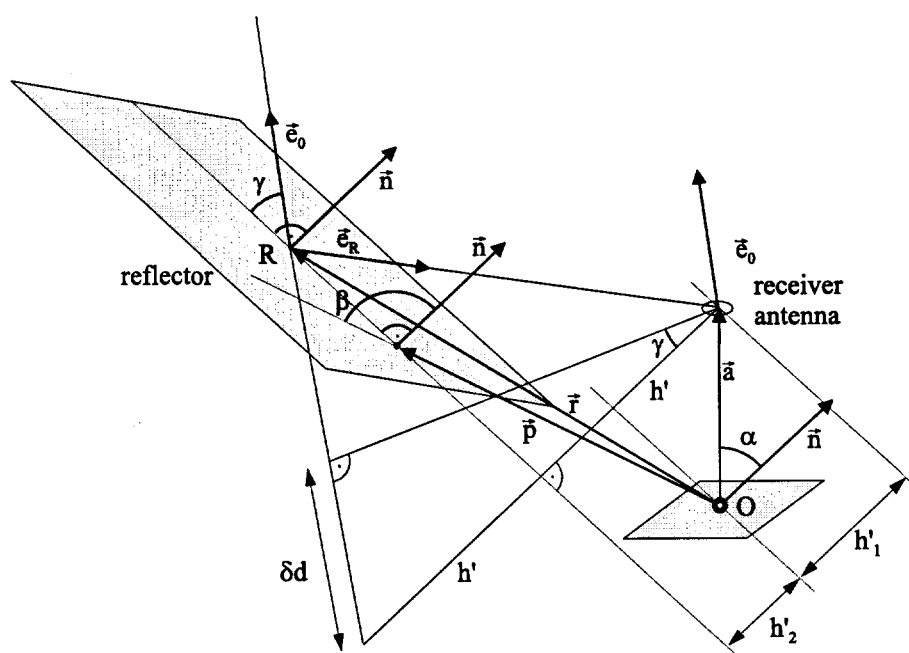


Figure 5.5.: Geometrical view of multipath with one reflector.

- $\delta d$  = range elongation
- $O$  = origin of coordinate system
- $R$  = reflection point
- $\vec{e}_0$  = unit vector to satellite
- $\vec{e}_R$  = unit vector from reflection point to antenna
- $\vec{n}$  = unit vector, perpendicular to the reflector plane
- $\vec{p}$  = vector from  $O$  to a known point on the reflector plane
- $\delta d$  = multipath induced range elongation
- $\vec{a}$  = vector from  $O$  to antenna of the form  $\vec{a} = [0, 0, h]^T$ , where  $h$  is the antenna height
- $h'$  = perpendicular distance from reflector plane to antenna composed of the parts  $h'_1$  and  $h'_2$
- $\alpha$  = angle between  $\vec{a}$  and  $\vec{n}$
- $\beta$  = angle between  $\vec{p}$  and  $\vec{n}$
- $\gamma$  = angle of incidence of the signal relative to the reflector plane

The multipath effect depends not only on the range elongation, but also from the reflection properties of the reflector. For this reason there is the need to know the reflection point  $R$  of the signal, which can be described with

$$\vec{r} = \vec{a} + v \cdot \vec{e}_R, \quad (5.10)$$

where

$$\begin{aligned} \vec{r} &= \text{vector from } O \text{ to } R \\ v &= \text{length from antenna to } R. \end{aligned}$$

The vector  $\vec{e}_R$  can be derived as

$$\begin{aligned} \vec{e}_R &= \vec{e}_0 + 2 \left( \vec{n} \cdot \cos \left( \frac{\pi}{2} - \gamma \right) - \vec{e}_0 \right) \\ &= 2 \cdot \vec{n} \cdot \cos \left( \frac{\pi}{2} - \gamma \right) - \vec{e}_0 \\ &= 2\vec{n} (\vec{n}^T \vec{e}_0) - \vec{e}_0. \end{aligned} \quad (5.11)$$

It follows

$$\begin{aligned} v &= -\frac{h'}{\sin \gamma} \\ &= -\frac{h'}{\sin \left( \frac{\pi}{2} - \arccos (\vec{e}_0^T \vec{n}) \right)} \\ &= -\frac{h'}{\cos (\arccos (\vec{e}_0^T \vec{n}))} \\ &= -\frac{h'}{\vec{e}_0^T \vec{n}}. \end{aligned} \quad (5.12)$$

The negative sign is due to the direction of  $\vec{e}_R$ .

The amplitude of the reflected signal with one reflector is usually smaller than the amplitude of the direct signal. The amplitude reduction depends on the incident angle  $\gamma$  of the signal and on the reflection properties of the reflector, which can be estimated with the knowledge of the location of the reflection point  $R$ . Additionally the amplitude depends also on the antenna characteristic.

### 5.1.3. Delay Lock Loop

The previous chapter gives an overview about the geometrical connections of multipath. The resulting effect is mainly the range elongation  $\delta d$ . Further multipath effects are produced in the receiver itself. The receiver tries to correlate the internally created signal with the received signal to determine the time of signal reception. A multipath environment creates a signal, which is composed of an overlay of time shifted signals. A proper correlation is then insure.

An estimation of this effect is done by using the Delay Lock Loop (DLL) technique described in [van Nee, 1992, Townsend *et al.*, 1995, Jülg, 1997]. The DLL is a commonly used technique in GPS receivers to measure the range. The input signal of the loop is written in the complex notation as:

$$x(t) = \sum_{i=0}^M a_i \sqrt{2} p(t - \tau_i) e^{j[(\omega + \omega_i)t + \theta_i]}, \quad (5.13)$$

where

- $M$  = number of reflectors
- $a_i$  = amplitude of  $i^{th}$  signal
- $\tau_i$  = delay of  $i^{th}$  signal
- $\omega_i$  = angular doppler frequency of  $i^{th}$  signal
- $\theta_i$  = phase of  $i^{th}$  signal = range elongation  $\delta d$  of the  $i^{th}$  signal
- $p(t)$  = spread spectrum code ( $\pm$  valued code)
- $\omega$  = angular carrier frequency of the GPS signal.

The input signal  $x(t)$  is coherently correlated with two local spread-spectrum codes with a relative spacing of 1 chip time, the early code  $e(t)$  and the late code  $l(t)$ :

$$\begin{aligned} e(t) &= \frac{1}{\sqrt{2}} p(t - \tau - \frac{T_c}{2}) e^{-j\omega t} \\ l(t) &= \frac{1}{\sqrt{2}} p(t - \tau + \frac{T_c}{2}) e^{-j\omega t}, \end{aligned} \quad (5.14)$$

where

$T_c$  = chip duration.



The early and late autocorrelation functions  $y_e(\tau, t)$  and  $y_l(\tau, t)$  are

$$y_e(\tau, t) = \sum_{i=0}^M a_i R \left( \tau - \tau_i + \frac{T_c}{2} \right) \cdot e^{j(\omega_i t + \theta_i)} \quad (5.15)$$

$$y_l(\tau, t) = \sum_{i=0}^M a_i R \left( \tau - \tau_i - \frac{T_c}{2} \right) \cdot e^{j(\omega_i t + \theta_i)} \quad (5.16)$$

with

$$R(\vartheta) = \begin{cases} \frac{1+\frac{1}{N}}{T_c} \cdot \vartheta + 1 & -T_c \leq \vartheta \leq 0 \\ -\frac{1+\frac{1}{N}}{T_c} \cdot \vartheta + 1 & 0 \leq \vartheta \leq T_c \\ \frac{1}{N} & |\vartheta| > T_c \end{cases}, \quad (5.17)$$

where

$\tau$  = difference between received and local code

$\vartheta$  = time variable.

The DLL now gives the phase difference between the received code and the local code by measuring the phase  $\tau$  for which the output signal  $z(\tau, t)$  is zero while the slope  $\frac{\partial z}{\partial \tau}$  is negative.

$$z(\tau, t) = \int_{t-T}^t (|y_e(\tau, t)|^2 - |y_l(\tau, t)|^2) dt = 0, \quad \frac{\partial z}{\partial \tau} \leq 0. \quad (5.18)$$

The function  $z(\tau, t)$  is called S-function (see figure 5.6). The bold line shows the S-function for a direct signal. The negative slope of the function crosses the x-axis at 0. An indirect signal would create the dashed line which negative slope crosses the x-axis at a different point than 0.

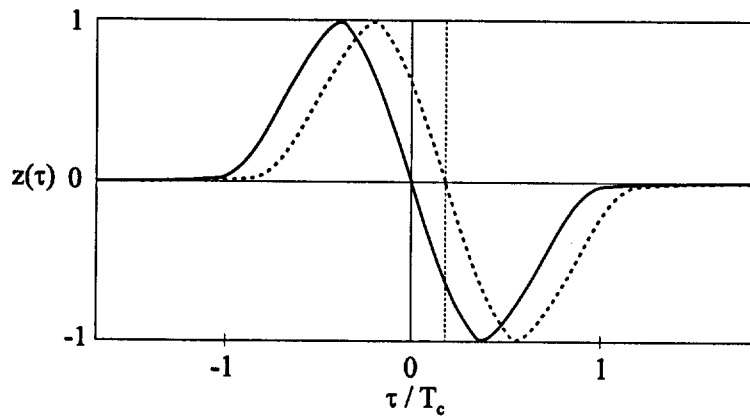


Figure 5.6.: S function of Delay Lock Loop.

#### 5.1.4. Verification of the Multipath Model

[Cerniar, 1997] has written a program to verify the multipath model by using the characteristics described in the two previous chapters. The test site was selected in a way that one main reflector (wall of a building) affects the signal with multipath. The antenna with choke rings was placed on the floor to avoid multipath from the ground. A satellite was chosen for the tests, which could be expected to create multipath effects with the given geometry. The  $\omega_i$  was set to zero in equation (5.13) and  $T$  to 1 in equation (5.18). Figure 5.7 on top shows the results of this test. The grey line is the range error, which was estimated by using the code and carrier phase measurements. The black line represents the modeled multipath. The x-axis is given in angular length which describes the angle that the satellite has flown since it is arisen at the horizon. The y-axis represents the range error. It is seen, that the frequency of the repeatability of the error is described quite good from an angular length of 3.5 onwards. The amplitude has a larger error and may be caused by using simplified reflection properties and antenna characteristics. The area of angular length from 3.0 to 3.5 does not seem to match the model at all. It was assumed, that a second reflector would probably affects the measurements. Better results were achieved by including a balustrade which was in the near environment (figure 5.7 bottom). Nevertheless the amplitude modeled does still differ clearly from the amplitude measured.

It was further noted, that the modeling of the environment has to be in the centimeter level. Small variations clearly provoke different multipath effects. This demands a large effort to reach the required model accuracy. For this reason it was renounced to model the antenna environment in Lugano-Agno. It further follows, that this method is only applicable on stationary GPS receivers.

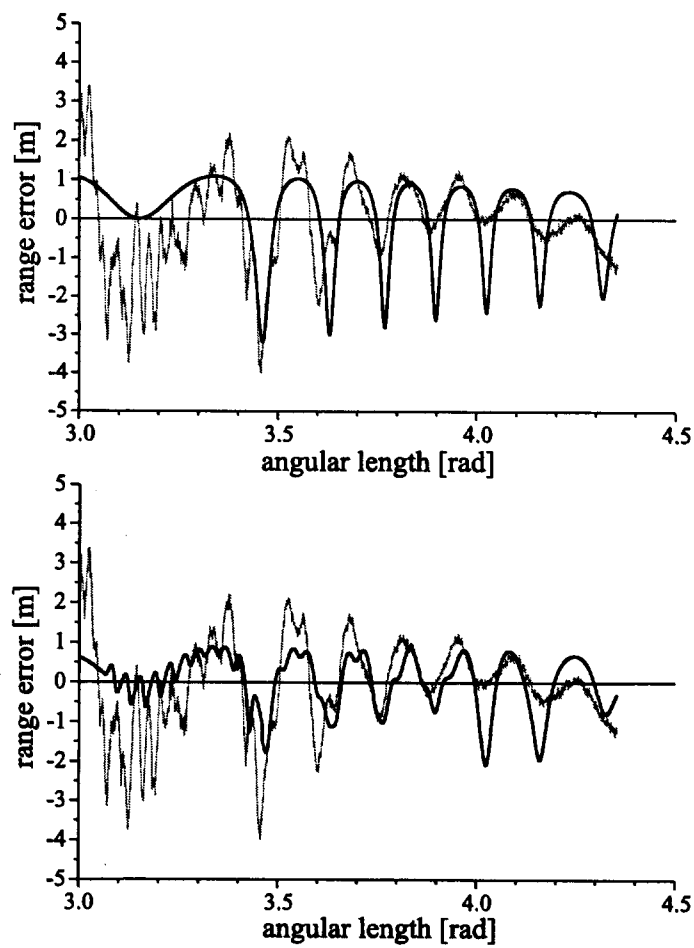


Figure 5.7.: Modeled multipath (black lines) and measured multipath and noise (grey lines) for one (top) and two (bottom) reflectors.

### 5.1.5. Signal Loss Caused by Carrier Phase Multipath

A loss of lock of the GPS signal was noted during preliminary measurements at the airport of Lugano-Agno. The GPS antenna was not fitted with any multipath suppress constructions (e.g. choke rings etc.). The signal loss took place at specific satellite elevations. Figure 5.8 shows an azimuth-elevation diagram with the position of the tracked satellites. The light grey area represents the terrain horizon, which is estimated out of a digital terrain model. The bold, dark grey lines indicates the regions with the loss of the GPS signal.

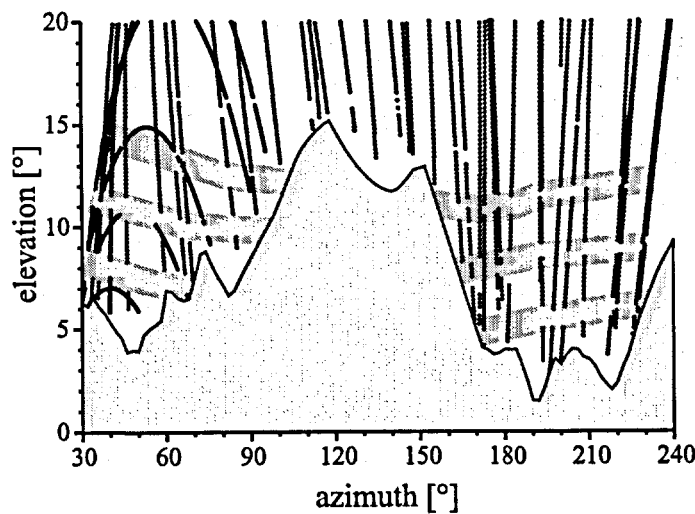


Figure 5.8.: Signal loss is located mostly in the bold, dark grey lines. The bottom, light grey area represents the terrain horizon.

It is surmised, that these loss of signals are caused, when the reflected signal has a similar amplitude like the direct signal and its range elongation is

$$\delta d = \left(i + \frac{1}{2}\right) \lambda_{L1}, \quad i = 0, 1, 2, \dots, \quad (5.19)$$

where

$$\lambda_{L1} = \text{wavelength of } L1 \text{ signal} = 19.05 \text{ cm.}$$

The overlay of both signals produces the loss of the GPS signal. The  $\delta d$  refers to the  $L1$  signal as the measurements were done at this frequency. The same effect can also occur at other frequencies.

The modeling of this effect is based on figure 5.5. A simplified model is used in a first step. As the measurements were carried out near the runway at the airport, it can be assumed, that the environment is a horizontal plane. Furthermore it is assumed,

that the reflections occurred on the ground. The reflector can consequently be set equal to the horizontal ground plane and the origin of the coordinate system is put on the reflector under the antenna (see figure 5.9).

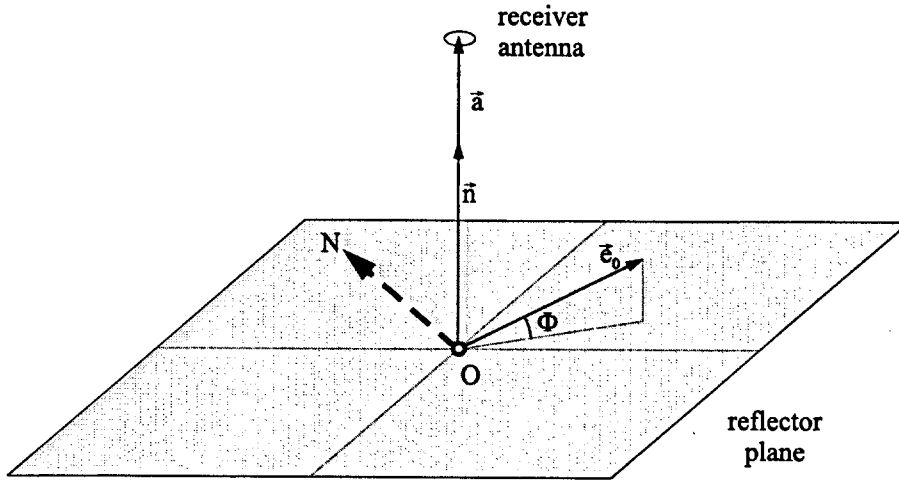


Figure 5.9.: Geometrical view of multipath for an horizontal reflector set equal to the soil.

$\Phi$  = satellite elevation  
 $N$  = direction of north.

It results

$$\vec{p} = \begin{bmatrix} 0 \\ 0 \\ 0 \end{bmatrix}, \quad \vec{a} = \begin{bmatrix} 0 \\ 0 \\ h \end{bmatrix}, \quad \vec{n} = \begin{bmatrix} 0 \\ 0 \\ 1 \end{bmatrix}, \quad (5.20)$$

and

$$|\vec{a}| = h = h'. \quad (5.21)$$

The height  $h$  of the antenna over the ground has to be known, which is usual for a static measurement. It follows with equations (5.9), (5.19) and (5.21)

$$\Phi(i) = \arcsin \left( \frac{(i + \frac{1}{2}) \lambda_{L1}}{2h} \right), \quad i = 0, 1, 2, \dots \quad (5.22)$$

The satellite elevation  $\Phi$ , which obliterate the GPS signal depends only on  $i$ . It follows, that  $\Phi$  remains constant for a given  $i$ . Figure 5.8 shows contrary to this result, that the elevation  $\Phi$  varies for some degrees, depending on the azimuth.

A second step in this multipath modeling can be done by assuming that the reflector plane is inclined. Figure 5.10 shows the modified geometry for this case.

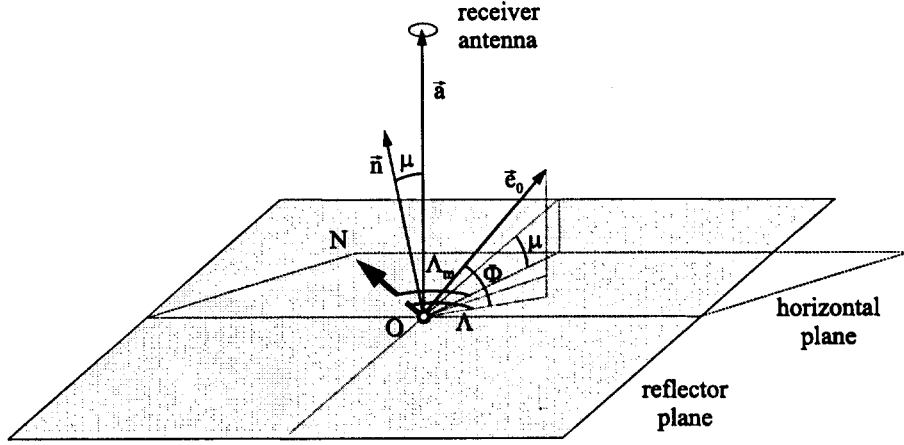


Figure 5.10.: Geometrical view of multipath for an inclined reflector set equal to the soil.

- $\mu$  = inclination of reflector
- $\Lambda$  = azimuth of satellite
- $\Lambda_m$  = azimuth of gradient of plane.

It follows

$$\vec{p} = \begin{bmatrix} 0 \\ 0 \\ 0 \end{bmatrix}, \quad \vec{a} = \begin{bmatrix} 0 \\ 0 \\ h \end{bmatrix}, \quad (5.23)$$

$$\vec{n} = \begin{bmatrix} -\sin \Lambda_m \sin \mu \\ -\cos \Lambda_m \sin \mu \\ \cos \mu \end{bmatrix}, \quad \vec{e}_0 = \begin{bmatrix} \sin \Lambda \cos \Phi \\ \cos \Lambda \cos \Phi \\ \sin \Phi \end{bmatrix}. \quad (5.24)$$

The vectors  $\vec{e}_0$  and  $\vec{n}$  in (5.7) gives

$$\begin{aligned}
 \gamma &= \frac{\pi}{2} - \arccos(\vec{e}_0^T \vec{n}) \\
 &= \frac{\pi}{2} - \arccos(-\sin \Lambda \cos \Phi \sin \Lambda_m \sin \mu - \\
 &\quad \cos \Lambda \cos \Phi \cos \Lambda_m \sin \mu + \sin \Phi \cos \mu) \\
 &= \frac{\pi}{2} - \arccos(-\sin \mu \cos \Phi (\sin \Lambda_m \sin \Lambda + \cos \Lambda_m \cos \Lambda) + \\
 &\quad \sin \Phi \cos \mu) \\
 &= \frac{\pi}{2} - \arccos(-\sin \mu \cos \Phi \cdot \\
 &\quad \left( \frac{1}{2} \cos(\Lambda_m - \Lambda) - \frac{1}{2} \cos(\Lambda_m + \Lambda) + \right. \\
 &\quad \left. \frac{1}{2} \cos(\Lambda_m - \Lambda) + \frac{1}{2} \cos(\Lambda_m + \Lambda) \right) + \\
 &\quad \sin \Phi \cos \mu) \\
 &= \frac{\pi}{2} - \arccos(-\sin \mu \cos \Phi (\cos(\Lambda_m - \Lambda)) + \sin \Phi \cos \mu) \\
 &= \sin \Phi \cos \mu - \sin \mu \cos \Phi (\cos(\Lambda_m - \Lambda)). \tag{5.25}
 \end{aligned}$$

Equations (5.21) and (5.25) in (5.9) gives

$$\begin{aligned}
 \delta d &= 2h (\sin \Phi \cos \mu - \sin \mu \cos \Phi (\cos \Lambda_m - \Lambda)) \\
 &= \left( i + \frac{1}{2} \right) \lambda_{L1}. \tag{5.26}
 \end{aligned}$$

It follows

$$\frac{\left( i + \frac{1}{2} \right) \lambda_{L1}}{2h} = \sin \Phi \cos \mu - \sin \mu \cos \Phi (\cos(\Lambda_m - \Lambda)). \tag{5.27}$$

The elevation  $\Phi$  can be calculated numerically. Figure 5.11 shows the resulting  $\Phi$  for  $i = 1 \dots 3$  with good fitting of signal loss. It has to be mentioned, that  $\Phi$  is very sensible to small differences between the modeled reflector and the topography in the near environment of the antenna. Similar effects were also detected by [Axelrad, 1994].

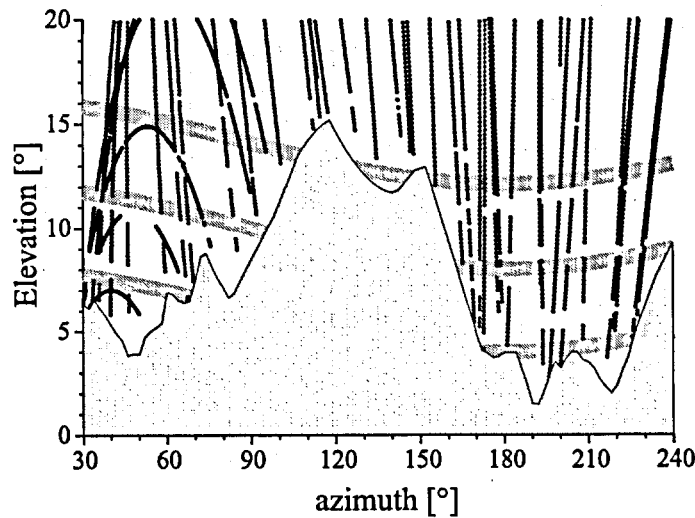


Figure 5.11.: Modeled signal loss (grey bands) due to carrier phase multipath. The bottom light grey area represents the terrain horizon.

The multipath effect derived needs a modeled reflector to determine the satellite position which causes the signal loss. Vice versa the knowledge of the satellite position with the signal loss gives information about the reflector. This inverse way of looking at multipath gives the possibility to estimate the physical environment of the antenna with a high grade of accuracy. Such a method was suggested by [Clark, 1992], where phase and amplitude data could be useful to make a holographic map of the multipath environment. The receivers he had access to at the time did not provide sufficient amplitude resolution to get experimental results.

These investigations can be used to make predictions on the available satellite constellations including carrier phase multipath for a ground station. Counter measure can then be applied in the case of too few available satellite signals due to carrier phase multipath (e.g. choke rings, low antenna gain for reflected incoming signals with negative elevation).

## 5.2. Interference

### 5.2.1. Introduction

One of the major tasks, that has to be solved before applying GNSS for critical use like sole mean navigation is the unintentional and intentional Radio Frequency Interference (RFI). RFI's can produce degraded or total loss of the GPS signal, which was widely reported by different users at different locations and points of time. The potential sources of interference can be found either outside (e.g. [Stevens, 1995,



Ward, 1995]) or inside the aircraft (e.g. [Moore, 1995, Perry and Geppert, 1996]) and consists of VHF communication harmonics and intermodular products, satellite communication, mobile satellite service, DME, VOR harmonics, TV harmonics and much more [Johnson, 1994]. The RFI can further be divided into three categories:

- in-band RFI: harmonics, spurious, and intermodulation products falling in the nominal GNSS bandwidth
- out-of-band RFI: powerful signals near the nominal GNSS bands, which are strong enough to overcome the receiver's passive RF filtering
- physical interference: multipath, shadowing, terrain masking, and other interference caused by the physical environment.

Different techniques were developed to mitigate in-band and out-of-band RFI, among them filters, nulling antennas, physical isolation etc. [Johnson, 1994, Braasch and Snyder, 1998]. There is still no guarantee, that all types of RFI can be rejected by these techniques.

Programs were further called into being to assess and control electromagnetic interference to GNSS. Among them the Working Group 6 of Special Committee 159 of RTCA makes efforts on developing the capability to monitor the environment from the air and from the ground to identify and quickly locate environmental interference when it is detected [Williams, 1996].

### 5.2.2. RFI in the Region of Lugano-Agno

Early terrestrial GPS measurements (since 1986) in the region of Lugano-Agno revealed receiver problems at special spots. By flying over the region a more consistent view of the problem has been established. Special GPS test flights of the TU Braunschweig in 1994 encountered severe interferences. Some further test flights with the aircraft of the Federal Directorate of Surveying confirmed these findings. Dedicated measurement flights and spectrometric analysis carried out by Swisscontrol showed severe interferences on the L1 band [Schulte, 1995a, Schulte, 1995b].

Figure 5.12 shows the influence of the interference on the signal to noise ratio (SNR) during one of the flights carried out by Swisscontrol in 1996. SNR values of less than 35db were plotted, where the thickness of the line gives information on the size of the SNR. The circle shows the location of Lugano-Agno. The triangles indicate potential interfering stations. The characteristics of the SNR leads to the assumption, that the lower left station creates the disturbances with two radiating beams represented by the grey shaded areas.

This data is used to derive a radiation characteristic of the assumed station, which is represented in figure 5.13 [Geiger, 1996]. The dots represents measurements during the Swisscontrol flight in a polar plot as seen from the assumed station. The corresponding SNR are gridded, where the distance of the aircraft to the station is

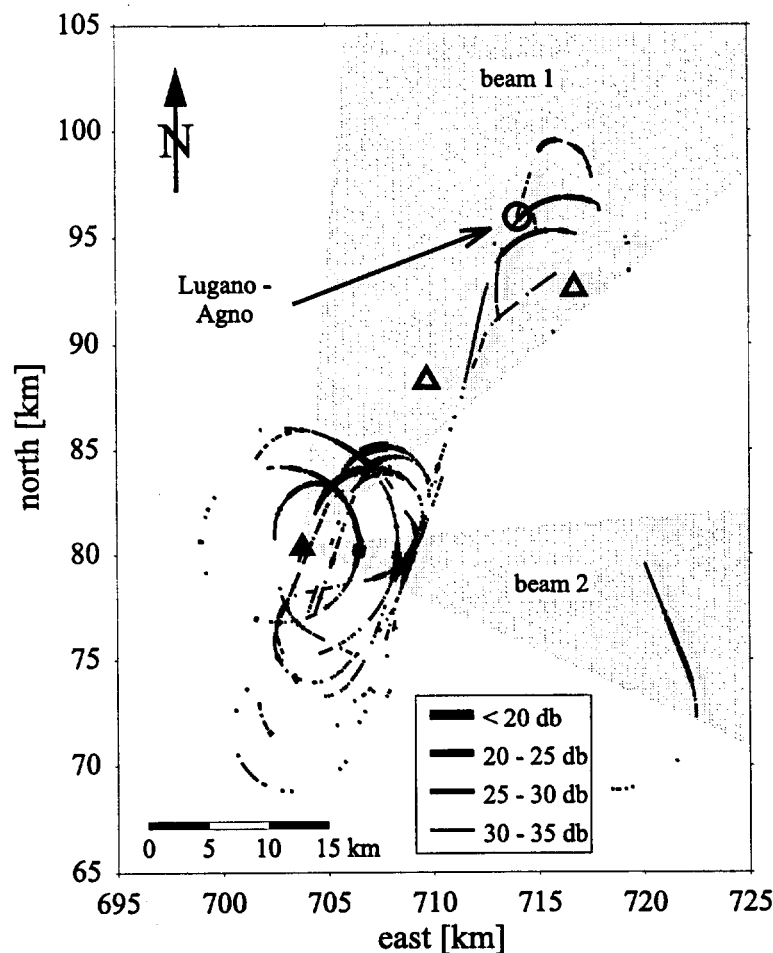


Figure 5.12.: Signal to Noise Ratio (SNR) of an on-board GPS receiver during Swisscontrol flights in the region of Lugano-Agno. The thickness of the line represents the size of the SNR. The white triangles indicate potential interfering stations, where the black triangle is the assumed interfering station. The grey areas represent the assumed radiating beams.

taken into consideration. The results shows, that two radiating beams (low SNR) can be detected at an azimuth of  $20^\circ$  and  $95^\circ$  and with low elevation, which are similar to the grey, shaded area in figure 5.12.

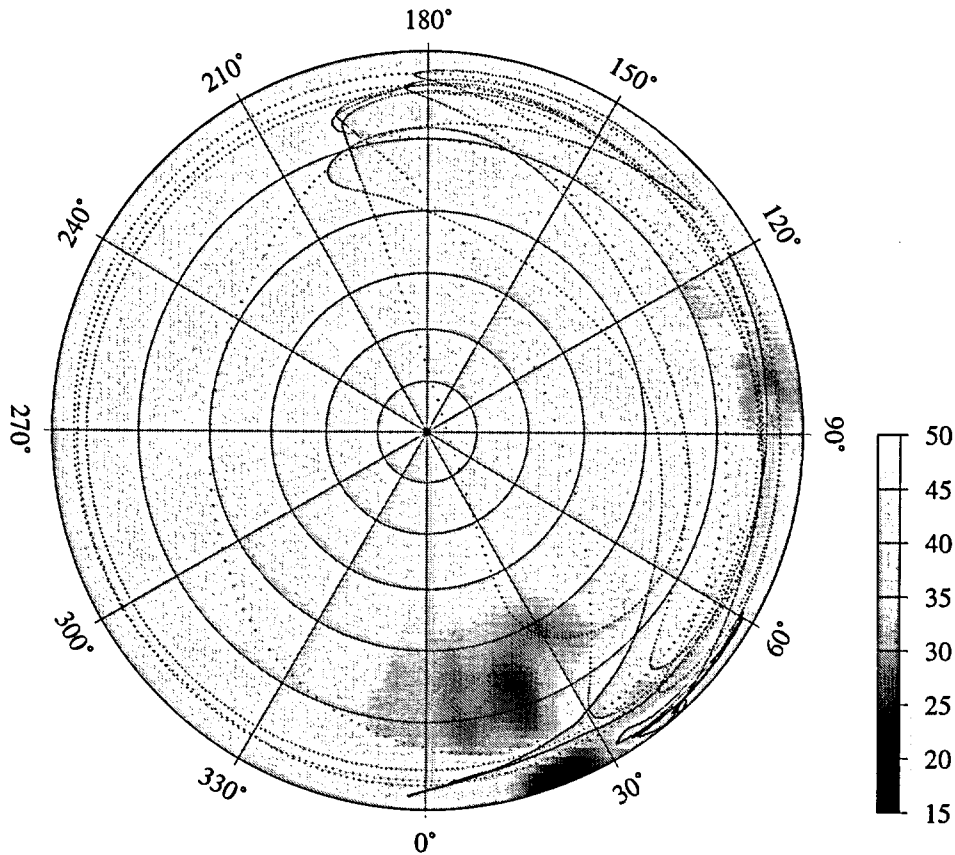


Figure 5.13.: Signal to Noise Ratio (SNR) of an on-board GPS receiver as measured from the Swisscontrol test flights (dots). The colours mark the size of the SNR. Two radiating beams can be identified at about  $20^\circ$  and  $95^\circ$ .

### 5.2.3. Use of Digital Terrain Models for Detection of Potentially Interfering Zones

It becomes necessary to create an easy tool which could give an overview about regions that are potentially influenced by a jamming station. The result should be represented in a map or as a layer, which could be overlaid over an existing map. With such a map a prediction of possible interference problems are simplified [Scaramuzza and Geiger, 1995].

A Digital Terrain Model (DTM) has to be at one's disposal together with the location of the assumed interfering station. The DTM is filtered to a grid resolution of

250m in this case. The extension of the investigated area is  $30\text{km} \times 30\text{km}$ , which is represented in figure 5.14. The dot on the lower edge of the grid indicates the location of the supposed interfering station.

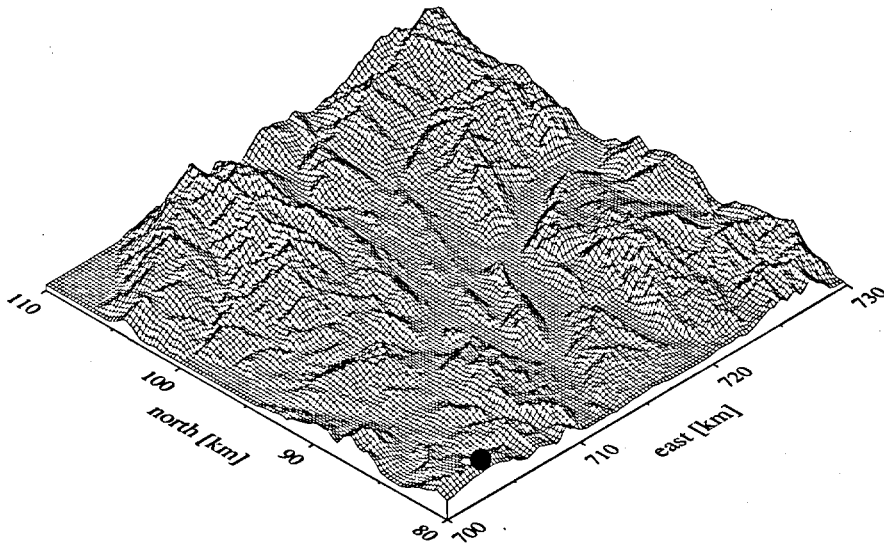


Figure 5.14.: Digital Terrain Model of the region north-east of the assumed interfering station. The black dot on the bottom corner indicates the location of the assumed interfering station.

Sections are cut through the grid, radial to the assumed station. Such a cross section can be analysed in detail as represented in figure 5.15.

The dot is the supposed interfering station. With this cross section it is possible to find the boundary line between the shadowed, medium grey areas and the illuminated, light grey areas. The line between the light grey and dark grey area shows the points on the ground, which are exposed to the interference. The boundary line shows, in other words, the limit, from where the station is visible or not. At this point it is to note, that corrections caused by the curvature of the earth and refraction of electromagnetic waves have to be included into the calculation.

A boundary surface (figure 5.16) can be constructed with the creation of the boundary lines over the whole area, radial to the station. Points, which are above this surface are possibly exposed to the interference and points below the surface should be safe against interference.

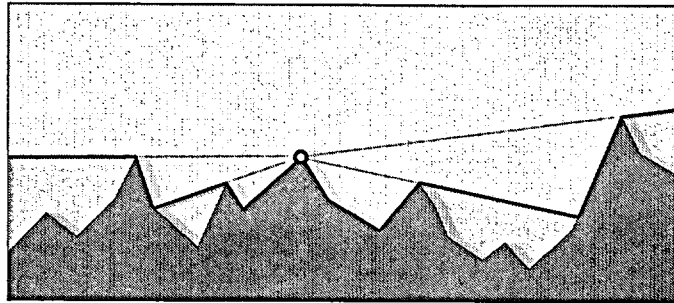


Figure 5.15.: Cross section through the Digital Terrain Model showing the shadowed zones (medium grey area) and the illuminated zones (light grey area). The dark grey area represents the terrain.

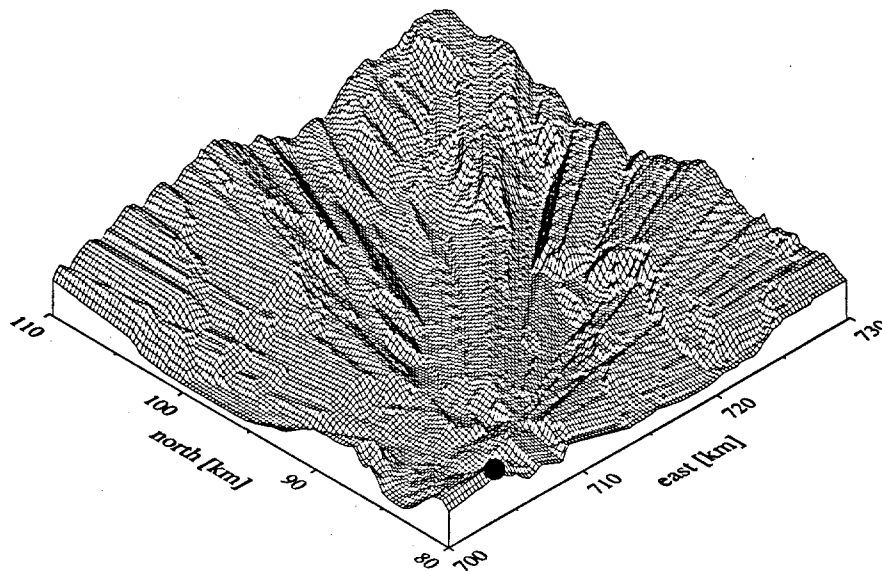


Figure 5.16.: Surface of shadow boundary. The black dot on the bottom corner indicates the location of the assumed interfering station

This surface is now represented as a map in figure 5.17. The grey regions show locations on the ground, which are visible from the station, that means, that interference could occur. The isolines indicate the minimum altitude in meters, which is needed to get into the field of visibility of the station. The isolines on the grey areas correspond directly to the isolines of the terrain.

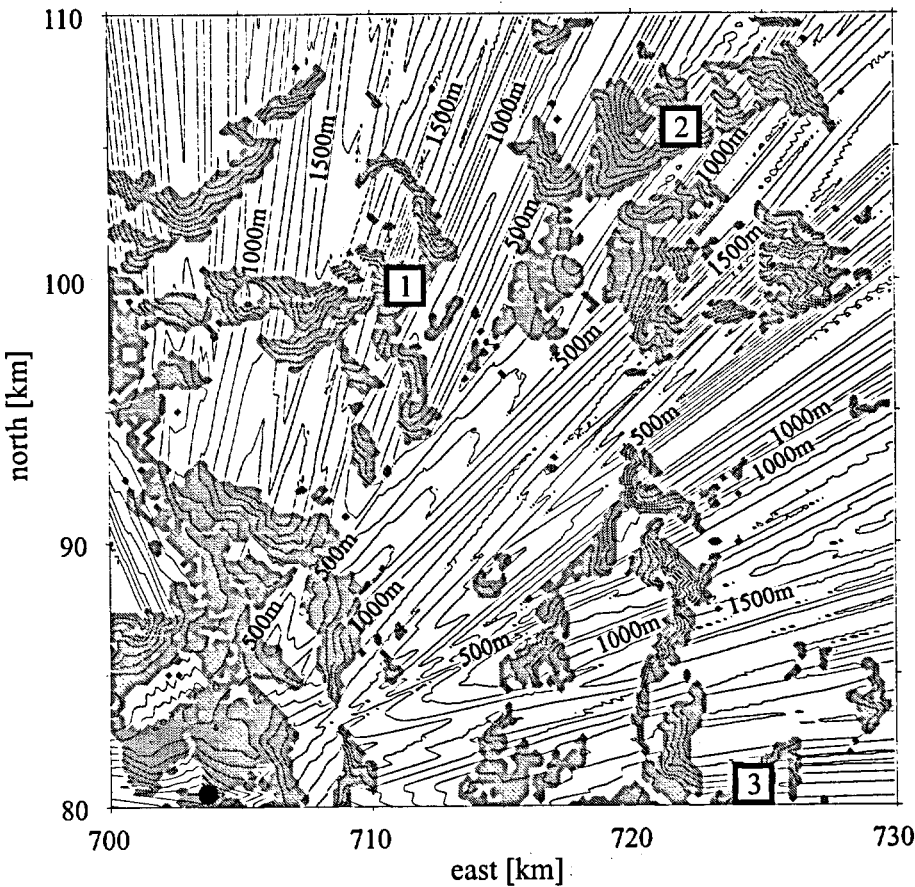


Figure 5.17.: Map with potentially interfering zones on ground (grey areas) or over the ground given with isolines. The black dot on the left bottom corner represents the assumed interfering station. The three numbered boxes indicate the locations, which were chosen for the field tests in August 1997.

Such a map can be used, among others, to find parts of flight tracks, which are potentially exposed to the interference and to find locations, where additional measurements can be carried out on ground.

It is remarked, that for the production of the present map it has been supposed, that the transmission characteristics is omnidirectional. However, link stations will, in most cases, show directional pattern. In these cases the map should be cut in corresponding sections.

### 5.2.4. Lugano Field Tests August 1997

A better comprehension of the radiating characteristic of the interfering station is needed to understand its influence on the GPS receivers used. One of the main interests is to have knowledge on the power and frequency of the interference signal. No information is available from the user of the station as it is a military transmitter. The attempt via official agencies was also in vain.

Consequently the needed information has to be gained by measurements. This was the object among others of the field tests, that were carried out in August 1997 in the environs of Lugano-Agno. The measurements were carried out by means of a spectrum analyzer of the Institute of Navigation of the University of Stuttgart. The following results are part of [Butsch, 1997].

The spectra of the signals received by active GPS antennas were determined. The GPS antennas were tilted in the direction of the transmitter to have the best possible reception of the interference signal. For easier comparison with susceptibility masks of GPS receivers the spectra were transformed from the interface antenna cable/antenna input of the GPS receiver to the interface GPS antenna output/preamplifier input by addition of the cable loss and subtraction of the preamplifier gain. Since nearly all GPS antennas have omnidirectional antenna patterns they have comparable gains and therefore the interface between antenna and preamplifier is suitable for comparison of received signals.

Three locations were chosen by using the map in figure 5.17, where a good reception of the interfering station could be expected. Two of them were located in the northern beam and one in the eastern beam.

The figures 5.18 to 5.20 shows the measured spectra (black line) at each location. Additionally a dark grey curve indicates the power of an interference signal, that must not cause a degradation of the GPS receiver's performance. This curve was defined in the Minimum Operational Performance Standard (MOPS) of [RTCA, 1991]. The light grey curve represents the power of an interference signal, that is required to cause a loss of lock of the code tracking loop of a typical C/A-code receiver.

No signal within the L1-frequency band of GPS could be detected at the first location in the beam 1 (figure 5.18). The only signal in the vicinity of the GPS band was at 1548MHz. This signal is unlikely to cause degradation of the GPS signal due to its weakness. Even a closer location to the interfering station would probably not cause a degradation of the GPS signal.

Additional signals (1557MHz, 1562.5MHz, 1583MHz) and 1588MHz were found at the second location, still in the beam 1. These signals were closer to L1, but still not strong enough to cause a degradation of the GPS signal. This signal would probably affect the GPS signal at closer locations. It is not clear, why this spectrum differs from the one measured at the first location. It is assumed, that the transmitter signal changes from time to time.

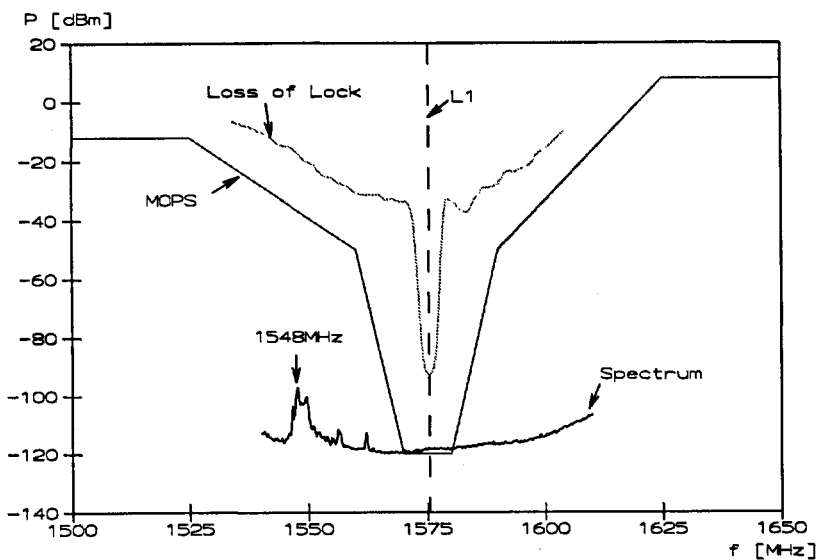


Figure 5.18.: Spectrum (black line) at location 1 [Butsch, 1997]. The dark grey line indicates the minimum signal power defined by RTCA to degrade a GPS receiver. The light grey curve indicates the signal power that is required to cause a loss of lock of the code tracking loop of a typical C/A-code receiver as defined by Butsch.

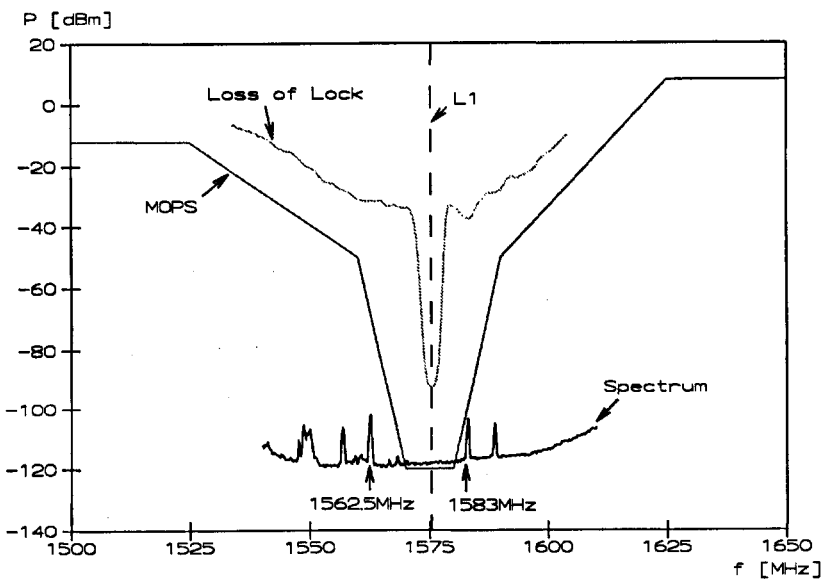


Figure 5.19.: Spectrum at location 2 [Butsch, 1997].



As expected the spectrum at the third location differs from the first two. Signals were found within the L1-band. Others were detected in the vicinity. The signals at and near L1 would not fulfil the RTCA requirements, but would still be too weak to noticeably degrade a GPS receiver.

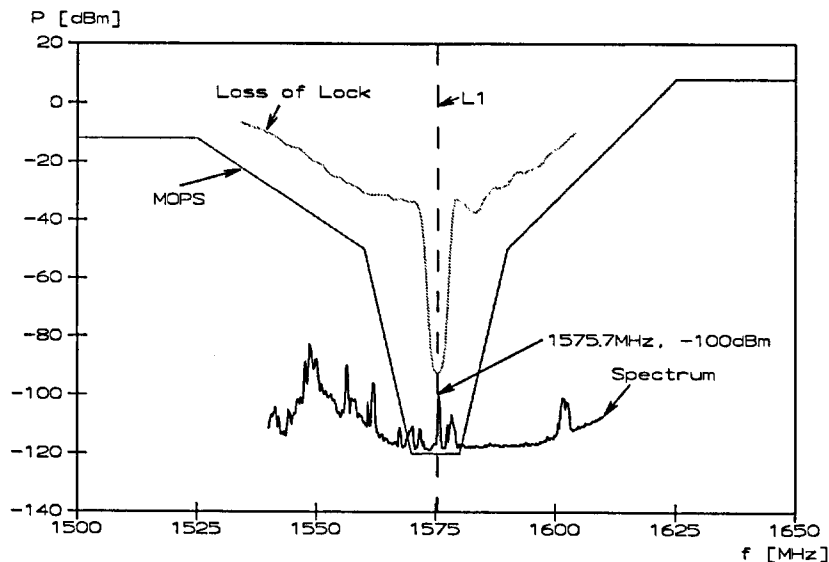


Figure 5.20.: Spectrum at location 3 [Butsch, 1997].

It resulted from this field tests, that a GPS receiver would be more sensitive to the second beam than to the first one. It is also possible, that the spectrum changes from time to time, so that it is difficult to make a realistic prediction of the possible interference to a GPS receiver in this region. The use of GPS for sole means navigation is critical in the cases of interference, especially when loss of lock take place during periods longer than a few seconds. The integration of supplemental navigation systems (e.g. INS) is necessary, but not sufficient, as the duration of loss of lock is not predictable.

### 5.3. Findings

Many influences can cause degradation of GPS signals. Two of them are investigated: multipath and interference. These two GPS degradation sources are of interest, as they cannot be detected by a ground based integrity monitoring system.

#### Multipath

The range noise and multipath of the ground station has been estimated by subtracting the carrier phase from the code measurements and by eliminating other biases. It can be shown, that systematic errors are repeatable day by day with identical satellite constellations.

The multipath error was modeled with respect to the environment geometry and a receivers Delay Lock Loop (DLL). The verification of this model was carried out on a location with a well known environment geometry. It is seen, that the modeled error characteristics principally matches the measured multipath, but differences in the error size are present. It is also seen, that the multipath errors are very sensitive to small changes in the environment geometry.

Losses of lock of GPS signal during preliminary measurements at the airport of Lugano-Agno were recorded at certain satellite elevations. It is shown with a model, that these signal losses can be attributed to carrier phase multipath with reflections on the ground. This model can be used to make predictions on the satellite availability including loss of lock due to carrier phase multipath at ground stations.

#### Interference

Radio Frequency Interference (RFI) was detected on preliminary flights as well as during the test flights. The RFI influence on the flights is of main interest. For this purpose a software tool was created, which generates a map with potential regions exposed to RFI. Not only the location of potential interference but also the spectrum and the timely variation of the disturbing signal is of interest. Field tests with a spectrum analyzer were carried out. It is seen, that the disturbing signals did only partially cover the GPS L1 frequency. Furthermore the measured signal was too weak to create serious disturbance to the GPS receivers. Therefore it can be deduced, that timely variations were present and that the frequency environment and the RFI potential has to be monitored continuously.

## 6. Integrity Monitoring

### 6.1. Basics on Integrity Monitoring

#### 6.1.1. Introduction

The integrity parameter as defined in chapter 3.4 is the ability of a system to provide timely warnings to users when the system should not be used for navigation [RTCA, 1991], that means, when the system fails to meet the accuracy needed for a phase of flight. On the one hand, there are no requirements on the methods to be used for this purpose. On the other hand, the RTCA has defined following four GPS position integrity performance requirements:

Phase of Flight	Alarm Limit ( $AL$ )	Maximum Allowable Alarm Rate ( $MAAR$ )	Time to Alarm ( $TtA$ )	Minimum Detection Probability
En Route	2.0 $NM$	$0.002\ h^{-1}$	30 $sec$	0.999
Terminal	1.0 $NM$	$0.002\ h^{-1}$	10 $sec$	0.999
RNAV Approach (Non-Precision)	0.3 $NM$	$0.002\ h^{-1}$	10 $sec$	0.999

Table 6.1.: GPS position integrity performance requirements as defined by the RTCA.

These four parameters have to be understood as follows:

- Alarm Limit ( $AL$ ): a failure is defined to exist, when the GPS horizontal radial position error is outside the specified alarm limit.
- Maximum Allowable Alarm Rate ( $MAAR$ ): this parameter refers to the total alarm rate with the equipment in normal operation with no satellite malfunction.

- Time to Alarm (*TtA*): this parameter is defined to be the maximum allowable elapsed time from the onset of the failure until the time that the integrity alarm is annunciated.
- Minimum Detection Probability: detection probability is defined as 1 minus miss probability ( $P_{MD}$ ). Miss probability is the conditional probability that the detection algorithm decides that a failure is not present when, in fact, a failure exists.

These requirements are related to the detection of an error. That means, that after a detection the system is no more available. For this reason some algorithm tries to isolate the satellite with the malfunction. In such a way it is possible to delete the isolated satellite and to continue to navigate with the other ones, if integrity is given for these ones. The RTCA SC-159 Integrity Working Group has now defined, that a detection leads only to an alert, when the attempt, to exclude the anomalous satellite(s), fails [Lee *et al.*, 1996].

As shown in figure 6.1 it is mainly of interest to know the two probabilities  $P_{MD}$  of a missed detection and  $P_{FA}$  of a false alarm of a system.





	no alarm	alarm
normal operation		<div><div><math>P_{FA}</math></div><div>uneconomical</div></div>
failure	<div><div><math>P_{MD}</math></div><div>hazardous</div></div>	

Figure 6.1.: Integrity matrix describing the four possible combinations merged by the situation 'no alarm'/'alarm' and 'normal operation'/'failure'.

$P_{MD}$  can be calculated as follows:

$$P_{MD} = 1 - \text{Minimum Detection Probability}$$

(6.1)

The estimation of  $P_{FA}$  has to be derived from the *MAAR*, which depends highly on its interpretation. The definition given by the RTCA says, that the alarm rate should not be larger than a given value, when there is no malfunction of any satellite. This rate does not include the situations, where the position error is larger than the alarm limit (*AL*) due to the poor geometry of the satellites (high DOP's). An activation

of the alarm would be correct in this case, even if there is no satellite malfunction. These cases should be subtracted from the *MAAR* to achieve the  $P_{FA}$ . It is further noted, that errors caused by multipath or interference should also be subtracted from the *MAAR*, as these errors are not due satellite malfunction.

Different interpretations of the *MAAR* and calculation of the  $P_{FA}$  were found in the literature. [Lee, 1993] says, that the rate of alarm shall not be more than the *MAAR*, independent whether there is a true or false alarm. This interpretation does not exclude, that there is a true alarm due a satellite malfunction, which differs from the definition given by the RTCA.

[Sturza, 1990] derives  $P_{FA}$  as follows:

$$P_{FA} = \frac{TtA}{3600sec} \cdot MAAR \quad (6.2)$$

where the assumption is done, that an integrity decision is done in time steps equal to the *TtA*. Formula 6.2 can be used only, when it is excluded, that the position error would not violate the alarm limit due to poor satellite geometry without satellite malfunction.

Furthermore one has to distinguish between error detection, exclusion and isolation. A detection says that an error has occurred in the system. After a detection, the system is no more usable. An exclusion isolates some satellites, where one or more of them are the erroneous ones. Isolation, at least, isolates only the erroneous ones. Exclusion and isolation give the possibility to delete the erroneous satellites and to continue to navigate with the other ones. A post integrity check is required after the deletion of satellites to ensure, that no erroneous satellites are left in the calculations. The integrity requirements given by the RTCA relates only to the detection of an error.

Existing or proposed integrity monitoring techniques can mainly be divided into two categories, external and internal methods.

### 6.1.2. External Methods

These methods use informations, which are collected outside of the aircraft to achieve the required GPS integrity. These techniques are highly reliable in detecting and isolating erroneous satellites, as they are based on many redundant measurements and include important a priori information. The main disadvantage is, that it cannot detect or isolate errors, which are produced in the vicinity of the users (e.g. multipath and interference).

#### Integrity Channel

Most of the proposed solutions are using a network of ground based monitoring stations which collect GPS data and transfer them to a master station for

an integrity check. The result is disseminated mostly via satellite (see e.g. [Kalafus, 1989, Bellen and Naerlich, 1997]). Examples of this technique can be found on the Wide Area Augmentation System (WAAS) planned in the USA and on EGNOS in Europe. Similar methods can also be adapted to a smaller regions like the terminal area of an airport and with an uplink for the dissemination of information instead of a satellite. This could be connected with a Local Area Augmentation System (LAAS).

### 6.1.3. Internal methods (RAIM and AAIM)

These methods refer to techniques, which use either information from only the GPS receiver, known as Receiver Autonomous Integrity Monitoring (RAIM), or uses additional information from other aircraft sensors (e.g. inertial sensors), known as Aircraft Autonomous Integrity Monitoring (AAIM).

The main idea of internal methods is to calculate a test variable with the available information and to compare it against a threshold value to determine if integrity is given or not.

These methods have the ability to detect or isolate not only errors based on satellite failures, but also those which are created in the environment of the user. The main disadvantage is, that these methods have to work with less redundant measurements than external methods.

#### Position Comparison

This technique calculates the position by using all ( $n \geq 5$ ) tracked satellites and by using  $n$  subset with  $n - 1$  satellites. If there is no failure, then all position solutions obtained should cluster closely together. A failed satellite would scatter this cluster. A RAIM statistics can be calculated with these positions (e.g. size of cluster). The comparison of this RAIM statistics with precalculated thresholds values gives information on the system integrity [Lee, 1986, Misra *et al.*, 1993, Michalson, 1995].

#### Range Comparison

The range comparison technique is analogous to the position comparison technique. The only difference is, that the measurements residuals are used for comparison instead of the positions itself [Lee, 1986].

### Least Square Residuals (LSR)

This method is based on equation (3.1). The position is then calculated as

$$\vec{x} = (\mathbf{A}^T \mathbf{P} \mathbf{A})^{-1} \mathbf{A}^T \mathbf{P} \vec{f}. \quad (6.3)$$

The residuals of the measurements are

$$\begin{aligned} \vec{v} &= \vec{f} - \mathbf{A} \vec{x} \\ &= (\mathbf{I} - \mathbf{A}(\mathbf{A}^T \mathbf{P} \mathbf{A})^{-1} \mathbf{A}^T \mathbf{P}) \vec{f}, \end{aligned} \quad (6.4)$$

where

$\vec{v}$  = vector of measurement residuals.

[Parkinson and Axelrad, 1988] proposes to calculate the test variable  $r$  by means of the square sum of the residuals:

$$r = SSE = \vec{v}^T \vec{v}, \quad (6.5)$$

where

$SSE$  = test variable.

The threshold has to be selected in a way, that it fulfils the integrity requirements. The integrity procedure proposed by [Parkinson and Axelrad, 1988] calculates first a residual parameter  $r$  based on  $SSE$  for all satellites in view (at least six). If  $r$  is less than a detection threshold  $r_D$ , then it is assumed that all satellites are working properly. Otherwise a failure is detected and the residual parameters  $r^1, r^2, \dots, r^n$  are computed for the  $n$  subsets of  $n - 1$  satellites. If one  $r^i$  is larger than  $r_D$ , then the  $i^{th}$  satellite is assumed to be the erroneous one. An isolation is not possible, if there are more than one  $r^i$ 's larger than  $r_D$ .

[Walter and Enge, 1995] propose to fill the diagonal elements of the weight matrix  $\mathbf{P}$  depending on the elevation of the satellites to achieve a better result.

### Parity Method

The parity method was first suggested by [Sturza, 1988]. The design matrix  $\mathbf{A}$  in equation (6.3) is first transformed in a matrix representing a state space and a parity space. A parity vector can be constructed with the transformed design matrix and

the measurements  $\vec{f}$ . The parity vector is then used for fault detection. It is further shown in [Sturza, 1988] that the LSR and parity method yields the same results.

[Brown *et al.*, 1994] proposes an algorithm based on the parity method, which isolates two satellites, where one of them has to be the erroneous one. The isolation and skipping of two or more satellites, even if there are correct ones among them, is called partial identification.

## Integrated Systems

The use of additional information may help integrity monitoring algorithm to better detect an error. The aid of the barometric altitude is proposed by e.g. [Lee, 1993]. Combination with inertial navigation systems is described by e.g. [Brenner, 1990, Butzmühlen, 1996]. There is also the possibility to use radionavigation facilities (see e.g. [Brown, 1988]), but its availability depends strongly on the location. All these methods are called Aircraft Autonomous Integrity Monitoring (AAIM) and are more robust, but technically more complex than RAIM.

### 6.1.4. Combination of External and Internal Methods

The combination of external and internal RAIM methods as proposed by [Brown, 1989] would show some advantages. On the one hand, the external methods can fall back on a network of measurements. This allows, due to the large redundancy, a quick detection and isolation of a satellite failure. On the other hand, the internal RAIM method should be able to detect errors caused in the vicinity of the aircraft like multipath or interference. By this way, the internal and external methods can complement with each other.

### 6.1.5. Test Variable Thresholds

The selection of the threshold is as important as the construction of the test variables. In general there are three approaches to define threshold values:

- a threshold may keep a constant value during the entire phase of flight
- a threshold may keep a constant value only during a measurement epoch and changes e.g. with the satellite constellation
- a threshold is defined for each satellite separately

It is expected, that the quality of detection and isolation depends on the refinement of the threshold. The third point in the list above allows the detection and isolation of an erroneous satellite in one step.



## 6.2. Derivation of a LSR Based RAIM Method for Single Failure

### 6.2.1. Introduction

In this chapter an enhanced RAIM method is derived, which can be used for a single satellite failure situation. This method is based on the measurement residuals obtained from the least squares adjustment (see chapter 6.1.3, Least Square Residuals). The enhancement lies in the determination of thresholds for each measurement residual instead of the calculation of one threshold by means of the measurement residuals square sum. By this way the satellite constellation geometry can be taken better into consideration. Further this method allows to detect and isolate an erroneous satellite in one step.

The starting point is based analogously to the LSR method in equation (3.1). The weight matrix  $P$  is set equal to the unit matrix  $I$ . The position solution  $\vec{x}$  is then

$$\begin{aligned}\vec{x} &= (A^T A)^{-1} A^T \vec{f} \\ &= A^* \vec{f},\end{aligned}\tag{6.6}$$

where

$$A^* = (A^T A)^{-1} A^T.$$

The measurement residuals  $\vec{v}$  are

$$\begin{aligned}\vec{v} &= \vec{f} - A\vec{x} \\ &= (I - AA^*)\vec{f}.\end{aligned}\tag{6.7}$$

The assumption is made, that the measurement residuals  $\vec{v}$  are uncorrelated with normal distribution.

### 6.2.2. Modeled Errors

Measurement residuals  $\delta v_i$  will now be constructed for defined measurement errors  $\delta f_i$ . It is noted, that the measurements in equation (6.7) are replaced by measurement errors.  $\delta \vec{f}_i$  is a  $m$ -vector ( $m$  is the number of measurements) with zeros except the  $i^{th}$  element, which is set to  $\delta f_i$ :

$$\begin{aligned}\delta \vec{f}_i &= \delta f_i \vec{e}_i \\ &= [0, \dots, 0, \delta f_i, 0, \dots, 0]^T,\end{aligned}\tag{6.8}$$

where

$\vec{e}_i$  = unit vector in direction  $i$ .

$\delta \vec{f}_i$  represents an erroneous measurement of the  $i^{th}$  satellite.

Now  $\delta f_i$ 's have to be estimated so, that the position error is equal to the alarm limit  $AL$ .  $\vec{f}$  is replaced by  $\delta \vec{f}_i$  in equation (6.6):

$$\delta \vec{x}_i = \mathbf{A}^* \cdot \delta \vec{f}_i, \quad (6.9)$$

where

$\delta \vec{x}_i$  = position displacement induced by  $\delta \vec{f}_i$ .

The vector  $\delta \vec{x}_i$  has the following form:

$$\delta \vec{x}_i = [\delta x_{i1}, \delta x_{i2}, \delta x_{i3}, \delta x_{i4}]^T \quad (6.10)$$

where

$$\begin{aligned} \delta x_{i1} &= \mathbf{A}_{1i}^* \cdot \delta f_i \\ \delta x_{i2} &= \mathbf{A}_{2i}^* \cdot \delta f_i \\ \delta x_{i3} &= \mathbf{A}_{3i}^* \cdot \delta f_i \\ \delta x_{i4} &= \mathbf{A}_{4i}^* \cdot \delta f_i. \end{aligned} \quad (6.11)$$

The integrity boundary in the horizontal plane is given by a circle with radius  $AL$ . The following relation holds for a violation of the limits:

$$AL \leq \sqrt{\delta x_{i1}^2 + \delta x_{i2}^2}. \quad (6.12)$$

Equation (6.11) in (6.12) gives:

$$\delta f_i \geq \frac{AL}{\sqrt{\mathbf{A}_{1i}^{*2} + \mathbf{A}_{2i}^{*2}}}. \quad (6.13)$$

$\delta \vec{f}_i$  is now defined by equation (6.13) and the corresponding measurement residuals  $\delta \vec{v}_i$  can be estimated with equation (6.7):

$$\delta \vec{v}_i \geq (\mathbf{I} - \mathbf{A}\mathbf{A}^*)\delta \vec{f}_i. \quad (6.14)$$

### 6.2.3. Relations between the Measurement Residuals

The main idea is now, that every measurement of an epoch contributes with its noise and bias to the range residual  $\vec{v}$ . This means, that  $\vec{v}$  is a linear combination of  $\delta\vec{v}_i$ 's:

$$\vec{v} = \alpha_1\delta\vec{v}_1 + \alpha_2\delta\vec{v}_2 + \dots + \alpha_n\delta\vec{v}_n \quad (6.15)$$

where

$\alpha_i$  = contribution of  $i^{th}$  measurement.

Equation (6.15) can be written as:

$$\vec{v} = \mathbf{V}\vec{\alpha} \quad (6.16)$$

with

$$\mathbf{V} = [\delta\vec{v}_1, \delta\vec{v}_2, \dots, \delta\vec{v}_n] \quad (6.17)$$

and

$$\vec{\alpha} = [\alpha_1, \alpha_2, \dots, \alpha_n]^T. \quad (6.18)$$

The vector  $\vec{\alpha}$  contains the magnitude of the  $\delta\vec{v}_i$  contributing to  $\vec{v}$  and acts as test variable. A large error on the  $i^{th}$  range measurement invokes a large  $\alpha_i$ . An  $\alpha_i$  larger than 1 points at a violation of the alarm limit caused by the  $i^{th}$  satellite. The test variable  $\vec{\alpha}$  allows to detect and isolate a single failure. This test variable can be defined as follow:

$$\vec{\alpha} = \mathbf{V}^{-1}\vec{v}. \quad (6.19)$$

Unfortunately the matrix  $\mathbf{V}$  is singular as it will be shown.

Define a matrix  $\mathbf{U}$ :

$$\begin{aligned} \mathbf{U} &= (\vec{u}_1 \dots \vec{u}_n) \\ &= \mathbf{I} - \mathbf{A}\mathbf{A}^*, \end{aligned} \quad (6.20)$$

where  $\vec{u}_i$  is the  $i^{th}$  column-vector of matrix  $\mathbf{U}$ . With equation (6.20) in (6.14) it follows

$$\begin{aligned} \delta\vec{v}_i &= \mathbf{U}\delta\vec{f}_i \\ &= \mathbf{U}(\delta f_i \vec{e}_i), \end{aligned} \quad (6.21)$$

where

$$\vec{e}_i = i^{th} \text{ unit vector.}$$

Matrix  $\mathbf{V}$  can be written as

$$\begin{aligned} \mathbf{V} &= [\delta \vec{v}_1, \delta \vec{v}_2, \dots, \delta \vec{v}_n] \\ &= [\delta f_1 \vec{u}_1, \delta f_2 \vec{u}_2, \dots, \delta f_n \vec{u}_n]. \end{aligned} \quad (6.22)$$

It follows that

$$\det(\mathbf{V}) = \delta f_1 \cdot \delta f_2 \cdot \dots \cdot \delta f_n \cdot \det(\mathbf{U}). \quad (6.23)$$

If the determinant of  $\mathbf{V}$  is zero, then it follows that the determinant of  $\mathbf{U}$  is also zero. The  $\delta f_i$ 's have to be different to zero, otherwise this would mean that a  $\vec{f}_i$  without an error would create an error in the position, which does not make sense.

It can be shown, that  $\mathbf{U}$  is idempotent, that means that  $\mathbf{U}^2 = \mathbf{U}$ :

$$\begin{aligned} \mathbf{U}^2 &= (\mathbf{I} - \mathbf{A}(\mathbf{A}^T \mathbf{A})^{-1} \mathbf{A}^T)(\mathbf{I} - \mathbf{A}(\mathbf{A}^T \mathbf{A})^{-1} \mathbf{A}^T) \\ &= \mathbf{I} - 2 \cdot (\mathbf{A}(\mathbf{A}^T \mathbf{A})^{-1} \mathbf{A}^T) + (\mathbf{A}(\mathbf{A}^T \mathbf{A})^{-1} \mathbf{A}^T)^2 \\ &= \mathbf{I} - 2 \cdot (\mathbf{A}(\mathbf{A}^T \mathbf{A})^{-1} \mathbf{A}^T) + (\mathbf{A}(\mathbf{A}^T \mathbf{A})^{-1} \mathbf{A}^T \mathbf{A}(\mathbf{A}^T \mathbf{A})^{-1} \mathbf{A}^T) \\ &= \mathbf{I} - 2 \cdot (\mathbf{A}(\mathbf{A}^T \mathbf{A})^{-1} \mathbf{A}^T) + (\mathbf{A}(\mathbf{A}^T \mathbf{A})^{-1} \mathbf{A}^T) \\ &= \mathbf{I} - (\mathbf{A}(\mathbf{A}^T \mathbf{A})^{-1} \mathbf{A}^T) \\ &= \mathbf{U}. \end{aligned} \quad (6.24)$$

[Kshirsagar, 1983] shows, that if  $\mathbf{U} = \mathbf{I} - \mathbf{H}$  is an idempotent matrix, then

$$\begin{aligned} \text{rank}(\mathbf{I} - \mathbf{H}) &= \text{trace}(\mathbf{I} - \mathbf{H}) \\ &= \text{trace}(\mathbf{I}) - \text{trace}(\mathbf{H}) \\ &= m - r, \end{aligned} \quad (6.25)$$

where  $\mathbf{H}$  is the generalized inversion:

$$\mathbf{H} = \mathbf{A} \mathbf{A}^*. \quad (6.26)$$

[Kshirsagar, 1983] shows also, that

$$\begin{aligned} r &= \text{trace}(\mathbf{H}) \\ &= \text{rank}(\mathbf{H}) \\ &= \text{rank}(\mathbf{A}). \end{aligned} \quad (6.27)$$

The rank  $r$  of the  $m \times n$  matrix  $\mathbf{A}$  is at maximum the smaller value of  $m$  and  $n$  [Papula, 1990]. The rank  $r$  of  $\mathbf{A}$  has also to be at minimum  $n$ , otherwise it would not be possible to solve equation (6.6). It follows, that  $\text{rank}[\mathbf{A}] = n$ .

It follows, that the rank of  $\mathbf{U}$  is smaller than its dimension and consequently the determinant of  $\mathbf{U}$  and  $\mathbf{V}$  is equal to zero [Papula, 1990], respectively  $\mathbf{U}$  and  $\mathbf{V}$  are singular.

#### 6.2.4. Methods to Solve the Test Variable $\alpha$

Three approaches to solve the problem of the singular matrix  $\mathbf{V}$  are given. The first two are based on particular solutions of equation (6.16). The third approach tries to find similarities between the vectors  $\delta\vec{v}_i$  and  $\vec{v}$ .

##### Single Value Decomposition (SVD)

This method is based on a theorem, which says, that any  $m \times n$  matrix  $\mathbf{V}$  can be written as a product of an  $m \times n$  column-orthogonal matrix  $\mathbf{D}$ , an  $n \times n$  diagonal matrix  $\mathbf{E}$  with positive or zero diagonal elements  $e_i$ , and the transpose of an  $n \times n$  matrix [Press *et al.*, 1990]:

$$\mathbf{V} = \mathbf{D} \cdot [\text{diag}(e_i)] \cdot \mathbf{F}^T, \quad (6.28)$$

where  $\text{diag}(x_i)$  stands for a diagonal matrix  $\mathbf{X}$  with the  $i^{\text{th}}$  diagonal element equal to  $x_i$ .

It follows, that

$$\mathbf{D}^T \mathbf{D} = \mathbf{F}^T \mathbf{F} = \mathbf{I} \quad (6.29)$$

and

$$\mathbf{E}^{-1} = \left[ \text{diag} \left( \frac{1}{e_i} \right) \right] \quad (6.30)$$

for  $e_i \neq 0$ .

The inverse of  $\mathbf{V}$  is then:

$$\mathbf{V}^{-1} = \mathbf{F} \cdot \left[ \text{diag} \left( \frac{1}{e_i} \right) \right] \cdot \mathbf{D}^T \quad (6.31)$$

for  $e_i \neq 0$ . In the case, that  $e_i$  is very close or equal to zero, [Press *et al.*, 1990] recommends to replace  $\frac{1}{e_i}$  with zero. The amount of  $e_i$ 's equal to zero is equal to the rank defect of  $\mathbf{V}$ . Equation (6.31) finds a particular solution  $\vec{\alpha}_p$  for equation (6.16)

for the case, that  $\vec{v}$  is not in the range of  $\mathbf{V}$ .  $\vec{\alpha}_p$  does not exactly solve equation (6.16), but among all possible vectors  $\vec{\alpha}$ , it will do the closest possible job in the least square sense. That means

$$res = \min(|\mathbf{V}\vec{\alpha}_p - \vec{v}|) \quad (6.32)$$

where

$res$  = residual of solution.

More detailed explanations on SVD are also given in [Schwarz, 1988].

A procedure for the decomposition of  $\mathbf{V}$  to  $\mathbf{D}$ ,  $\mathbf{E}$  and  $\mathbf{F}$  is given in [Press *et al.*, 1990] and is used to find the needed variable  $\vec{\alpha}_p$ . Preliminary simulations with this procedure did not give satisfactory results. The resulting  $P_{MD}$  and  $P_{FA}$  are far away from the requirements. The problem may be, that the SVD does not solve the equation exactly, but tries to find a solution by means of equation (6.32).

### Similarity-Transformation

The similarity transformation (S-transformation) is used in geodesy to solve the problem of the network adjustment. There is also the problem of the inversion of a matrix with a rank defect (datum defect). It is possible to find with the S-transformation a particular solution  $\vec{x}$  with the condition:

$$\vec{x}^T \vec{x} = \text{minimal.} \quad (6.33)$$

[Just, 1979] has shown a way to find this particular solution  $\vec{x}$ , which can be adapted to the equation (6.15). The starting point is equation (6.7), which can be written as:

$$\vec{v} = \vec{f} - [\mathbf{A}_1 \mathbf{A}_2] \cdot \begin{bmatrix} \vec{x}_1 \\ \vec{x}_2 \end{bmatrix}, \quad (6.34)$$

where

$\vec{x}$  :  $\vec{x}$  is divided in a  $r$ -dimensional part  $\vec{x}_1$  and a  $(m-r)$ -dimensional part  $\vec{x}_2$ ,  
 $\mathbf{A}$  : observation matrix divided in  $\mathbf{A}_1$  and  $\mathbf{A}_2$  depending on  $\vec{x}_1$  and  $\vec{x}_2$ .

It follows the normal equation system:

$$\begin{bmatrix} \mathbf{A}_1^T \mathbf{A}_1 & \mathbf{A}_1^T \mathbf{A}_2 \\ \mathbf{A}_2^T \mathbf{A}_1 & \mathbf{A}_2^T \mathbf{A}_2 \end{bmatrix} \begin{bmatrix} \vec{x}_1 \\ \vec{x}_2 \end{bmatrix} - \begin{bmatrix} \mathbf{A}_1^T \vec{f} \\ \mathbf{A}_2^T \vec{f} \end{bmatrix} = 0. \quad (6.35)$$

Equation (6.35) can be written with the corresponding substitutions as:

$$\begin{bmatrix} \mathbf{N}_{11} & \mathbf{N}_{12} \\ \mathbf{N}_{21} & \mathbf{N}_{22} \end{bmatrix} \begin{bmatrix} \vec{x}_1 \\ \vec{x}_2 \end{bmatrix} - \begin{bmatrix} \vec{n}_1 \\ \vec{n}_2 \end{bmatrix} = 0, \quad (6.36)$$

where

$$\begin{aligned} \mathbf{N}_{11} &= \mathbf{A}_1^T \mathbf{A}_1 & \mathbf{N}_{12} &= \mathbf{A}_1^T \mathbf{A}_2 \\ \mathbf{N}_{21} &= \mathbf{A}_2^T \mathbf{A}_1 & \mathbf{N}_{22} &= \mathbf{A}_2^T \mathbf{A}_2 \\ \vec{n}_1 &= \mathbf{A}_1^T \vec{f} & \vec{n}_2 &= \mathbf{A}_2^T \vec{f}. \end{aligned}$$

By reducing the equation system (6.36) by the unknown parameters of  $\vec{x}_2$  it follows:

$$\mathbf{N} \vec{x}_1 = \vec{n}, \quad (6.37)$$

where

$$\begin{aligned} \mathbf{N} &= \mathbf{N}_{11} - \mathbf{N}_{12} \mathbf{N}_{22}^{-1} \mathbf{N}_{21} \quad \text{and} \\ \vec{n} &= \vec{n}_1 - \mathbf{N}_{12} \mathbf{N}_{22}^{-1} \vec{n}_2. \end{aligned}$$

$\mathbf{N}$  has still rank defect  $r$ . A particular condition is now defined as:

$$\mathbf{I}_0 \cdot \mathbf{H} \cdot \vec{x}_0 = 0, \quad (6.38)$$

where

- $\mathbf{I}_0$  = diagonal matrix with  $d$ -times diagonal element equal 1 and rest 0.
- $\mathbf{H}$  = matrix, which columns contains eigenvectors  $\vec{h}_i$  of the eigenvalues  $\lambda_i$  for  $\lambda_i \neq 0$  of  $\mathbf{N}$
- $\vec{x}_0$  = particular solution.

The relation between  $\vec{x}_1$  of equation (6.37) and  $\vec{x}_0$  is given by the S-transformation

$$\vec{x}_0 = \mathbf{S}_0 \vec{x}_1, \quad (6.39)$$

where

$$\mathbf{S}_0 = \mathbf{I} - \mathbf{H}(\mathbf{H}^T \mathbf{I}_0 \mathbf{H})^{-1} \mathbf{H}^T \mathbf{I}_0. \quad (6.40)$$

The particular solution  $\vec{x}_0$  fulfils the condition in equation (6.33). This solution is also identical to the Moore-Penrose-Inverse (Pseudoinverse) [Just, 1979].

This procedure is used to solve the problem in equation (6.16) but does not give satisfactory results, similar to the Single Value Decomposition. The problem may be, that the particular solution fulfils the condition in equation (6.33), which does not have to correspond to the exact solution in equation (6.16).

### 6.2.5. Comparison of Measurement Residuals

The procedures described in the two previous chapters do not give the expected results by finding a particular inverse. So a different approach has to be found to solve this problem. The main idea is, that the measurement residual  $\vec{v}$  for a single failure has to show some similarities to one of the vectors  $\delta\vec{v}_i$ . It should be possible to find the erroneous satellite by comparing the lengths of the projections of  $\vec{v}$  on  $\delta\vec{v}_i$  and the angles between these vectors.

The column vectors  $\delta\vec{v}_i$  of matrix  $\mathbf{V}$  span a  $(n - r)$ -dimensional, affin measurement residual space. Calculation in this space has to be done with respect to its characteristics, which can be described by the metric tensor  $\mathbf{G}$ :

$$\mathbf{G} = g_{ij} = \delta\vec{v}_i^T \delta\vec{v}_j. \quad (6.41)$$

The vector  $\vec{v}$  in equation (6.7) lies in this space. An error on the  $i^{\text{th}}$  measurement invokes a growth of  $\vec{v}$  in direction of  $\delta\vec{v}_i$  due to equation (6.14).

The vectors  $\vec{v}_{pi}$  are now defined as the projection of  $\vec{v}$  on  $\delta\vec{v}_i$ . The length of  $\vec{v}_{pi}$  is:

$$|\vec{v}_{pi}| = |\vec{v}| \cdot \cos \beta_i, \quad (6.42)$$

where the length of a vector  $\vec{v}$  is

$$|\vec{v}| = \sqrt{\vec{v}^T \cdot \mathbf{G} \cdot \vec{v}} \quad (6.43)$$

and the angle  $\beta_i$  between the vectors  $\vec{v}$  and  $\delta\vec{v}_i$  is:

$$\beta_i = \angle(\vec{v}, \delta\vec{v}_i) = \arccos \left( \frac{\vec{v}^T \cdot \mathbf{G} \cdot \delta\vec{v}_i}{|\vec{v}| \cdot |\delta\vec{v}_i|} \right). \quad (6.44)$$

Equation (6.43) and (6.44) in (6.42) gives:

$$|\vec{v}_{pi}| = \frac{\vec{v}^T \cdot \mathbf{G} \cdot \delta\vec{v}_i}{\sqrt{\delta\vec{v}_i^T \cdot \mathbf{G} \cdot \delta\vec{v}_i}}. \quad (6.45)$$

The factor  $\mu_i$  is defined as the relation between the lengths of  $\vec{v}$  and  $\delta\vec{v}_i$ :

$$\mu_i = \frac{|\vec{v}_{pi}|}{|\delta\vec{v}_i|}. \quad (6.46)$$



The test variables are now  $\mu_i$  and  $\beta_i$ . A violation of the *HAL* boundary by the  $i^{th}$  satellite is given, when following two conditions apply:

$$\begin{aligned} \mu_i &\geq 1 \quad \text{and} \\ \beta_i &\text{ minimal for } i = 1 \dots n. \end{aligned} \quad (6.47)$$

### 6.2.6. Time to Alarm *TtA*

The derived RAIM algorithm is a snapshot method. This means, that a test on integrity of the measurements can be done by using only one measurement epoch. The Time to Alarm (*TtA*) given in the requirements allows a latency of the alarm. This latency can be used to reduce the noise of the measurements by calculating mean values of the measurements of the last *TtA* seconds. The standard deviation of the resulting noise decreases to  $\sigma'_0$ :

$$\sigma'_0 = \frac{\sigma_0}{\sqrt{TtA \cdot SR}}, \quad (6.48)$$

where

$\sigma_0$  = measurement noise,  
 $SR$  = sampling rate of GPS receiver.

### 6.2.7. Simulations

Simulations are needed to verify the quality of the derived RAIM algorithm. These simulations have to cover an entire day to test different satellite geometries. Different strategies are possible in the selection of the satellites, which are used in the RAIM test. On the one hand the worst geometry with respect to the DOP's for the minimal needed number of satellites can be selected and gives very conservative results. On the other hand all possible combinations of all visible satellites can be chosen to represent the situations in a more operational use of GPS. All values of the measurement vector  $\vec{f}$  are selected randomly with a given standard deviation  $\sigma_0$  describing the noise in a fault-free situation. The simulations are based on DGPS, so that it can be assumed, that all biases are eliminated.

The size of  $\sigma_0$  is composed by forming the square sum of the single  $\sigma_x$  of the different error sources. Table 6.2 gives an overview of the selected  $\sigma_x$ , which are based on [Parkinson, 1994].  $\sigma_0$  is then

$$\sigma_0 = \sqrt{2(\sigma_{eph}^2 + \sigma_{clk}^2 + \sigma_{ion}^2 + \sigma_{trp}^2 + \sigma_{mpt}^2 + \sigma_{rec}^2)}. \quad (6.49)$$

The factor 2 has to be included due to the use of two receivers in the differential GPS mode.

Error Source	$\sigma_x[m]$
Ephemeris Data $\sigma_{eph}$	0.0
Satellite Clock $\sigma_{clk}$	0.7
Ionosphere $\sigma_{ion}$	0.7
Troposphere $\sigma_{trp}$	0.5
Multipath $\sigma_{mpt}$	1.0
Receiver $\sigma_{rec}$	0.2

Table 6.2.:  $\sigma$  values for differential GPS mode used in the simulations.

A loop ( $i = 1 \dots m$ ) is done for each satellite of a given constellation, where a linear growing bias is set on the  $i^{th}$  satellite. The loop is terminated, when the horizontal position shift reaches  $2 \cdot HAL$ . The position error can be calculated with equation (6.9) when using the measurement errors instead of the ranges and is used to test the RAIM alarm.

The integrity monitoring requirements are selected for the phase of flight of the non-precision approach (see table 6.1).

### 6.2.8. Verification and Modification

A first run is done with the method developed in the chapters 6.2.1 to 6.2.6. In a first step it is of interest to know, how the results of the simulations characterize the RAIM algorithm. The values  $P_{FA}$  and  $P_{MD}$  will be estimated only in a further step, after having done some modifications on the algorithm.

This simulation does not try to isolate and exclude the erroneous satellite yet and is also limited to the worst combination of six satellites with respect to the HDOP. The results of this simulation are represented in figure 6.2 top. The  $x$ -axis indicates the horizontal position shift. The vertical, bold line is set equal to the  $HAL$ . The  $y$ -axis indicates the probability of false alarm for the region left of  $HAL$ , respectively the probability of missed detections missed for the region right of  $HAL$ .

The diagram on the top can be characterized by three curves shown in the bottom diagram and denoted with 1 to 3. The solid part of curve 1 corresponds to the false alarms. Curve 2 can be interpreted analogous for the missed detections. The solid part of these two curves have their origin in the noise of the measurements as the modeled measurements  $\delta \tilde{f}_i$  in equation (6.8) does not contain noise terms. The peak of curve 1 and 2 can be reduced drastically by detecting and excluding the assumed erroneous satellite before the horizontal position shift reaches the  $HAL$ .

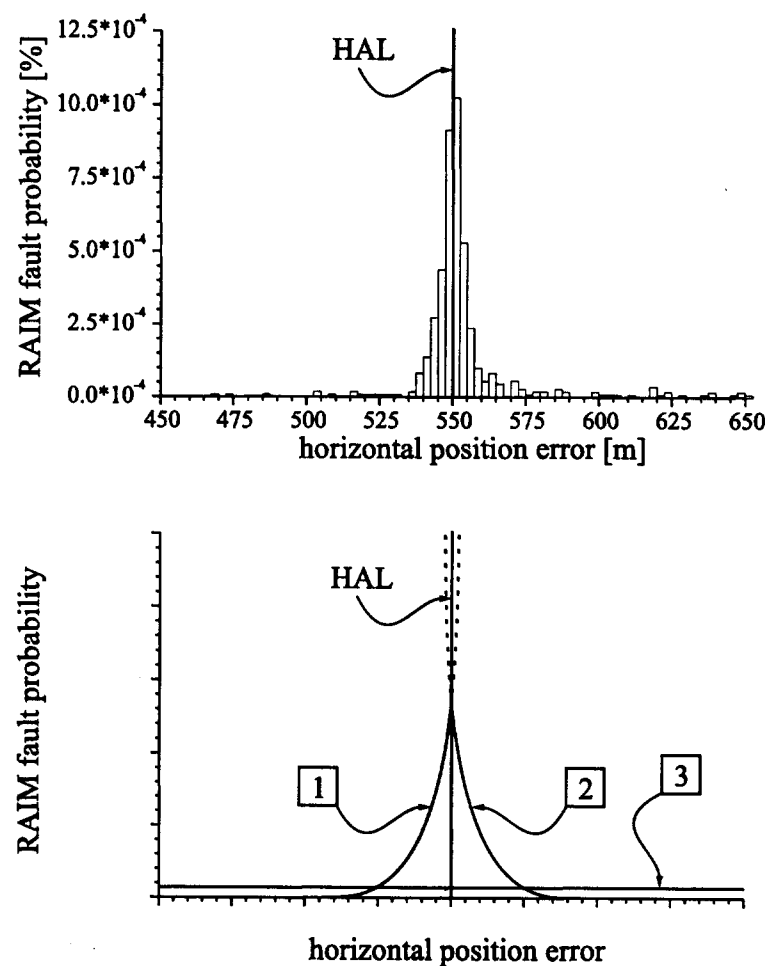


Figure 6.2.: Simulation results on the probability of false alarms  $P_{FA}$  and missed detections  $P_{MD}$  depending on the horizontal position error (top). The vertical bold line is set equal to the  $HAL$ . The region left of the  $HAL$  represents the probabilities of false alarms where the right side represents the probabilities of missed detections. The algorithm does not exclude a failed satellite in these simulations. This distribution can be modeled with three curves (bottom).

For this purpose a Horizontal Detection Limit (*HDL*) has to be defined as

$$HDL \leq HAL - \delta H, \quad (6.50)$$

where  $\delta H$  can be described as the detection noise induced by the measurement noise. The  $\delta H$  can be estimated as

$$\delta H = a \cdot \max |P_H A^* \vec{f}_\sigma| \quad (6.51)$$

where

$$P_H = \begin{bmatrix} 1 & 0 & 0 & 0 \\ 0 & 1 & 0 & 0 \\ 0 & 0 & 0 & 0 \\ 0 & 0 & 0 & 0 \end{bmatrix} \quad (6.52)$$

is the projection matrix of the resulting vector into the horizontal plane and

$$\vec{f}_\sigma = [\pm\sigma_0, \dots, \pm\sigma_0]^T. \quad (6.53)$$

All sign combinations for the elements of  $\vec{f}_\sigma$  have to be tested to find the largest  $\delta H$ . The value  $a$  defines the confidence interval.

Curve 3 is somewhat different. These faults are caused by a few satellites during a longer period of measurement bias growth. The vectors  $\delta\vec{v}_i$  have to be examined for these specific constellations to understand the cause for these faults. The angles  $\nu_{ij}$  between the vectors  $\delta\vec{v}_i$  and  $\delta\vec{v}_j$  can be calculated with equation (6.44). Two satellites  $i$  and  $j$  invoking faults of the type of curve 3 have small angles  $\nu_{ij}$ . This means, that the two satellites invoke residual vectors with similar direction, but normally with different lengths. Such a situation is represented in figure 6.3 and shows what happens during the detection and isolation process.

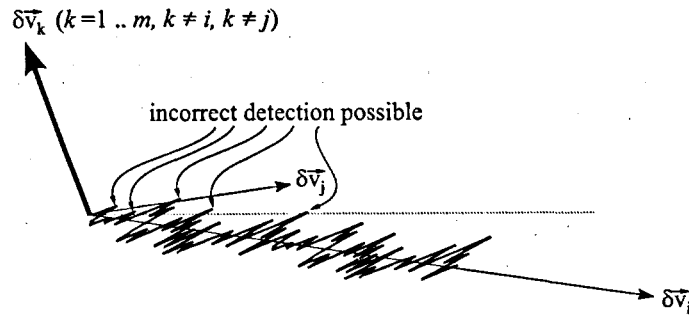


Figure 6.3.: Small angles between  $\delta\vec{v}_i$  and  $\delta\vec{v}_j$  can cause false detections when the range noise is enough large.

The two straight, thin arrows represent the residual vectors of the satellites  $i$  and  $j$ . The vertical vector represents the remaining  $(m - 2)$ -dimensional residual space. A measurement with a bias and noise on satellite  $i$  would create the 'noisy' line. The dashed line is the bisector between the two residual vectors. If the noise on the measurement residual is so large, that it passes the dashed line, then the algorithm assumes, that the error was invoked by satellite  $j$ . In these cases the algorithm checks the size of  $\mu_j$  instead of  $\mu_i$  and can cause false alarms, respectively missed detections.

A further simulation is done with a modified RAIM algorithm, which tries to isolate and exclude the erroneous satellite. The Horizontal Detection Limit  $HDL$  is set to  $500m$ . That means, that if an assumed horizontal position error of  $500m$  is reached, then the algorithm tries to isolate and exclude the erroneous satellite and checks the integrity with the reduced satellite constellation. All possible satellite constellation combinations are tested in this simulation with a time step of one hour. The results are presented in figure 6.4, analogous to figure 6.2. It is seen, that the peak at  $HAL$  disappears due to  $HDL \leq HAL - \delta H$ .

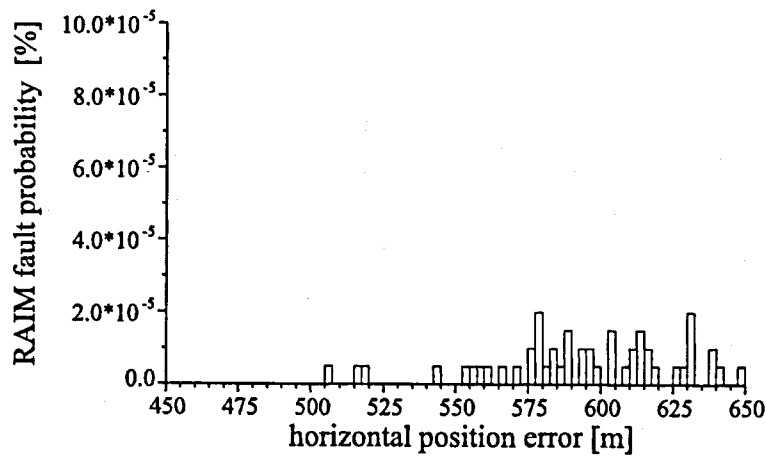


Figure 6.4.: Simulation results on the probability of false alarms  $P_{FA}$  and missed detections  $P_{MD}$  depending on the horizontal position error. The algorithm excludes failed satellites in these simulations.

### 6.2.9. RAIM Quality Prediction

The effect of small angles  $\nu_{ij}$  can be used for RAIM quality prediction. These angles can be estimated a priori, as they depend on the satellite constellation only. The  $\nu_{ij}$  has to be larger than a  $\nu_{min}$ , which depends mainly on the measurement noise  $\sigma_0$ .

Figure 6.5 shows the correlation between the amount of RAIM failures and the angle  $\nu_{ij}$  for a simulation with the *HDL* set to 500m. The y-axis represents the missed detections, respectively false alarms in dependence of the smallest  $\nu_{ij}$  of the constellation. It is seen, that the envelope lines do increase for smaller  $\nu_{ij}$ , which is a confirmation of the effect mentioned in chapter 6.2.8. The largest  $\nu_{ij}$  for missed detections is about 3.5° and for false alarms about 50°.

It is also noted, that problems with small  $\nu_{ij}$  appear only for constellations with few satellites. The  $\nu_{ij}$ 's for five satellites are either about 0° or 180° (figure 6.6). This means, that the  $\delta\vec{v}_i$ 's have all the same direction and differ only in its length and sign. The partial redundancy factors  $r_{ii}$

$$r_{ii} = \text{diag}(\mathbf{I} - \mathbf{A}\mathbf{A}^*) \quad (6.54)$$

with

$$r_{ii} \in [0, 1]. \quad (6.55)$$

describes the influence of the  $i^{th}$  measurement to the result  $\vec{x}$ . A  $r_{ii} = 0$  means, that the  $i^{th}$  measurement does not have any influence to the result. Investigations showed, that one  $r_{ii}$  is nearly always close to zero for the case of five satellites.

By increasing the number of satellites, the  $\nu_{ij}$  converges to 90° (figure 6.6) and the  $r_{ii}$  are much less close to zero.

The following check

$$\nu_{ij} > \nu_{min}, i = 1 \dots m, j = 1 \dots m, i \neq j \quad (6.56)$$

can be inserted into the RAIM algorithm just after the knowledge of  $\mathbf{A}$ . Should equation (6.56) not be fulfilled, then the satellite with the smaller  $|\delta\vec{v}_i|$  has to be deleted, if seven or more satellites are available. False alarms, respectively missed detections, can be avoided by this way, but requires to track more than six satellites.

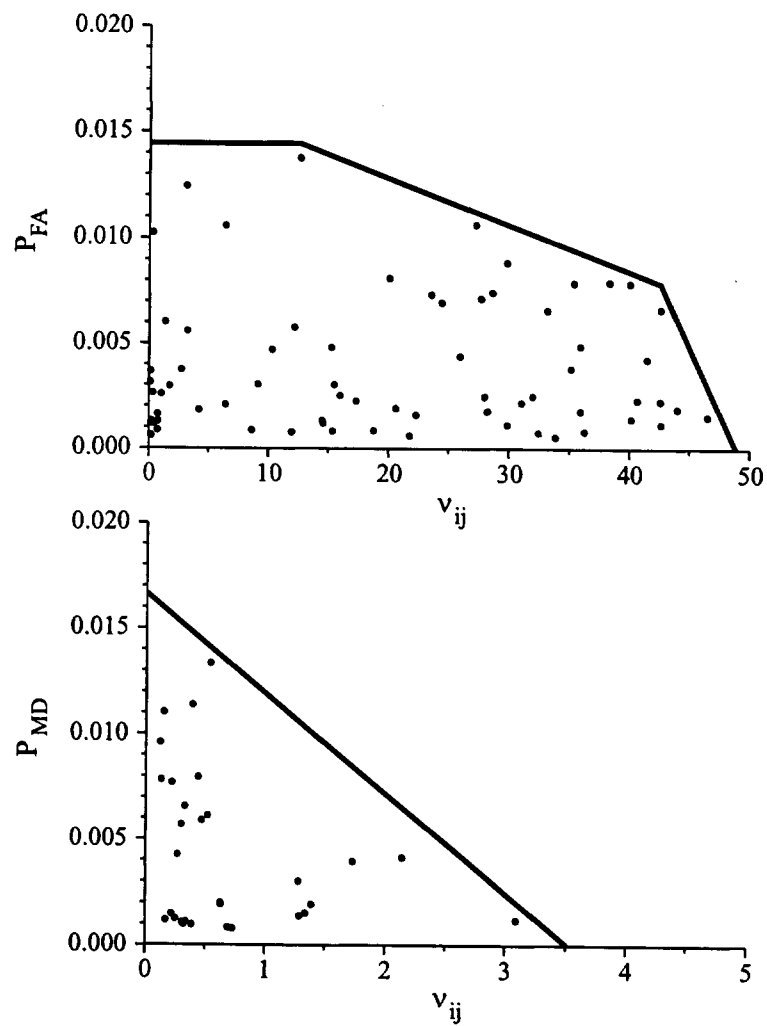


Figure 6.5.: False alarms (top) and missed detections depending on the angle  $\nu_{ij}$  between the residual vectors.

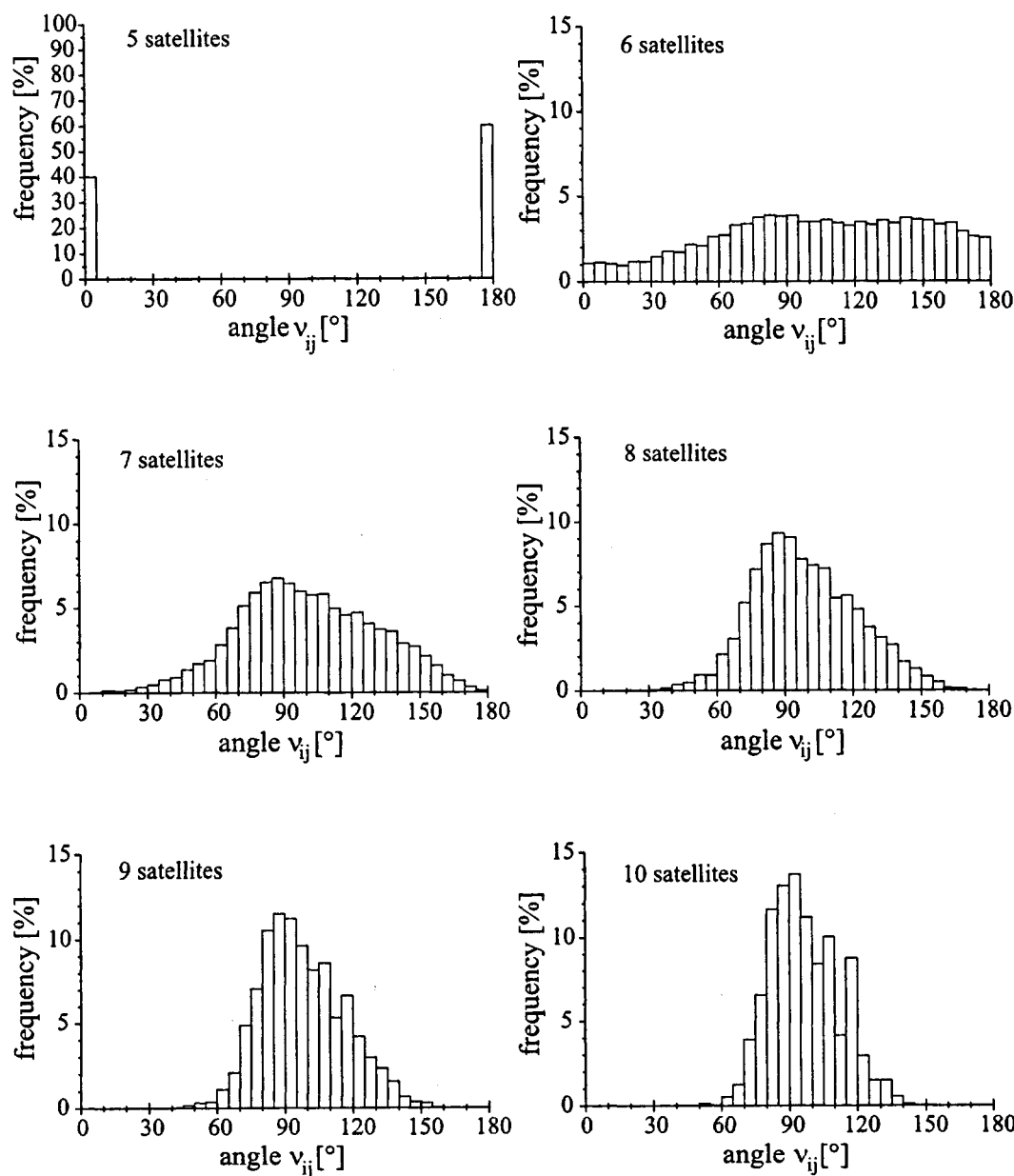


Figure 6.6.: Convergence of the amount of  $\nu_{ij}$ 's from 0°, respectively 180° towards 90° by increasing the number of satellites, which can be interpreted as a de-correlation of the residual vectors.



### 6.2.10. Single Failure RAIM Overview

An overview of the derived RAIM algorithm for the single failure case is shown as flow chart in figure 6.7. The first step comprises the determination of  $\mathbf{A}$  and  $\vec{f}$ , which is then modified to the mean of all measured  $\vec{f}$ 's during the period of the last  $TtA$  seconds. The angles  $\nu_{ij}$  are calculated to predict the RAIM quality for the given constellation, where satellites have to be deleted if necessary. The vectors  $\vec{v}$ ,  $\vec{v}_{pi}$  and the values  $\mu_i$  are then calculated with the remaining constellation. If  $\mu_i$  and the angle between  $\vec{v}$  and  $\delta\vec{v}_j$  do not fulfil equation (6.47) then no failure is assumed. Otherwise an alarm is set if only six or less satellites are available. If there are more satellites available, then  $i^{th}$  satellite has to be deleted.

### 6.2.11. RAIM Simulation Results

A simulation using all possible satellite constellations during one day with time steps of one hour is done. The range error increases with  $2ms^{-1}$ . This simulation comprises  $7.1 \cdot 10^6$  tests with 5658 different satellite constellations. The amount of false alarms is 251. It follows a

$$P_{FA} = 3.5 \cdot 10^{-5}, \quad (6.57)$$

which is 6.3 times poorer than the required  $5.56 \cdot 10^{-6}$  (see equation (6.2)).

The amount of missed detections is 114 with

$$P_{MD} = 1.6 \cdot 10^{-5}, \quad (6.58)$$

which is 62.5 times better than the required  $10^{-3}$  (see equation (6.1)).

It follows, that this RAIM algorithm does only partially fulfil the requirements. It is to point out, that these results are conservative, as the main part of the tested constellations comprise the minimum number of satellites. Further the quality of the results depends directly on the selected size of the noise and on the sampling rate of the GPS receiver (see equation (6.48)).

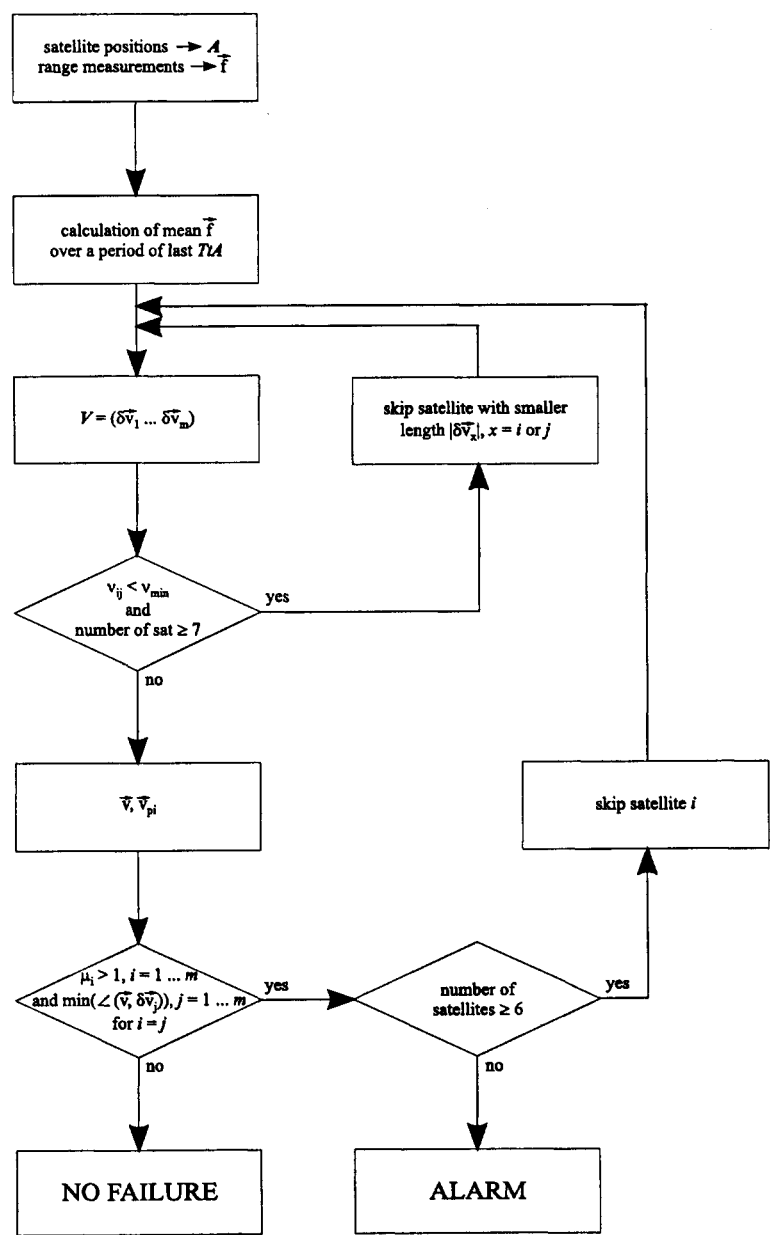


Figure 6.7.: Flow chart of derived RAIM algorithm for single satellite failure.

## 6.3. RAIM Enhancements

### 6.3.1. Dual Failure RAIM

The derived RAIM algorithm is designed for detection and isolation of only one failed satellite. Two or more failures are no more properly detected. An approach to solve the dual satellite failure case is based on the single satellite failure. Problems of this approach are further pointed out.

The matrix  $\mathbf{V}$  in equation (6.17) is needed as starting point. It is assumed, that the satellites  $i$  and  $j$  have a bias and the other measurement error are zero so that the measurement vector  $\delta \vec{f}_{ij}$  has the form:

$$\delta \vec{f}_{ij} = [0, \dots, 0, \delta f_i, 0, \dots, 0, \delta f_j, 0, \dots, 0]^T \quad (6.59)$$

analogous to equation (6.8).

The resulting measurement residual  $\vec{v}$  is then a linear combination of the  $\delta \vec{v}_i$  and  $\delta \vec{v}_j$  of  $\mathbf{V}$

$$\delta \vec{v}_{ij} = \mu_i \delta \vec{v}_i + \mu_j \delta \vec{v}_j, \quad (6.60)$$

where  $\mu_i$  and  $\mu_j$  are calculated with equation (6.46).

The square of the horizontal position shift  $b_{ij}^2$  induced by  $\delta \vec{f}_{ij}$  can be modeled as follow

$$\begin{aligned} b_{ij}^2 &= (\mathbf{P}_H \mathbf{A}^* \vec{f})^2 \\ &= (\mathbf{P}_H \mathbf{A}^* (\mu_i \delta \vec{f}_i + \mu_j \delta \vec{f}_j))^2 \\ &= (\mu_i \delta \vec{x}_i + \mu_j \delta \vec{x}_j)^2 \\ &= \mu_i^2 \delta \vec{x}_i^2 + 2\mu_i \mu_j \delta \vec{x}_i \delta \vec{x}_j + \mu_j^2 \delta \vec{x}_j^2, \end{aligned} \quad (6.61)$$

where  $\mathbf{P}_H$  is the projection matrix of the position into the horizontal plane (equation(6.52)). It follows for the length of  $b_{ij}^2$ :

$$\begin{aligned} |b_{ij}|^2 &= \mu_i^2 |\delta \vec{x}_i|^2 + 2 \cos(\nu_{ij}) \cdot \mu_i \mu_j |\delta \vec{x}_i| |\delta \vec{x}_j| + \mu_j^2 |\delta \vec{x}_j|^2 \\ &= \begin{bmatrix} \mu_i \\ \mu_j \end{bmatrix}^T \begin{bmatrix} |\delta \vec{x}_i|^2 & \cos \nu_{ij} |\delta \vec{x}_i| |\delta \vec{x}_j| \\ \cos \nu_{ij} |\delta \vec{x}_i| |\delta \vec{x}_j| & |\delta \vec{x}_j|^2 \end{bmatrix} \begin{bmatrix} \mu_i \\ \mu_j \end{bmatrix}, \end{aligned} \quad (6.62)$$

where  $\nu_{ij}$  can be obtained with equation (6.44) by using the  $\delta \vec{v}_i$  and  $\delta \vec{v}_j$  as vectors. The value  $|b_{ij}|$  is the first test variable and corresponds to  $\mu_i$  in equation (6.47). The

second test variable is the angle  $\gamma_{ij}$  between the vector  $\vec{v}$  and the plane builded by the vectors  $\delta\vec{v}_i$  and  $\delta\vec{v}_j$  as shown in figure 6.8. The angle  $\gamma_{ij}$  is zero for  $\delta f_{ij}$ .

A violation of the *HAL* boundary by the  $i^{th}$  and  $j^{th}$  satellites assumes following conditions:

$$\begin{aligned} \mu_{ij} &\geq 1 \quad \text{and} \\ \gamma_{ij} &\text{ minimal for } i = 1 \dots n, j = 1 \dots n \text{ and } i \neq j. \end{aligned} \quad (6.63)$$

Simulations with this algorithm have given very poor results. The main problem lies in the linear dependence of some  $\delta\vec{v}_i$ 's (see chapter 6.2.3). The angles  $\gamma_{ij}$  and  $\gamma_{il}$  are identical for the case of linear dependence of  $\delta\vec{v}_i$ ,  $\delta\vec{v}_j$  and  $\delta\vec{v}_l$ . In this case it is not possible to isolate the failed satellites.

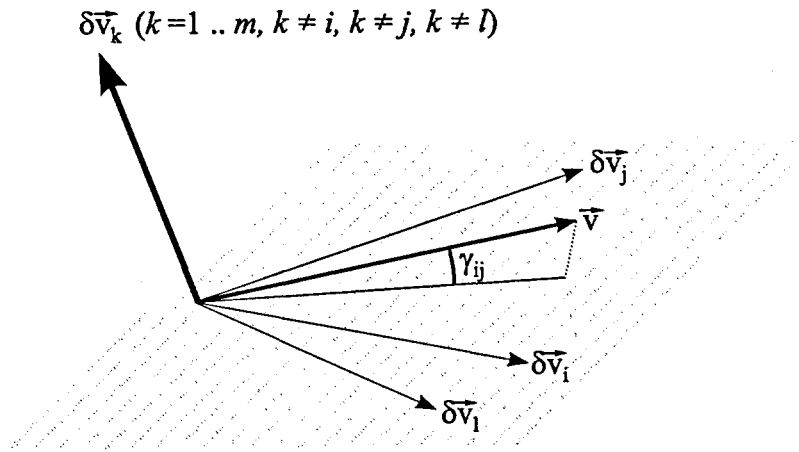


Figure 6.8.: Geometric representation of the residual vectors for a dual satellite failure RAIM algorithm approach.

### 6.3.2. Barometric Aided Integrity Monitoring

The RAIM algorithm derived shows some instabilities when using few satellites. Any additional measurement would improve the RAIM quality.

An additional measurement can be obtained with the barometric altitude (being a standard low cost aircraft equipment) without augmenting the number of unknowns. The design matrix  $\mathbf{A}$  can be extended by one row of the following form

$$[0, 0, 1, 0]. \quad (6.64)$$

The vector  $\vec{f}$  has to be extended with a value  $R_E + h$ , where

$R_E$  = earth radius  
 $h$  = altitude over sea level.

The altitude  $h$  has to be corrected with respect to the reference ellipsoid, geoid and local air pressure to obtain a geometrical altitude.

The weight matrix  $P$  has now to be selected other than  $I$ , due to the different accuracy of the GPS range and the barometric altitude.  $P$  is then

$$P = \begin{bmatrix} (\sigma_0^{-1})^2 & 0 & \dots & 0 \\ 0 & \ddots & & \vdots \\ \vdots & & (\sigma_0^{-1})^2 & 0 \\ 0 & \dots & 0 & (\sigma_{baro}^{-1})^2 \end{bmatrix}, \quad (6.65)$$

where

$\sigma_{baro}$  = standard deviation of barometric altitude.

The starting equation (6.6) is then

$$\vec{x} = (A^T P A)^{-1} A^T P \vec{f} \quad (6.66)$$

and all following calculations have to be done with respect to  $P$ . This kind of integrity monitoring is also called Aircraft Autonomous Integrity Monitoring (AAIM), as it uses additional information from the aircraft itself.

The size of  $\sigma_{baro}$  increases with the altitude. Estimations for  $\sigma_{baro}$  are given in [FAA, 1992, RTCA, 1996]. The  $\sigma_0$  is selected identical to table 6.2 and equation (6.49).

A first simulation is done with the worst constellations (five satellites and one barometer) with respect to the  $HDOP$  and different  $\sigma_{baro}$  values. Figure 6.9 represents the resulting  $P_{FA}$  and  $P_{MD}$  depending on the  $\sigma_{baro}$ . Both probabilities increases nearly linear with increasing  $\sigma_{baro}$ .

A simulation using all possible satellite constellations during one day with time steps of one hour is done. The range error increases with  $2ms^{-1}$ . This simulation comprises  $6.7 \cdot 10^6$  tests with 5658 different satellite constellations. This simulation did not detect any false alarms

$$P_{FA} = 0. \quad (6.67)$$

The amount of missed detections is 2. It follows:

$$P_{MD} = 3.0 \cdot 10^{-7}, \quad (6.68)$$

which is  $3.3 \cdot 10^3$  times better than the required.

These simulations shows, that the aiding of the barometer altitude improves the derived RAIM algorithm in such a way, that it fulfils the integrity requirements.

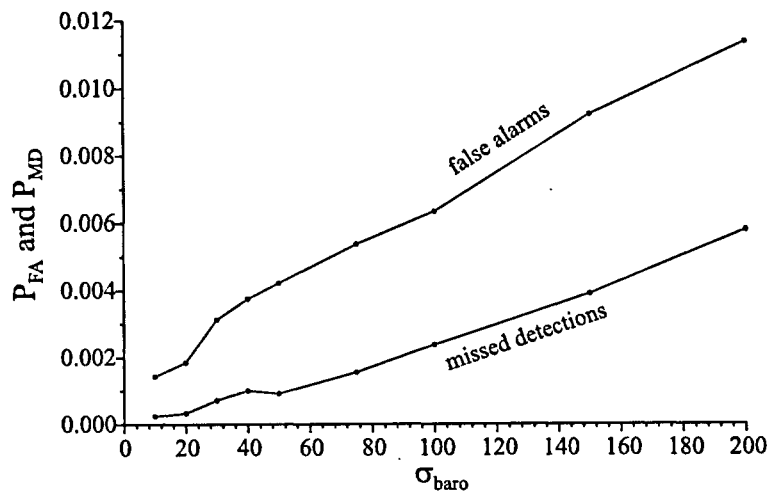


Figure 6.9.: Probability of false alarms  $P_{FA}$  and missed detections  $P_{MD}$  depending on the barometric error  $\sigma_{\text{baro}}$ .

## 6.4. Findings

The integrity of the navigation system, given by different parameters, has to be guaranteed. Different techniques were developed for this purpose. One of these is called Receiver Autonomous Integrity Monitoring (RAIM). This method tries to detect and exclude one or more failed satellites using only the information contained in the GPS signals. The reliability of RAIM algorithms is not always given due to the stringent integrity requirements.

A new, enhanced RAIM algorithm for one failed satellite is derived with the aim to fulfil the requirements. This algorithm is based on the least square range residuals as it is already used in other RAIM algorithms. The difference is, that alarm thresholds are defined for each signal in a vector space instead of only one scalar alarm threshold for all signals. This has the advantage, that error detection and isolation can be carried out in one step.

Extended simulations with different constellations and error sizes were carried out to test the RAIM quality. The probability of false alarm is 6 times poorer and of missed detection 28 times better than required. It is shown, that these errors strongly depend on the noise of the range measurements. It is also shown, that the RAIM quality is improved when increasing the number of used satellites.

Improvements can be reached by including measurements of additional airborne instruments resulting in an Aircraft Autonomous Integrity Monitoring (AAIM). The addition of the barometric altitude (being a standard low cost aircraft equipment) is selected, as these measurements can simply be implemented in the derived RAIM algorithm. Simulations were again carried out. No false alarm was detected where the probability of missed detection resulted to be  $3.3 \cdot 10^3$  times better than the requirements. It is seen, that the RAIM algorithm can be improved drastically and that the AAIM algorithm fulfils the requirements.

It is shown, that the extension of the RAIM algorithm for a dual failure situation fails. The main problem lies in the linear dependence of the modeled range residuals. Consequently this RAIM algorithm is applicable on single satellite failures only. However, the single satellite failure algorithm may be applied in an iterative manner in order to detect in favourable cases multi satellite failures.

## 7. Summary and Conclusions

### 7.1. The Lugano Trials

Satellite based navigation gives the opportunity to perform enhanced approach procedures. The Federal Office of Civil Aviation (FOCA) has initiated and leads in cooperation with different institutions the Lugano GPS approach trials. Their aim is to gain experience and insight into modern satellite navigation systems and its performance. The objective is planned to be achieved by carrying out a large number of approaches under operational conditions with data recording and scientific analysis.

Unfortunately, technical problems appeared so that, until now, only two missions with nine approaches were flown. Vertical guidance as well as the Course Deviation Indicator (CDI) during curved flight were not available. The Ground Proximity Warning System (GPWS) alarm was activated when overflying the mountain peak 'Cima dell'Uomo'. The first phase of the trials, which served for a fine tuning of the approach procedure and navigation system, could not be concluded successfully.

Nevertheless nine hours of data were recorded. Not all data labels were recorded during the first flight mission. The dataset of the second flight was complete. Consequently the investigations were done on the second flight. The ground station worked properly during the whole flight time. The investigations are based on the Required Navigation Performance (RNP) parameters (accuracy, integrity, availability, and continuity) as used for certifications of satellite based navigation systems.

### 7.2. Required Navigation Performance

The accuracy of the Pseudo Range Corrections (PRC), the GPS position of the aircraft operational system and the approach flights are analysed in this chapter.

The PRC of the operational and the measurement system shows very large differences, most of them lying in the range of  $\pm 20m$ . A systematic error, depending on the satellite elevation, is revealed. It is assumed that these errors are caused by the use of different atmospheric models for path delay reduction. This does not create problems when ground reference and airborne equipment uses both the same



atmospheric reduction models. These models would have to be prescribed for all receivers to avoid an accuracy degradation.

The accuracy of the aircraft position (Navigation System Error, NSE) is estimated for the stand-alone and differential GPS (DGPS) mode separately by comparing the positions of the operational system with the GPS carrier phase positions of the measurement system. The mean cross-track and along-track position differences are in the range of 0.5 to 1.5 *m*. The  $1\sigma$ -value is for the stand-alone mode in the range of 23 *m* and in the DGPS about 13 *m*. The mean vertical position difference is nearly 48 *m* in the stand-alone mode. It can be shown that this difference corresponds to the geoidal undulation. It is assumed that the operational system corrects its altitude with a geoidal undulation whilst the measurement system does not make this corrections. Similar to the atmospheric models, the geoid model has to be prescribed for all receivers to avoid accuracy degradation. This degradation is eliminated when operating in the DGPS mode. Nevertheless, the mean vertical difference is still more than 6 *m*.

The investigations on the Total System Error (TSE) of the approaches have to be restricted to the lateral fraction and to straight approach legs only due to the problems with the vertical guidance and the CDI. Reasonable investigations are possible on three, respectively four, approaches. This small number of approaches does not allow to make any statistical significant statement on the system accuracy. Nevertheless it gives an idea of the accuracy performance of the navigation system. The examined approaches are divided into a GPS stand-alone and a DGPS part. The mean Total System Error (TSE) in the stand-alone mode is -0.67% and the  $1\sigma$ -value 6.22% of the tunnel width. The corresponding values for the DGPS mode are -4.16% and 4.46% respectively. These values show the accuracy potential of satellite based navigation systems.

Investigations on the TSE probability distributions show that these errors are not normal distributed. Attention has to be given when statistics are carried out on such data.

Finally, the influence of the Selective Availability (SA) on the aircraft control system and consequently its accuracy is analysed. For this purpose a simple control system algorithm and modeled SA is chosen. It is seen that control systems can enter into resonance with the SA, causing an accuracy degradation.

Technical problems prevented a recording of the system integrity flag, so that statements on integrity, availability and continuity are not possible. These parameters are nevertheless treated theoretically in the following chapters.

### 7.3. Satellite Visibility and Geometry

The availability and continuity depends, among other factors, on the number of visible satellites and their constellation. Six visible satellites at minimum are manda-

tory in order to provide navigation and Receiver Autonomous Integrity Monitoring (RAIM) capability. Sufficient satellite visibility and resulting Dilution Of Precision (DOP) is conditional for the availability and continuity of the navigation system. Approach simulations with real satellite constellations are carried out including cut off angle, terrain masking extracted from a Digital Terrain Model (DTM), modeled flight dynamics (roll, pitch and heading of aircraft), and aircraft body masking. The first three mentioned influences can sometimes have a large impact on satellite visibility. Contrary to expectation, the aircraft body almost does not affect the satellite visibility as the antenna is mounted on top of the fuselage where the obstructions are negligible. The simulations shows, that the influences of terrain, aircraft attitude and cut off angle together can reduce the number of visible satellites during short periods to three. Six or less satellites are visible during 5.9 % of a day where a GDOP larger than 5 occurs during 1.34 % of a day. The flight through the gaps with less than six satellites would last 20 to 30sec. The GDOP reaches partially large values which would make the navigation system unusable.

Additional satellites and/or pseudolites would offer the possibility of bridging such critical situations. Simulations with GPS and additionally the Russian GLObal Navigation Satellite System (GLONASS), three geostationary INMARSATs, the planned European Navigation Satellite System (ENSS), and two pseudolites placed 2.5km in front of the runway showed significant improvements. The addition of GLONASS, respectively ENSS, can solve these problems. The pseudolites could enhance the continuity but at least three are needed. The INMARSATs can contribute only to a slight improvement.

A comparison of the number of tracked satellites during the flights with the predicted number of visible satellites using the real aircrafts position and attitude occasionally shows up to four non-tracked satellites. This is mainly caused by the unknown receiver antenna characteristics. It is also noted that sometimes more satellites than expected are tracked. It can be shown that these satellites lie down to  $-37^\circ$  beneath the antenna horizon. Multipath and refraction can be excluded as the cause. It is assumed, that the GPS signal is conducted via the aircraft fuselage shell to the antenna which can provoke uncontrolled effects on the range measurements and, consequently, also on the GPS position. For this reason it would be advantageous to use a small cut off angle in the aircraft fixed coordinate system.

## 7.4. Multipath and Interference

Many influences can cause degradation of GPS signals. Two of them are investigated: multipath and interference. These two GPS degradation sources are of interest, as they cannot be detected by a ground based integrity monitoring system.

The range noise and multipath of the ground station has been estimated by subtracting the carrier phase from the code measurements and by eliminating other biases.

It can be shown that systematic errors are repeatable day by day with identical satellite constellations.

The multipath error was modeled with respect to the environment geometry and a receivers Delay Lock Loop (DLL). The verification of this model was carried out on a location with a well-known environment geometry. It is seen that the modeled error characteristics principally matches the measured multipath, yet differences in the error size are present. It is also seen that the multipath errors are very sensitive to small changes in the environment geometry.

Losses of lock of GPS signal during preliminary measurements at the airport of Lugano-Agno were recorded at certain satellite elevations. It is shown with a model, that these signal losses can be attributed to carrier phase multipath with reflections on the ground. This model can be used to make predictions on the satellite availability including loss of lock due to carrier phase multipath at ground stations.

Radio Frequency Interference (RFI) was detected on preliminary flights as well as during the test flights. The RFI influence on the flights is of main interest. For this purpose a software tool was created which generates a map with potential regions exposed to RFI. Not only the location of potential interference but also the spectrum and the timely variation of the disturbing signal is of interest. Field tests with a spectrum analyzer were carried out. It is seen that the disturbing signals did only partially cover the GPS L1 frequency. Furthermore the measured signal was too weak to create serious disturbance to the GPS receivers. Therefore it can be deduced that timely variations were present and that the frequency environment and the RFI potential have to be monitored continuously.

## 7.5. Integrity Monitoring

The integrity of the navigation system, given by different parameters, has to be guaranteed. Different techniques were developed for this purpose. One of these is called Receiver Autonomous Integrity Monitoring (RAIM). This method tries to detect and exclude one or more failed satellites using only the information contained in the GPS signals. The reliability of RAIM algorithms is not always given due to the stringent integrity requirements.

A new, enhanced RAIM algorithm for one failed satellite is derived with the aim to fulfil the requirements. This algorithm is based on the least square range residuals as it is already used in other RAIM algorithms. The difference is that alarm thresholds are defined for each signal in a vector space instead of only one scalar alarm threshold for all signals. This has the advantage that error detection and isolation can be carried out in one step.

Extended simulations with different constellations and error sizes were carried out to test the RAIM quality. The probability of false alarm is 6 times poorer and of missed detection 28 times better than required. It is shown that these errors strongly

depend on the noise of the range measurements. It is also shown that the RAIM quality is improved when increasing the number of used satellites.

Improvements can be achieved by including measurements of additional airborne instruments resulting in an Aircraft Autonomous Integrity Monitoring (AAIM). The addition of the barometric altitude (being a standard low cost aircraft equipment) is selected, as these measurements can simply be implemented in the derived RAIM algorithm. Simulations were again carried out. No false alarm was detected where the probability of missed detection resulted to be  $3.3 \cdot 10^3$  times better than the requirements. It is seen that the RAIM algorithm can be improved drastically and that the AAIM algorithm fulfils the requirements.

It is shown that the extension of the RAIM algorithm for a dual failure situation fails. The main problem lies in the linear dependence of the modeled range residuals. Consequently this RAIM algorithm is applicable on single satellite failures only. However, the single satellite failure algorithm may be applied in an iterative manner in order to detect, in favourable cases, multi satellite failures.

## 7.6. Final Remarks

The results of the test flights show that satellite based approaches and landings are in principle possible. Statistic analysis of a large number of flights is nevertheless essential to assure the required system quality. The accuracy of the few flown approaches is much better than required. Theoretical investigations show that the continuity of the system can be critical at some parts of the approach, especially when flying with large roll angles at low altitudes in rugged terrain. Enhancement of GPS could be required. Availability of GPS is given for the stand alone mode where the correction values were not available when DGPS was required due to the mountainous area. The integrity of the operational system in use could not be tested as the system warning flags could not be recorded. Simulations with an enhanced RAIM/AAIM algorithm, developed at our institute, shows that single satellite failures or erroneous range measurements can be detected.

This project lead to an advantageous cooperation between different partners and resulted in an increased experience and knowledge in satellite navigation systems.

# Acknowledgment

My thanks are addressed to all those people who contributed to the successful completion of this work. These are in alphabetical order:

R. Aebersold, Swiss Federal Office of Civil Aviation  
 M.G. Bähler, Swisscontrol  
 T. Brandt, Crossair  
 T. Buchanan, Federal Office of Civil Aviation, now with Swisscontrol  
 F. Butsch, Institute of Navigation of the University of Stuttgart  
 M. Cerniar, Geodesy and Geodynamic Laboratory, ETH Zürich  
 M. Cocard, Geodesy and Geodynamic Laboratory, ETH Zürich  
 A. Dosé, Crossair  
 H. Doswald, Swiss Aircraft Factory  
 J. Dütsch, Swiss Federal Office of Civil Aviation  
 U. Ewert  
 E. Favey, Geodesy and Geodynamic Laboratory, ETH Zürich  
 A. Geiger, Geodesy and Geodynamic Laboratory, ETH Zürich  
 P. Genou, Swisscontrol  
 S. Glöckler  
 K. Green, Crossair  
 H. Grob, Swiss Federal Office of Civil Aviation  
 F. Härrli, Swiss Federal Office of Civil Aviation  
 R. Hübscher, Eidgenössische Vermessungsdirektion und Vermessungsflugdienst  
 M. Huwiler, Swisscontrol  
 H.-G. Kahle, Geodesy and Geodynamic Laboratory, ETH Zürich  
 H. Kummer, Swisscontrol  
 H. Lang, Swiss Federal Office of Civil Aviation  
 U. Lauener, Swisscontrol. now with Swiss Federal Office of Civil Aviation  
 W. Lechner, Telematica  
 G. Marcionni, Airport of Lugano-Agno  
 G. Meier, Swisscontrol  
 B. Meier-Joseph, Crossair  
 M. Montanari, Swisscontrol  
 I. Muntwiler, Swiss Air Force  
 Y. Peter, Geodesy and Geodynamic Laboratory, ETH Zürich

M. Rothacher, Astronomical Institute of the University of Berne  
D. Rusca, Airport of Lugano-Agno  
W. Santschi, Swiss Federal Office of Topography  
G. Scaramuzza  
M. Schulte-Elte, Swisscontrol  
M. Schwendener, Swisscontrol, now with Deutsche Flugsicherung  
R. Suter, Swisscontrol  
B. Tiemeyer, Eurocontrol Experimental Centre  
D. Waser, Crossair  
R. Waser, Crossair  
B. Werffeli, Swiss Air Force  
U. Wild, Swiss Federal Office of Topography

# Bibliography

- [Auber *et al.*, 1994] J.-C. Auber, A. Bibaut, and J.-M. Rigal. Characterization of Multipath on Land and Sea at GPS Frequencies, 1994. Proceedings of ION GPS-94, pp. 1155–1171.
- [Axelrad, 1994] P. Axelrad. Use of Signal-to-Noise Ratio for Multipath Error Correction in GPS Differential Phase Measurements: Methodology and Experimental Results, 1994. Proceedings of ION GPS-94, pp. 655–666.
- [Bauer, 1992] M. Bauer. Vermessung und Ortung mit Satelliten. Herbert Wichmann Verlag GmbH, Karlsruhe, 1992. 3. Auflage.
- [BAZL AG OPS, 1995] BAZL AG OPS. Protokoll 11. Sitzung DGPS Lugano AG OPS, August 1995. Reg. Nr. 544-pip, 30.8.1995.
- [Bellen and Naerlich, 1997] W. Bellen and S. Naerlich. Participation in the EG-NOS Project from the Viewpoint of the German Air Navigation Services (DFS). Proceedings of the First European Symposium on Global Navigation Satellite Systems, GNSS97, Volume I, p. 255–267, DGON, Munich, Germany, 1997.
- [Blomenhofer and Hein, 1995] H. Blomenhofer and G. W. Hein. Tropospheric Effects in DGPS and their Removal During Precision Approach and Automatic Landing. In *International Symposium on Precision Approach and Automatic Landing, 21–24 February 1995, Braunschweig, Germany*. Deutsche Gesellschaft für Ortung und Navigation, 1995.
- [BMV, 1996] BMV. Deutscher Funknavigationsplan 1996, 1996. Schlussbericht zum Forschungsvorhaben Nr. L-2/95-50137/95, Bundesministerium für Verkehr.
- [Braasch and Snyder, 1998] M. Braasch and C. Snyder. Running Interference: Testing a Suppression Unit. *GPS World*, 9(3):50–54, March 1998.
- [Braasch, 1994] M. Braasch. GPS and DGPS Multipath Effects and Signal Modelling, 1994. ION GPS-94 Tutorial, Course 625.
- [Brenner, 1990] M. Brenner. Implementation of a RAIM Monitor in a GPS Receiver and an Integrated GPS/IRS, 1990. Proceedings of ION GPS-90, pp. 397–406.
- [Brockhaus, 1994] R. Brockhaus. Flugregelung. Springer-Verlag, Berlin, 1994.

- [Brown *et al.*, 1994] R. Brown, J. Kraemer, and G. Nim. A Partial Identification RAIM Algorithm for GPS Sole Means Navigation, 1994. Proceedings of ION GPS-94, pp. 557–566.
- [Brown, 1988] A. K. Brown. Civil Aviation Integrity Requirements for the Global Positioning System. *Journal of The Institute of Navigation*, 35(1):23–40, Spring 1988.
- [Brown, 1989] R. G. Brown. RAIM and GIC Working Together: The Ultimate Solution to the GPS Integrity Problem. *Journal of The Institute of Navigation*, 36(2):173–178, Summer 1989.
- [Bürki *et al.*, 1992] B. Bürki, M. Cocard, A. Geiger, R. Gyger, and H.-G. Kahle. Development of a portable dual frequency microwave water vapor radiometer for geodetic applications. Proceedings of the Symposium in Refraction of Transatmospheric Signals in Geodesy, Publ. Geod., 36, p. 129 - 133, Neth. Geod. Comm., De Hague, 1992.
- [Butsch, 1997] F. Butsch. Lugano Field Tests, 1997. Institute of Navigation, University of Stuttgart.
- [Butzmühlen, 1996] C. Butzmühlen. Ensuring the GNSS Onboard Integrity Function under Adverse Conditions – Feasibility and Flight Test Results. ION National Technical Meeting, Santa Monica, CA, 1996.
- [CCIR, 1986] CCIR. Recommendations and Reports of the CCIR, 1986, Propagation in Non-Ionized Media, 1986. XVIth Plenary Assembly, International Telecommunication Union, International Radio Consultative Committee, Volume V.
- [Cerniar, 1997] M. Cerniar. Modellierung des Multipath-Effektes auf GPS Codemessungen. Semesterarbeit, GGL, ETH Zürich, Schweiz, 1997.
- [CH-RNP, 1998] CH-RNP. Schweizerischer Radionavigationsplan (CH-RNP), 1998. ed. Bundesamt für Zivilluftfahrt (FOCA), V0.12.
- [Chaperon, 1988] F. Chaperon. Vermessungskunde. Skript zur Vorlesung, Institut für Geodäsie und Photogrammetrie, ETH Zürich, 1988.
- [Clark, 1992] T. Clark. GPS Antennas. De-Mystifying Multipath, 1992.
- [Cobb and O'Connor, 1998] S. Cobb and M. O'Connor. Pseudolites: Enhancing GPS with Ground-based Transmitters. *GPS World*, 9(3):55–60, March 1998.
- [Cocard, 1994] Marc Cocard. *High Precision GPS Processing in Kinematic Mode*. PhD thesis, Swiss Federal Institute of Technology, Zürich, 1994.



- [Department of Defence, 1993] Department of Defence. Technical Characteristics of the NAVSTAR GPS. Navtech Seminars and Navtech Book and Software Store, Inc., from U.S. Government Document, 1993.
- [DoT and DoD, 1997] DoT and DoD. Federal Radionavigation Plan 1996. Department of Transportation and Department of Defense, Washington, DC, USA, 1997. DOD-4650.5/DOT-VNTSC-RSPA-97-2.
- [Duerr, 1992] T. Duerr. Effect of Terrain Masking on GPS Position Dilution of Precision. *Journal of The Institute of Navigation*, 39(3):317-323, Fall 1992.
- [EEC, 1994a] EEC. GNSS Integrity Monitoring at High Latitudes, Evaluation of Data Collected during Flight Trial in DRA BAC 1-11, October 1994. Executive Summary of EEC Report No.297, EEC Task AT65, EATCHIP Task FCO.ET3.ST07.
- [EEC, 1994b] EEC. GNSS Integrity Monitoring at High Latitudes, Flight Trial in DRA BAC 1-11, October 1994. Executive Summary of EEC Report No.296, EEC Task AT65, EATCHIP Task FCO.ET3.ST07.
- [FAA, 1992] FAA. Airborne Supplemental Navigation Equipment Using the Global Positioning System, October 1992. Technical Standard Order TSO-C129.
- [FAA, 1994] FAA. IFR Approval for Differential GPS Special Category I Instrument Approaches Using Private Ground Facilities, September 1994. FAA Order 8400.11.
- [Flament and Pieplu, 1997] D. Flament and J. M. Pieplu. GLONASS Contribution to EGNOS Performance. Proceedings of the First European Symposium on Global Navigation Satellite Systems, GNSS97, Volume I, p. 69-77, DGON, Munich, Germany, 1997.
- [Geiger, 1990] A. Geiger. Gravimetrisches Geoid der Schweiz: Potentialtheoretische Untersuchungen zum Schwerfeld im Alpenraum. Geodätisch-geophysikalische Arbeiten in der Schweiz, Band 43, Schweizerische Geodätische Kommission, 1990.
- [Geiger, 1996] Alain Geiger. Verzerrungs-Analyse, Interpolation und Approximation. Technical Report 254, Institute of Geodesy and Photogrammetry, ETHZ, Zürich, 1996.
- [Green *et al.*, 1989] G. Green, P. Massatt, and N. Rhodus. The GPS 21 Primary Satellite Constellation. *Journal of The Institute of Navigation*, 36(1):9-24, Spring 1989.
- [Hein *et al.*, 1997] G. Hein, H. Su, and B. Eissfeller. Orbit Determination of Geosynchronous Satellites of a European Satellite Navigation System (ENSS). Proceedings of the First European Symposium on Global Navigation Satellite Systems, GNSS97, Volume II, p. 479-488, DGON, Munich, Germany, 1997.

- [Herring, 1992] T. Herring. Modelling Atmospheric Delays in the Analysis of Space Geodetic Data. In *Refraction of Transatmospheric Signals in Geodesy, Proceedings of the Symposium*, volume Publ. Geod. 36, pages 157–164, 1992.
- [Höflinger *et al.*, 1992] W. Höflinger, M. Cocard, and A. Geiger. IODEL, Ionosphärenmodellierung mit GPS 2-Frequenzmessungen. Technical Report 200, Institute of Geodesy and Photogrammetry, ETHZ, Zürich, 1992. IGP-Bericht.
- [Höflinger, 1993] W. Höflinger. Entwicklung von 3D Meteo-Modellen zur Korrektur der troposphärischen Refraktion bei GPS-Messungen. Technical Report 216, Institute of Geodesy and Photogrammetry, ETHZ, Zürich, 1993. IGP-Bericht.
- [Hoots and Roehrich, 1980] F. Hoots and R. Roehrich. Model for Propagation of NORAD Elements Sets, December 1980.
- [Hurrass and Hickmann, 1997] K. Hurrass and D. Hickmann. Multipath Effects at GPS L1-Frequency. Proceedings of the First European Symposium on Global Navigation Satellite Systems, GNSS97, Volume II, p. 707–716, DGON, Munich, Germany, 1997.
- [ICAO, 1990] ICAO. Rules of the Air, July 1990. International Standards, Annex2, Ninth Edition.
- [ICAO, 1993] ICAO. Aircraft Operations, 1993. Procedures for Air Navigation Services, Doc 8168-OPS/611, Volume I.
- [ICAO, 1994b] ICAO. Manual on Required Navigation Performance (RNP), 1994b. Doc 9613-AN/937, first edition.
- [Johnson, 1994] M. Johnson. Interference to GNSS Receivers in the Civil Aviation Environment, 1994. Proceedings of ION GPS-94, pp. 1127–1136.
- [Jülg, 1997] Thomas Jülg. *Einfluss der Mehrwegesignalausbreitung auf die Laufzeit- und Phasenmessungen beim Globalen Navigationssystem GPS*, volume 97 of 28. Deutsche Forschungsanstalt für Luft- und Raumfahrt, Oberpfaffenhofen, Juli 1997.
- [Just, 1979] Christian Just. Statistische Methoden zur Beurteilung der Qualität einer Vermessung. Technical Report 27, Institut für Geodäsie und Photogrammetrie, ETH Zürich, November 1979. Mitteilungen.
- [Kalafus, 1989] R. Kalafus. GPS Integrity Channel RTCA Working Group Recommendations. *Journal of The Institute of Navigation*, 36(1):25–44, Spring 1989.
- [Kee and Parkinson, 1994] C. Kee and B. Parkinson. Calibration of Multipath Errors on GPS Pseudorange Measurements, 1994. Proceedings of ION GPS-94, Part1, pp. 353–362.

- [Kelly and Davis, 1994] R. J. Kelly and J. M. Davis. Required Navigation Performance (RNP) for Precision Approach and Landing with GNSS Application. *Journal of The Institute of Navigation*, 41(1):1-30, Spring 1994.
- [Kelso, 1992a] T. S. Kelso. Documentation for NORAD SGP4/SDP4 Units, October 1992.
- [Kelso, 1992b] T. S. Kelso. Documentation for NORAD SGP4/SDP4 Units, Interface Documentation, October 1992.
- [Kshirsagar, 1983] A. M. Kshirsagar. *A Course in Linear Models*. Marcel Dekker Inc., New York, 1983.
- [Laginja, 1993] T. Laginja. RNP Tunnel Concept for Precision Approach and Landing. All Weather Operations Panel, AWOP-WP/644, Fourteenth Meeting, Montreal, 1993.
- [Lautenbach, 1997] P. Lautenbach. The European Contribution to GNSS 2 - Institutional, Organisational and Financial Aspects. Proceedings of the First European Symposium on Global Navigation Satellite Systems, GNSS97, Volume I, p. 31-39, DGON, Munich, Germany, 1997.
- [Lee *et al.*, 1996] Y. Lee, K. van Dyke, B. Declene, J. Studenny, and M. Beckmann. Summary of RTCA SC-159 GPS Integrity Working Group Activities. *Journal of The Institute of Navigation*, 43(3), Fall 1996.
- [Lee, 1986] Y. Lee. Analysis of Range and Position Comparison Methods as a Means to Provide GPS Integrity in the User Receiver. *Proceedings of The Institute of Navigation*, June 1986. Forty-second Annual Meeting.
- [Lee, 1993] Y. Lee. RAIM Availability for GPS Augmented with Barometric Altimeter Aiding and Clock Coasting. *Journal of The Institute of Navigation*, 40(2):179-198, Summer 1993.
- [Lössner *et al.*, 1996] U. Lössner, C. Mattes, and U. Denksat. EEC Sapphire Data Update and Access Unit, User Requirements Document, May 1996.
- [Lowe *et al.*, 1997] D. Lowe, S. Capaccio, D. Walsh, P. Daly, G. Richards, A. Wolfe, and H. Mistry. GPS and GLONASS LAAS and RAAS Flight Trials with FMS Integration. Proceedings of the First European Symposium on Global Navigation Satellite Systems, GNSS97, Volume I, p. 99-108, DGON, Munich, Germany, 1997.
- [L+T, 1993] L+T. Digitales Höhenmodell DHM25. L+T, Wabern, August 1993. Produktinformation.
- [Luftfartsverket, 1994] Luftfartsverket. GNSS Landing Trials at Norrköpping/Kungsängen Airport, 1994.

- [Marchal and Carle, 1997] N. Marchal and C. Carle. Preparing the Transition from GNSS1 to GNSS2: Political and Technical Issues. Proceedings of the First European Symposium on Global Navigation Satellite Systems, GNSS97, Volume I, p. 41–48, DGON, Munich, Germany, 1997.
- [Michalson, 1995] W. Michalson. Ensuring GPS Navigation Integrity using Receiver Autonomous Integrity Monitoring. *IEEE Aerospace and Electronic Systems Magazine*, 10(10):31–34, October 1995.
- [Misra *et al.*, 1993] P. Misra, E. Bayliss, M. Pratt, and R. Muchnik. Receiver Autonomous Integrity Monitoring (RAIM) of GPS and GLONASS. *Journal of The Institute of Navigation*, 40(1):87–104, Spring 1993.
- [Moore, 1995] A. Moore. GPS Interference on Approach to Eddinburgh Airport, 1995.
- [Niell, 1996] A. Niell. Global Mapping Functions for the Atmospheric Delay at Radio Wavelengths. *Journal of Geophysical Research*, 101(B2):3227–3246, 1996.
- [Papula, 1990] Lothar Papula. *Mathematik für Ingenieure 2*. Vieweg Verlag, 1990.
- [Parkinson and Axelrad, 1988] B. Parkinson and P. Axelrad. Autonomous GPS Integrity Monitoring Using the Pseudorange Residuals. *Journal of The Institute of Navigation*, 35(2), Summer 1988.
- [Parkinson, 1994] B. Parkinson. Differential GPS (Part 1), 1994. ION GPS-94 Tutorial, Course 151A.
- [Peckham, 1997] R. Peckham. GNSS Architecture Optimisation. Proceedings of the First European Symposium on Global Navigation Satellite Systems, GNSS97, Volume I, p. 11–20, DGON, Munich, Germany, 1997.
- [Perry and Geppert, 1996] T. Perry and L. Geppert. Do Portable electronics endanger flight? The Evidence Mount. *IEEE Spectrum*, (9):26–33, September 1996.
- [Press *et al.*, 1990] W. Press, B. Flannery, S. Teukolsky, and W. Vetterling. Numerical Recipes in Pascal. Cambridge University Press, 1990.
- [Proakis, 1983] J. Proakis. *Digital Communication*. MacGraw Hill, New York, 1983.
- [RTCA, 1988] RTCA. Report of Special Committee 159 on Minimum Aviation System Performance Standards (MASPS) for Global Positioning System (GPS), 28 November 1988. RTCA/DO-202.
- [RTCA, 1991] RTCA. Minimum Operational Performance Standards (MOPS) for Airborne Supplemental Navigation Equipment Using Global Positioning System (GPS), July 1991. RTCA/DO-208.

- [RTCA, 1993] RTCA. Minimum Aviation System Performance Standards DGNSS Instrument Approach System: Special Category I (SCAT-I), 27 August 1993. RTCA/DO-217.
- [RTCA, 1995] RTCA. Minimum Operational Performance Standards for Global Navigation Satellite Systems (GNSS) Airborne Antenna Equipment, 20 October 1995. RTCA/DO-228.
- [RTCA, 1996] RTCA. Minimum Aviation System Performance Standards: Required Navigation Performance for Area Navigation, 5 August 1996. RTCA Paper No. 299-96, Final Draft, (Draft 9).
- [RTCA, 1996b] RTCA. Minimum Operational Performance Standards for Global Positioning System / Wide Area Augmentation System Airborne Equipment, 16 January 1996b. RTCA/DO-229.
- [RTCA, 1998] RTCA. Minimum Aviation System Performance Standards for the Local Area Augmentation System (LAAS), 1998. RTCA Paper No. 037-98/SC159-778, Proposed Final Draft (Draft 006).
- [RTCM SC-104, 1994] RTCM SC-104. RTCM Recommended Standards for Differential NAVSTAR GPS Service, 3 January 1994. RTCM Paper 194-93/SC104-STD.
- [Saastamoinen, 1973] J. Saastamoinen. Contributions to the Theory of Atmospheric Refraction / Introduction to Practical Computation of Astronomical Refraction. Bulletin géodésique Nrs 105, 106, 107, pp.50, 1973.
- [Scaramuzza and Geiger, 1995] Maurizio Scaramuzza and Alain Geiger. Use of Digital Terrain Model for Detection of Potentially Interfering Zones. In *Workshop GPS interference—is it a problem?, Proceedings*. Royal Institute of Navigation, London, 1995.
- [Schulte, 1995a] M. Schulte. Compte rendu final de la situation, 1995. Swisscontrol, Geneve.
- [Schulte, 1995b] M. Schulte. GPS Interference Search Around the Swiss Lugano/Agno Airport, 1995.
- [Schwarz, 1988] H. R. Schwarz. *Numerische Mathematik*. B. G. Teubner, 1988.
- [Seybold *et al.*, 1997] J Seybold, F. Gass, and U. Kälberer. Pseudolites - An Integral Part of LAAS (Local Area Augmentation Systems. Proceedings of the First European Symposium on Global Navigation Satellite Systems, GNSS97, Volume I, p. 277-286, DGON, Munich, Germany, 1997.

- [Sierk *et al.*, 1997] B. Sierk, B. Bürki, H. Becker-Ross, S. Florek, R. Neubert, L. Kruse, and H.-G. Kahle. Tropospheric water vapor derived from solar spectrometer, radiometer, and GPS measurements. *Journal of Geophysical Research*, Vol. 102, No. B10, p. 22411 - 22424, 10 October 1997.
- [Stevens, 1995] E. Stevens. Interference Trials on Aircraft GPS Receivers, 1995.
- [Sturza, 1988] M. Sturza. Navigation System Integrity Monitoring Using Redundant Measurements. *Journal of The Institute of Navigation*, 35(4), Winter 1988.
- [Sturza, 1990] M. Sturza. Comparison of Fixed and Variable Threshold RAIM Algorithms, 1990. Proceedings of ION GPS-90, pp. 437-443.
- [Townsend and Fenton, 1994] B. Townsend and P. Fenton. A Practical Approach to the Reduction of Pseudorange Multipath Errors in a L1 GPS Receiver, 1994. Proceedings of ION GPS-94, Part1, pp. 143-148.
- [Townsend *et al.*, 1995] B. R. Townsend, P. C. Fenton, K. J. van Dierendonck, and D. J. R. van Nee. Performance Evaluation of the Mutlipath Estimating Delay Lock Loop. *Journal of The Institute of Navigation*, 42(3):503-514, Fall 1995.
- [Vallot *et al.*, 1991] L. Vallot, S. Snyder, B. Schipper, N. Parker, and C. Spitzer. Design and Flight Test of a Differential GPS/Inertial Navigation System for Approach/Landing Guidance. *Journal of The Institute of Navigation*, 38(2):103-122, Summer 1991.
- [van Nee, 1992] R. D. J. van Nee. Multipath Effects on GPS Code Phase Measurements. *Journal of The Institute of Navigation*, 39(2):177-190, Summer 1992.
- [Vieweg and Lechner, 1994] S. Vieweg and W. Lechner. A GPS/GLONASS/INS Test Program. *IEEE Aerospace and Electronic Systems Magazine*, 9(7):23-28, July 1994.
- [Vieweg *et al.*, 1995] S. Vieweg, A. Lipp, and J. Wagner. Integrated Satellite- / Inertial Navigation with Low Cost Inertial Sensors for Precision Applications? - Feasibility, Test and Experiences -. Proceedings on ISPA95, International Symposium on Precision Approach and Automatic Landing, p. 303-310, Braunschweig, Germany, 1995.
- [Walter and Enge, 1995] T. Walter and P. Enge. Weighted RAIM for Precision Approach. Palm Springs, California, 1995. Proceedings on ION GPS-95.
- [Ward, 1995] D. Ward. UK Field Survey of RF radiation in the Environment, 1995.
- [Weiser, 1997] M. Weiser. Pseudolites - Chancen und Risiken lokaler Ergänzungen zu bestehenden GNSS-Systemen. DGON Fachausschuß Weltraumtechnik, Düsseldorf, 1997.

- 
- [Wells *et al.*, 1986] D. Wells, N. Beck, D. Delikaraoglou, A. Kleusberg, E. Krakiwsky, G. Lachapelle, R. Langley, M. Nakiboglu, K. P. Schwarz, J. Tranquilla, and P. Vaníček. Guide to GPS Positioning. Canadian GPS Associates, 1986.
- [Wild and Santschi, 1995] U. Wild and W. Santschi. GPS-Vermessung Flugplatz Agno, Grundlagemessungen für DGPS-Versuche des BAZL. L+T, Wabern, 1995. Technischer Bericht 95-26.
- [Williams, 1996] J. Williams. Unintentional Electromagnetic Interference to the GNSS, September 1996.
- [Wlaka, 1997] M. Wlaka. The European Contribution to GNSS 2, a Technical Concept. Proceedings of the First European Symposium on Global Navigation Satellite Systems, GNSS97, Volume I, p. 61–67, DGON, Munich, Germany, 1997.

## A. Abbreviations

2D	Two Dimensions
3D	Three Dimensions
A9	Amber 9 (airway)
AAIM	Aircraft Autonomous Integrity Monitoring
ADARS	Airborne Data Acquisition and Recording System
AIP	Aeronautical Information Publication
AIUB	Astronomical Institute of the University of Berne
AL	Alarm Limit
AOA	Angle of Attack
ARINC	Aeronautical Radio Incorporated
ATRK	Along-Track Error
ATS	Air Traffic Services
BIASC	waypoint of Lugano DGNSS approach
BMV	Bundesministerium des Verkehrs der Bundesrepublik Deutschland
CAA	Civil Aviation Authority
CAT-I	Category I
CAT-II/III	Category II and III
CCIR	Comite Consultatif Internationl de Radiocommunications
CDI	Course Deviation Indicator
CH	Switzerland
CHANG	waypoint of Lugano DGNSS approach
CPU	Central Processor Unit
CRX	Crossair
DGPS	Differential GPS
DGNSS	Differential Global Navigation Satellite System
DLL	Delay Lock Loop
DME	Distance Measuring Equipment
DO	Document
DoD	Department of Defence
DOP	Dilution of Precision
DoT	Department of Transportation
DRA	Defence Research Agency (now Defence Evaluation and Research Agency, DERA)
DTM	Digital Terrain Model



EATCHIP	European Air Traffic Control Harmonisation and Integration Programme
EEC	Eurocontrol Experimental Centre
EFIS	Electronic Flight Instrument System
ETH	Swiss Federal Institute of Technology
FAA	Federal Aviation Administration
FAF	Final Approach Fix
FANS	Future Air Navigation Systems
FMS	Flight Management System
FOCA	Swiss Federal Office of Civil Aviation
ft	Feet
FTE	Flight Technical Error
GB	Gigabyte
GDARS	Ground Data Acquisition and Recording System
GDOP	Geometrical Dilution of Precision
GGL	Geodesy and Geodynamics Laboratory
GIC	GPS Integrity Channel
GLONASS	Global Navigation Satellite System
GNSS	Global Navigation Satellite System
GPS	Global Positioning System (Navstar)
GPWS	Ground Proximity Warning System
GS	Glide Slope
HAL	Horizontal Alarm Limit
HDL	Horizontal Detection Limit
HDOP	Horizontal Dilution of Precision
Hz	Hertz
ICAO	International Civil Aviation Organization
IERS	International Earth Rotation Service
ILS	Instrument Landing System
INS	Inertial Navigation System
IRS	Inertial Reference System
ITRF	IERS Terrestrial Reference Frame
ITRS	IERS Terrestrial Reference System
LAAS	Local Area Augmentation System
LOC	Localizer
LORAN	Long Range Navigation
LSR	Least Square Residuals
LUKOM	waypoint of Lugano DGNSS approach
LV95	Landesvermessung 1995
L+T	Swiss Federal Office of Topography
MAAR	Maximum Allowable Alarm Rate
MASPS	Minimum Aviation System Performance Standard
MLS	Microwave Landing System
MOPS	Minimum Operational Performance Standards

---

NDB	Nondirectional Beacon
NM	Nautical Miles
NORAD	North American Aerospace Defence Command
NSE	Navigation System Error
PDOP	Position Dilution of Precision
PRC	Pseudo Range Correction
PRN	Pseudo Random Noise
RAIM	Receiver Autonomous Integrity Monitoring
RF	Radio Frequency
RFI	Radio Frequency Interference
RNAV	Area Navigation
RNP	Required Navigation Performance
RTCA	Radio Technical Commission for Aeronautics
RTCM	Radio Technical Commission for Maritime Services
SA	Selective Availability
SC	Special Committee
SC	Swisscontrol
SCAT-I	Special Category I
SCSI	Small Computer System Interface
SDI	Source Destination Identifier
SF	Swiss Aircraft Factory
SHARK	waypoint of Lugano DGNSS approach
SNR	Signal to Noise Ratio
SODES	waypoint of Lugano DGNSS approach
SSM	Sign Status Mix
SVD	Single Value Decomposition
TEC	Total Electron Content
TOUCH	waypoint of Lugano DGNSS approach
TSE	Total System Error
TtA	Time to Alarm
TV	Television
TW	Tunnel Width
UK	United Kingdom
UTC	Universal Time Coordinated
USA	United States of America
VD	Eidgenössische Vermessungsdirektion und Vermessungsflugdienst
VDOP	Vertical Dilution of Precision
VLF	Very Low Frequency
VMC	Visual Meteorological Conditions
VHF	Very High-Frequency
VOR	VHF Omnidirectional Range
WAAS	Wide Area Augmentation System
WGS-84	World Geodetic System 1984

## B. Glossary

### AAIM, Aircraft Autonomous Integrity Monitoring

A technique whereby a civil → *GNSS* receiver determines the → *integrity* of the → *GNSS* navigation signals with reference to other sensors or systems in the aircraft only. (→ *RAIM*, *Receiver Autonomous Integrity Monitoring*, → *RNP*, *Required Navigation Performance*)

### Accuracy

Accuracy is defined in the context of the approach phase of flight as the ability of the total system to maintain the aircraft position within a → *Total System Error (TSE)* with a 95% probability (inner tunnel) and to stay within a specified aircraft containment surface (outer tunnel) which defines the obstacle clearance and terrain avoidance. (→ *RNP*, *Required Navigation Performance*)

### Availability

Availability is defined as the ability of the total system to perform its function at the initiation of the intended operation. (→ *RNP*, *Required Navigation Performance*)

### Choke rings

Concentric rings on a ground plane of an antenna reduce → *multipath* effects.

### Continuity

Continuity is defined as the ability of the total system to perform its function without interruption during the intended operation. (→ *RNP*, *Required Navigation Performance*)

### Cut off angle

A fixed elevation angle referenced to the user's horizon in the horizontal coordinate system below which satellites are ignored for position calculations.

**DGNSS, Differential Global Navigation Satellite System**

Differential → *GNSS* is an augmentation, the purpose of which is to determine measurement errors at one or more known locations and subsequently transmit raw or derived information to other → *GNSS* receivers in order to enhance the → *accuracy*, → *integrity*, and → *availability*.

**DGPS, Differential GPS**

→ *GPS differential code mode*

**Ellipsoidal altitude/height**

Height above earth ellipsoid.

**Epoch**

→ *Measurement epoch*

**FTE, Flight Technical Error**

The FTE refers to the accuracy with which the aircraft is controlled. This corresponds to the deviation of the indicated position from the desired course. (→ *NSE*, *Navigation System Error*, → *TSE*, *Total System Error*)

**Geoid**

The equipotential surface of the earth's gravity field which best fits, in the least square sense, mean sea level.

**Geoidal undulation**

The up welling and depression of the → *geoid* with respect to the earth's ellipsoid.

**GNSS, Global Navigation Satellite System**

GNSS is a world-wide position, velocity, and time determination system, that includes one or more satellite constellations, receivers, and system integrity monitoring, augmented as necessary to support the required navigation performance for the actual phase of operation (→ *DGNSS*, *Differential Global Navigation Satellite System*).

**GPS carrier phase mode**

The GPS carrier phase mode refers to the position, velocity, and time estimation using the carrier phase of the GPS signal.

**GPS differential code mode**

The GPS differential code mode refers to the position, velocity, and time estimation using code measurements enhanced by  $\rightarrow$  *Pseudo Range Corrections (PRC)* derived and transmitted from one or more fixed ground stations.

**GPS stand alone mode**

The GPS stand alone mode refers to the position, velocity, and time estimation using only the code measurements by one single receiver.

**Integrity**

The system integrity refers to the ability of the system to provide timely warnings to the user when the system should not be used for navigation. ( $\rightarrow$  *RNP, Required Navigation Performance*)

**Measurement epoch**

A measurement epoch consists in a set of measurements carried out at one point in time.

**Multipath**

Multipath is caused by reflection or diffraction of the L-band signal on the aircraft, terrain, buildings etc. That means, that the signal travels from the satellite to the receiver antenna via multiple paths.

**NSE, Navigation System Error**

The NSE is the deviation the true (actual) position from the indicated position used for navigation purpose. This error is a combination of the navigation sensor error, airborne receiver error and reference position error. The navigation sensor error comprises navigation data transfer times, computation errors, display errors, sensor noise etc. Error components of the ground station receiver and atmosphere have to be added when using the  $\rightarrow$  *DGPS* mode. ( $\rightarrow$  *FTE, Flight Technical Error*,  $\rightarrow$  *TSE, Total System Error*)

**Orthometric altitude/height**

Altitude above → *geoid*.

**Path delay**

The path delay is caused by satellite signal transmission delay or signal refraction in the atmosphere (mainly troposphere and ionosphere). The path delay can be derived from the → *zenith path delay* using a mapping function depending on the elevation.

**PRC, Pseudo Range Correction**

Pseudo range corrections are estimates of the pseudo range errors. These corrections are calculated with a GPS receiver and its a priori known position.

**RAIM, Receiver Autonomous Integrity Monitoring**

A technique whereby a civil → *GNSS* receiver determines the → *integrity* of the → *GNSS* navigation signals without reference to other sensors or systems than the receiver itself. (→ *AAIM*, *Aircraft Autonomous Integrity Monitoring*, → *RNP*, *Required Navigation Performance* )

**RNP, Required Navigation Performance**

A measure of the navigation system performance within a defined airspace, route, or procedure, including the operating parameters of the navigation system used within the airspace. The RNP parameters used for approach and landing procedures are → *accuracy*, → *availability*, → *continuity*, and → *integrity*.

**Tracked satellite**

A tracked satellite refers in this context to a satellite, whose signal can be properly tracked by a receiver. (→ *visible satellite*)

**TSE, Total System Error**

The TSE corresponds to the deviation of the true position from the desired course. (→ *FTE*, *Flight Technical Error*, → *NSE*, *Navigation System Error*)

**Visible satellite**

A visible satellite refers in this context to a satellite, whose line of sight from a receiver antenna is not obstructed. ( $\rightarrow$  *Tracked satellite*)

**Zenith path delay**

The zenith path delay corresponds to the  $\rightarrow$  *path delay* for a satellite with an elevation of  $90^\circ$ . The path delay can be derived from the zenith path delay using a mapping function, which describes the atmosphere.

# C. Recorded Labels

## C.1. ADARS

The first three tables list the labels recorded by the ADARS, divided in a 25Hz, 10Hz and 1Hz table. It is noted, that additionally to nearly each label a Source Destination Identifier (SDI), a Sign Status Mix (SSM) and a parity bit are recorded, but not showed in the tables.

The fourth table shows the recorded labels of the GPS receiver of the measurement and monitoring system.

### Recording Rate 25Hz

Identifier	Description	Units	Range	Resolution
SAMPLE	sample	-	-	INT.
RECTIME	recording time	sec	-	0.01
GS	ground speed (IRS)	kts	±4096	0.125
TRK	track angle true (IRS)	degree	±180	$5.493 \cdot 10^{-3}$
PTRC	pitch rate (body)	degree/sec	±128	$3.906 \cdot 10^{-3}$
ROLR	roll rate (body)	degree/sec	±128	$3.906 \cdot 10^{-3}$
YAW	yaw rate (body)	degree/sec	±128	$3.906 \cdot 10^{-3}$
LONG	longitudinal acceleration (body)	g	±4	$1.221 \cdot 10^{-4}$
LATG	lateral acceleration (body)	g	±4	$1.221 \cdot 10^{-4}$
VRTG	normal acceleration (body)	g	±4	$1.221 \cdot 10^{-4}$
IALT	inertial vertical velocity	ft/min	32768	1.0

### Recording Rate 10Hz

Identifier	Description	Units	Range	Resolution
SAMPLE	sample	-	-	INT.
RECTIME	recording time	sec	-	0.01
RALT	radio height	ft	±8192	0.125
LOCD	LOC deviation	DDM	±0.4	$9.766 \cdot 10^{-5}$
GLS	GLS deviation	DDM	±0.8	$1.953 \cdot 10^{-4}$
MLSLOCD	LOC deviation	DDM	±0.4	$9.766 \cdot 10^{-5}$
MLSGLS	GLS deviation	DDM	±0.8	$1.953 \cdot 10^{-4}$



## Recording Rate 1Hz

Identifier	Description	Units	Range	Resolution
SAMPLE	sample	-	-	INT.
RECTIME	recording time	sec	-	0.01
ACUTC.HRS	UTC (GPS/A/C/FMS)	hrs	0-23	INT.
ACUTC.MINS	-	min	0-59	INT.
ACUTC.SEC	-	sec	0-59	INT.
IRDISC.B11	IRS discretes (bytes 11-29)	-	0-1	INT.
:				
IRDISC.B29	-	-	0-1	INT.
LATP	present position latitude (IRS)	degree	±180	$1.717 \cdot 10^{-4}$
LONP	present position longitude (IRS)	degree	±180	$1.717 \cdot 10^{-4}$
THDG	true heading (IRS)	degree	±180	$5.493 \cdot 10^{-3}$
WS	wind speed (IRS)	kts	±256	$7.813 \cdot 10^{-3}$
WD	wind angle (IRS)	degree	±180	$5.493 \cdot 10^{-3}$
PTCH	pitch angle	degree	±180	$5.493 \cdot 10^{-3}$
ROLL	roll angle	degree	±180	$5.493 \cdot 10^{-3}$
IALT	inertial altitude	ft	±131'072	0.125
DME	DME distance	nmi	512	$7.813 \cdot 10^{-3}$
ALT	altitude (1013.25 hPa)	ft	±131'072	1.0
BCALT	baro corrected altitude	ft	±131'072	1.0
CAS	computed air speed	kts	2048	$6.250 \cdot 10^{-2}$
TAS	true air speed	kts	2048	$6.250 \cdot 10^{-2}$
TAT	static air temperature	°Celsius	±512	0.25
SAT	total air temperature	°Celsius	±512	0.25
ADCWD1.B12	ADC discrete word 1 - Byte 12	-	0-1	INT.
ADCWD1.B13	ADC discrete word 1 - Byte 13	-	0-1	INT.
ADCWD1.B19	ADC discrete word 1 - Byte 19	-	0-1	INT.
ADCWD1.B22	ADC discrete word 1 - Byte 22	-	0-1	INT.
ADCWD1.B23	ADC discrete word 1 - Byte 23	-	0-1	INT.
ADCWD1.B26	ADC discrete word 1 - Byte 26	-	0-1	INT.
RWYHDG1	runway heading	degree	360	0.1
ILSFREQ	ILS frequency	MHz	100-180	0.01
ILSFREQ.CAT	ILS category	-	0-3	INT.
ILSFREQ.CF	ILS control function	-	0-3	INT.
RWYHDG2	runway heading (active in MLS)	degree	±180	$8.789 \cdot 10^{-2}$
MLSGNDID1	MLS GND station identification	α-num	-	2 CHAR.
MLSGNDID2	MLS GND station identification	α-num	-	2 CHAR.
ILSGNDID1	ILS GND station identification	α-num	-	2 CHAR.
ILSGNDID2	ILS GND station identification	α-num	-	2 CHAR.
HDOP	HDOP	-	1024	$3.125 \cdot 10^{-2}$
VDOP	VDOP	-	1024	$3.125 \cdot 10^{-2}$
HINTL	horizontal integrity limit	nm	16	$6.104 \cdot 10^{-5}$
SATV	GPS sensor status - sat. visible	-	0-15	INT.
SATT	GPS sensor status - sat. tracked	-	0-15	INT.
GMODE	GPS sensor status - op. Mode	-	0-7	INT.
B2L273.SSM	-	-	0-3	INT.
GLAT	GNSS latitude	degree	±180	$1.717 \cdot 10^{-4}$
GLON	GNSS longitude	degree	±180	$1.717 \cdot 10^{-4}$
GLATF	GNSS latitude fine	degree	±1.7173·10 <sup>-4</sup>	$8.382 \cdot 10^{-8}$
GLONF	GNSS longitude fine	degree	±1.7173·10 <sup>-4</sup>	$8.382 \cdot 10^{-8}$
UTCFF	UTC fine	sec	1	$9.537 \cdot 10^{-7}$
UTCFF	UTC fine fraction	sec	±9.5373·10 <sup>-7</sup>	$9.313 \cdot 10^{-10}$
UTC.HRS	UTC	hrs	0-23	INT.
UTC.MINS	-	min	0-59	INT.
UTC.SECs	-	sec	0-59	INT.
YEAR	date	year	0-99	INT.
MONTH	-	month	0-11	INT.
DAY	-	day	0-31	INT.
B2L260.SSM	-	-	0-3	INT.
GALT	GPS altitude (MSL)	ft	±131'072	0.125
CNO00 ... CNO11	measurement status - C/N ratio	dBhz	0-63	INT.
SVN00 ... SVN11	measurement status - satellite id.	-	0-31	INT.
PRC00 ... PRC11	pseudo range	m	268'435'456	256
PRF00 ... PRF11	pseudo range fine	m	256	0.125
RR00 ... RR11	range rate	m/sec	±4096	$3.9063 \cdot 10^{-3}$
DR00 ... DR11	delta range	m	±4096	$3.9063 \cdot 10^{-3}$
UTC00 ... UTC11	UTC measure time	sec	10.0	$9.5373 \cdot 10^{-6}$

Recording Rate 5Hz

Identifier	Description	Units	Range	Resolution
SAMPLE	sample	-	-	INT.
GUTC	recording time	sec	-	0.01
NVRECSTAT	Receiver Status	-	-	INT.
SVN00 ... SVN11	satellite id	-	-	INT.
CNO00 ... CNO11	signal to noise ratio	dBHz	20-51	1
LT00 ... LT11	lock time	sec	0-65536	0.031
IP00 ... IP11	Accumulated Doppler range	cycle	-	0.004
RR00 ... RR11	Doppler frequency	Hz	-	0.004
PRC00 ... PRC11	Pseudorange	m	-	0.008
SIP00 ... SIP11	StdDev Accumulated Doppler	cycle	-	0.002
SPRC00 ... SPRC11	StdDev pseudorange	m	-	0.062
TRK00 ... TRK11	tracking state	-	-	INT.
CHN00 ... CHN11	channel number	-	0-31	INT.
FLA00 ... FLA11	phase parity known flag	-	0-1	INT.
FLB00 ... FLB11	phase lock flag	-	0-1	INT.
FLC00 ... FLC11	code lock flag	-	0-1	INT.

C.2. GDARS

Following two tables list the labels recorded by the GDARS. The first table refers to the labels of the operational system. Three message types are possible and are divided in the table by an horizontal line. The second table shows the recorded labels of the GPS receiver of the measurement and monitoring system. The recording rate is 1Hz from 6am to 10pm and is increased to 5Hz during the period when a test flight is carried out.

Recording Rate 1Hz

Identifier	Description	Units	Range	Resolution
TYPE	message type	-	1-3	INT.
SID	station identifier	-	0-1023	INT.
TIME	seconds since GPS start	sec	-	-
ZCNT	Z-count	sec	0-3599.4	-
SN	sequence number	-	0-7	INT.
SH	station health	-	0-7	INT.
message type 1				
SC	satellite count	-	-	INT.
PRC	pseudo range correction	m	-	-
RRC	range rate correction	m/s	-	-
UDRE	user diff. range error	-	0-3	INT.
IOD	issue of data	-	0-7	INT.
message type 2				
SC	satellite count	-	-	INT.
DPRC	delta pseudo range correction	m	-	-
DRRC	delta range rate correction	m/s	-	-
UDRE	user diff. range error	-	0-3	INT.
IOD	issue of data	-	0-7	INT.
message type 3				
ECEF <sub>X</sub>	x-coordinates of ground station			
ECEF <sub>Y</sub>	y-coordinates of ground station			
ECEF <sub>Z</sub>	z-coordinates of ground station			

Recording Rate 1Hz respectively 5Hz

Identifier	Description	Units	Range	Resolution
SAMPLE	sample	-	-	INT.
GUTC	recording time	sec	-	0.01
NVRECSTAT	Receiver Status	-	-	INT.
SVN00 ... SVN11	satellite id	-	-	INT.
CNO00 ... CNO11	signal to noise ratio	dBHz	20-51	1
LT00 ... LT11	lock time	sec	0-65536	0.031
IP00 ... IP11	Accumulated Doppler range	cycle	-	0.004
RR00 ... RR11	Doppler frequency	Hz	-	0.004
PRC00 ... PRC11	Pseudorange	m	-	0.008
SIP00 ... SIP11	StdDev Accumulated Doppler	cycle	-	0.002
SPRC00 ... SPRC11	StdDev pseudorange	m	-	0.062
TRK00 ... TRK11	tracking state	-	-	INT.
CHN00 ... CHN11	channel number	-	0-31	INT.
FLA00 ... FLA11	phase parity known flag	-	0-1	INT.
FLB00 ... FLB11	phase lock flag	-	0-1	INT.
FLC00 ... FLC11	code lock flag	-	0-1	INT.



## **“Geodätisch-geophysikalische Arbeiten in der Schweiz”**

**(Fortsetzung der Publikationsreihe “Astronomisch-geodätische Arbeiten in der Schweiz”)  
der Schweizerischen Geodätischen Kommission (ab Bd. 40):**

- 40 1989 Integrale Schwerefeldbestimmung in der Ivrea- Zone und deren geophysikalische Interpretation. B. Bürki. 186 Seiten.
- 41 1990 ALGESTAR satellitengestützte Geoidbestimmung in der Schweiz. U. Marti. 61 Seiten plus Punktprotokolle.
- 42 1990 Höhensysteme, Schwerepotentiale und Niveauflächen: Systematische Untersuchungen zur zukünftigen terrestrischen und GPS-gestützten Höhenbestimmung in der Schweiz. B. Wirth. 204 Seiten.
- 43 1990 Gravimetrisches Geoid der Schweiz: Potentialtheoretische Untersuchungen zum Schwerefeld im Alpenraum. A. Geiger. 231 Seiten.
- 44 1991 Rapid Differential Positioning with the Global Positioning System (GPS). E. Frei. 178 Seiten.
- 45 1992 Dreidimensionales Testnetz Turtmann 1985-1990 Teil I. F. Jeanrichard (Hrsg.) Autoren: A. Geiger, H.-G. Kahle, R. Köchle, D. Meier, B. Neiningen, D. Schneider, B. Wirth. 183 Seiten.
- 46 1993 Orbits of Satellite Systems in Space Geodesy. M. Rothacher. 243 Seiten.
- 47 1993 NFP 20. Beitrag der Geodäsie zur geologischen Tiefenstruktur und Alpendynamik. H.-G. Kahle (Hrsg.) Autoren: I. Bauersima, G. Beutler, B. Bürki, M. Cocard, A. Geiger, E. Gubler, W. Gurtner, H.-G. Kahle, U. Marti, B. Mattli, M. Rothacher, Th. Schildknecht, D. Schneider, A. Wiget, B. Wirth. 153 Seiten plus 90 Seiten Anhang.
- 48 1994 Ionosphere and Geodetic Satellite Systems: Permanent GPS Tracking Data for Modelling and Monitoring: Urs Wild, 155 Seiten.
- 49 1994 Optical Astrometry of Fast Moving Objects using CCD Detectors: Thomas Schildknecht, 200 Seiten.
- 50 1995 Geodätische Alpen traverse Gotthard: A. Elmiger, R. Köchle, A. Ryf und F. Chaperon. 214 Seiten.
- 51 1995 Dreidimensionales Testnetz Turtmann 1985-1993, Teil II (GPS-Netz). F. Jeanrichard (Hrsg.) Autoren: G. Beutler, A. Geiger, M. Rothacher, Stefan Schaer, D. Schneider, A. Wiget, 173 Seiten.
- 52 1995 High Precision GPS Processing in Kinematic Mode: M. Cocard. 139 Seiten.
- 53 1995 Ambiguity Resolution Techniques in Geodetic and Geodynamic Applications of the Global Positioning System. L. Mervart. 155 Seiten.
- 54 1997 SG 95: Das neue Schweregrundnetz der Schweiz: F. Arnet und E. Klingelé. 37 Seiten.
- 55 1997 Combination of Solutions for Geodetic and Geodynamic Applications of the Global Positioning System (GPS). Elmar Brockmann, 211 Seiten.
- 56 1997 Geoid der Schweiz 1997. Urs Marti, 140 Seiten.
- 57 1998 Astrometry and Satellite Orbits: Theoretical Considerations and Typical Applications. Urs Hugentobler, 209 Seiten.
- 58 1998 Systematic Investigations of Error- and System-Modelling of Satellite Based Flight Approaches and Landings in Switzerland. Maurizio Scaramuzza, 165 Seiten.

